Okinawa Institute of Science and Technology
Graduate University

Thesis submitted for the degree

Doctor of Philosophy

Quenched and Driven Dynamics of One-Dimensional Quantum Systems

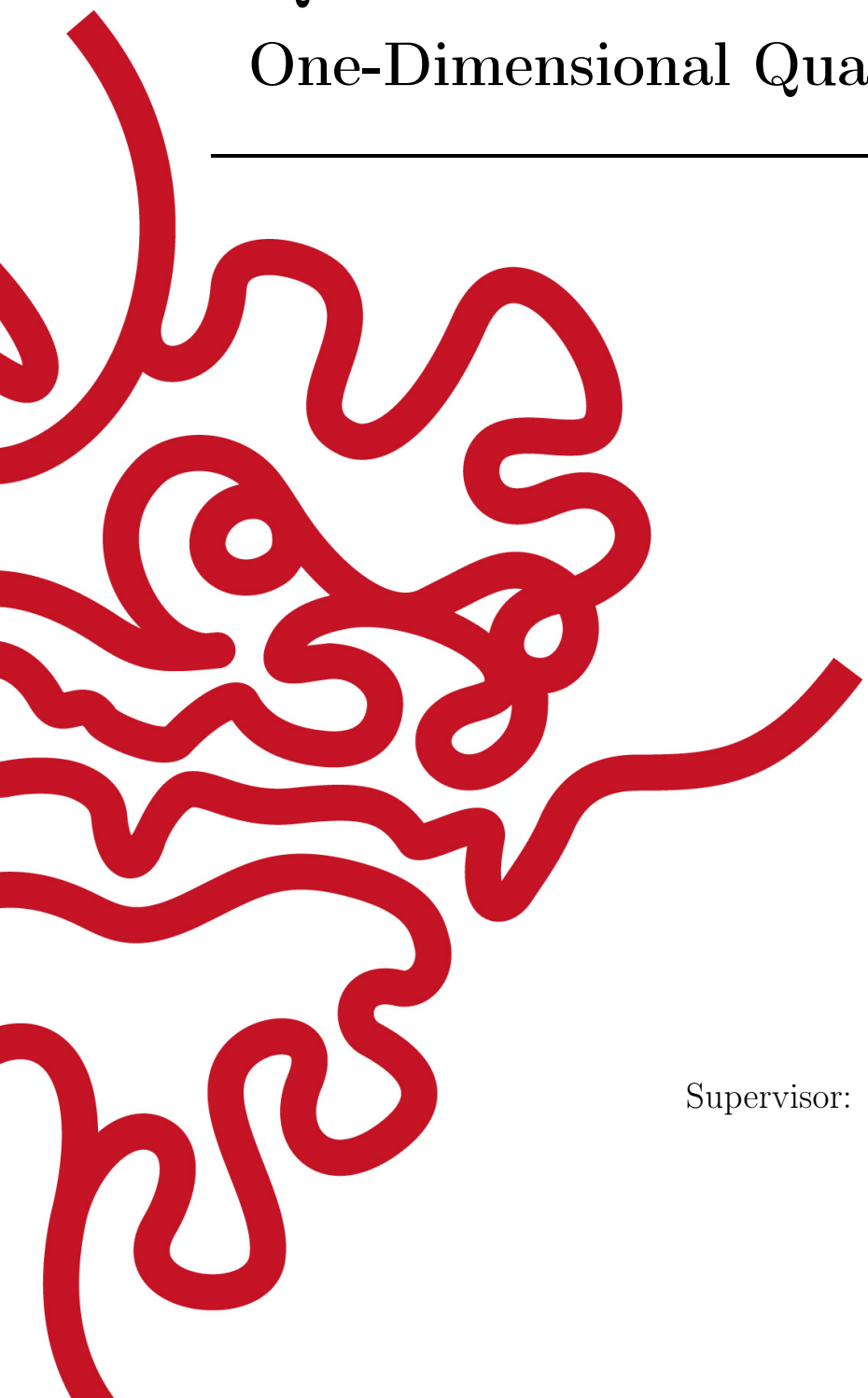

by

Mathias Mikkelsen

Supervisor: **Professor Thomas Busch**

April 2021

Declaration of Original and Sole Authorship

I, Mathias Mikkelsen, declare that this thesis entitled *Quenched and Driven Dynamics of One-Dimensional Quantum Systems* and the data presented in it are original and my own work.

I confirm that:

- No part of this work has previously been submitted for a degree at this or any other university.
- References to the work of others have been clearly acknowledged. Quotations from the work of others have been clearly indicated, and attributed to them.
- In cases where others have contributed to part of this work, such contribution has been clearly acknowledged and distinguished from my own work.
- None of this work has been previously published elsewhere, with the exception of the following:

  Chapter 4 contains a short summary of my work published as Mathias Mikkelsen, Thomás Fogarty and Thomas Busch, *Static and dynamic phases of a Tonks–Girardeau gas in an optical lattice*, New Journal of Physics, **20** 113011, 2018.

  Part of the work presented in chapter 5 is available as a pre-print manuscript: Mathias Mikkelsen, Thomás Fogarty and Thomas Busch, *Connecting scrambling and work statistics for short-range interactions in the harmonic oscillator* arXiv:2009.14478.

  Chapter 7 contains a short summary of my work published as Mathias Mikkelsen, Thomás Fogarty, Jason Twamley and Thomas Busch, *Optomechanics with a position-modulated Kerr-type nonlinear coupling*, Physical Review A, **96**, 043832, 2017.

  The published articles mentioned above have been published under the Creative Commons license and I therefore have permission to reuse any material from them for the purpose of this thesis. For these projects I did all of the technical work, did the interpretation and chose the directions of the projects in discussion with my co-authors, and wrote the first draft and final edit for each paper.

Date: April 2021

Signature: 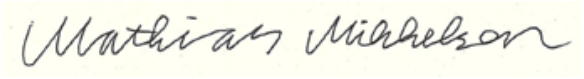

Abstract

Quenched and Driven Dynamics of One-Dimensional Quantum Systems

This thesis focuses on quenched and driven dynamics in interacting quantum systems that cannot be treated with mean-field approximations. The majority of the work is related to the unitary dynamics induced in one-dimensional systems due to a sudden change in a physical parameter (a quench). Such systems can be realized in cold atomic gases where the degree of experimental control also enables sudden changes in the physical parameters. The dynamics associated with underlying many-body phases and phase transitions for strongly interacting particles in a one-dimensional optical lattice and the relation between work statistics and scrambling dynamics for interacting particles in a harmonic trap are investigated. A more accurate exact diagonalization method useful for calculating the quench dynamics of small finitely interacting systems is also presented. Finally an investigation of an optomechanical system with a new type of nonlinear position-modulated Kerr coupling is presented. This is treated as an open quantum system which reaches a steady-state due to the interplay of driving and dissipation.

Acknowledgment

I would like to acknowledge the support of both current and former members of the Quantum Systems unit at OIST. Throughout the approximately 5 years I have spend with the group its various members have always done their best to make it a relaxed environment encouraging both scientific and non-scientific discussions.

A particular thank you goes to my main collaborator within the Quantum Systems unit Dr. Thomás Fogarty (Mossy) and my PhD supervisor Professor Thomas Busch. Working closely with Mossy has lead to many useful discussions, suggestions for interesting research directions, how to further characterize interesting aspects of my results and more broadly interpretations of results in general. I would like to thank him for always taking the time to discuss results! I would like to thank Thomas Busch for both academic and administrative support, creating a relaxing and encouraging environment in the group and of course for scientific discussions of results and methods. I'd also like to thank Professor Jason Twamley whom was a collaborator on my research project on optomechanics and who's insight into the field was invaluable. Finally I would like to thank my thesis committee as well.

I would like to acknowledge the Okinawa Institute of Science and Technology (OIST) Graduate University which has hosted and financially supported me during my PhD, as well as the Japanese Society for the Promotion of Science for financial support through a DC2 fellowship (and JSPS KAKENHI Grant No. 19J10852).

I also want to thank those who have made OIST a fun place to hang out outside of work, including but not limited to, Irinia, Leonidas, Andreas, Stefan, Rike, Juan and Rux. Finally I'd like to thank the regulars of the boardgame cafe Saikorodou located in Naha and the owner Goki for creating a welcoming space where I have enjoyed playing boardgames and practicing my Japanese.

Abbreviations

CM	Center-of-mass
HO	Harmonic Oscillator
SP	Single Particle
DE	Diagonal Ensemble
EDE	Extended Diagonal Ensemble
OTOC	Out-of-time-ordered correlation function
BEC	Bose-Einstein condensate

Nomenclature

$\hbar$ Planck constant ($1.054\ 572\ 66 \times 10^{-34}$ Js)

List of Publications

1. Mathias Mikkelsen, Thomás Fogarty and Thomas Busch, *Static and dynamic phases of a Tonks–Girardeau gas in an optical lattice*, New Journal of Physics, **20** 113011, 2018.

    - I did all of the technical work, did the interpretation and chose the directions of the project in discussion with my co-authors, and wrote the first draft and final edit of the paper.

2. Mathias Mikkelsen, Thomás Fogarty, Jason Twamley and Thomas Busch, *Optomechanics with a position-modulated Kerr-type nonlinear coupling*, Physical Review A, **96**, 043832, 2017.

    - I did all of the technical work, did the interpretation and chose the directions of the project in discussion with my co-authors, and wrote the first draft and final edit of the paper.

Contents

List of Figures

Introduction and overview

Quantum mechanics has been an integral part of the physical framework utilized to describe the world for approximately 100 years [3]. The basic laws that govern quantum mechanics have therefore been understood for a long-time and the unified expression of the electromagnetic, weak and strong force for fundamental particles within this framework have similarly been understood for almost 50 years [3]. In light of this one might think that quantum mechanics is essentially done and there is nothing interesting left to be solved. Contrary to this expectation, however, quantum mechanics is a thriving field with many interesting developments having taken place over the last 25 years. This is largely because modern quantum physics is not just concerned with the reductionist application of quantum mechanics to smaller and smaller elements, but rather with the application of quantum mechanics to explain complex physical phenomena and engineer useful results. This is not to say that modern research does not yield fundamental insights, however. Indeed recent progress in condensed matter physics, quantum thermodynamics and quantum information has led to the discovery of many intriguing properties of quantum mechanics. The application of quantum physics in many-body systems can lead to insights into emergent behaviours that play a fundamental role in nature and can yield information about universal structures that arise from the underlying microscopic physics [4, 5]. The attempt to understand simple quantum systems for applications in quantum information processing has lead to new insights into our fundamental understanding of quantum state tomography, measurement and entanglement [6]. Quantum mechanics in the presence of a lossy environment is required for quantum engineering and the field of open quantum systems theory has correspondingly become a topic of intense research interest [7, 8]. This also relates to the more fundamental problem of quantum decoherence and quantum thermodynamics. In addition to thermodynamics of open systems, the investigation of thermodynamics for closed systems governed by unitary time-evolution and hermitian Hamiltonians has led to considerable progress in understanding the interplay between quantum mechanics and classical statistical physics [9–12].

The emergence of new experimental fields such as cold atomic gases has furthermore lead to the growing field of quantum simulation in which fundamental models can be tested in clean, tunable experimental setups [13]. While experimental progress in condensed matter physics has lead to the possibility of creating specific material structures, these fields are still largely an attempt at explaining given natural phenomena. With the advent of the experimental revolution in cold atomic gases, however, one is no longer restricted to these very specific physical parameters and theoretical inquiry

is no longer limited to explaining given phenomena. Indeed, by utilizing cold atomic gases, specific experimental setups can be designed that allow for a clearer understanding of the physical mechanisms that govern a particular physical phenomenon as it is possible to isolate systems and change variables independently. Cold gases are therefore interesting both as a platform for quantum technology, but also as a platform for quantum simulation. This allows for insights obtained with cold atoms to feed back into fundamental fields such as nuclear physics [14] and condensed matter [13, 15, 16]. While these are very diverse fields that happen at different energy scales, the same theoretical framework can often be applied across these scales and it is the existence of such universality that allows for the usefulness of quantum simulation.

The main topic of this thesis is the dynamics of interacting quantum systems going from the few-body to the many-body limit. The models under investigation are partly chosen because exact solutions can be obtained which gives general insights into the topic of quantum dynamics in strongly correlated systems. However, they are also chosen because they can be experimentally realized utilizing cold atomic gases which means that the results and predictions are of experimental relevance. The thesis consists of two parts. In the first part relevant concepts, physical background and mathematical as well as numerical methods required to understand the presented work is explained. In the second part, my original research is presented split into 4 specific projects. An overview of each chapter is as follows:

- **Part 1**
  - Chapter 1: This chapter contains a brief introduction to quantum dynamics and an overview of unitary quantum quench dynamics for closed systems. This includes a basic mathematical description as well as a variety of ways to characterize post-quench dynamics and the quench itself, including the diagonal ensemble and the work probability distribution. I also discuss some of the ways quantum quenches have been utilized to investigate fundamental quantum physics in recent years, such as equilibration properties and dynamical phase transitions.
  - Chapter 2: This chapter contains an overview of the field of cold atomic gases. This includes an introduction to the field, an overview of experimental techniques and the most common mathematical models used to describe these systems. In addition I discuss experimentally realizable limits of these models where theoretical solutions can be found. In particular, I introduce the one-dimensional Hamiltonian describing a gas of N particles with short-range two-body interactions which will be the basic model under investigation in this thesis.
  - Chapter 3: This chapter discusses analytic and numeric techniques that can be applied to solve the specific models of interest in this thesis. I discuss the Bose-Fermi mapping theorem which allows one to map strongly interacting bosons to non-interacting fermions for any external potential. I then outline the analytic solution for two particles with finite short-range interaction in a harmonic trap. Finally I discuss second quantization and the diagonalization

of many-body systems in Fock-space.

- **Part 2**
  - Chapter 4: This chapter contains a discussion of the Tonks-Girardeau gas in a lattice exploring the full phase diagram as a function of the lattice depth and the ratio of number of particles to sites. Additionally the dynamics induced when the lattice is suddenly set into motion is discussed with particular attention to how this relates to the underlying many-body phases and critical points also pointing out some analogies with models for classical friction. All of the results and their interpretation is to be found in the paper *New Journal of Physics*, **20** 113011, 2018 [1]. The chapter itself will contain a brief summary of the results and how they connect to my overall work.
  - Chapter 5: This chapter investigates information scrambling utilizing the paradigmatic model consisting of two interacting particles in a harmonic trap and the canonical operators. A general overview of operator scrambling as defined through the squared commutator and the related out-of-time ordered correlation functions will be given. Analytic expressions for these quantities are derived for the relative-coordinate Hamiltonian and they are used to investigate the post-quench behaviour. This includes an investigation of the average scrambling which is shown to be proportional to the work fluctuations thus connecting the concept of operator scrambling with the work statistics of the quench. Additionally the dynamics of the quench are investigated and shown to be qualitatively different for interaction and trap quenches which can also be explained in terms of the work probability distribution and the non-equilibrium excitations in the system. This chapter partially corresponds to the arXiv paper arXiv:2009.14478 [17], but also contains additional material which will be presented in a second upcoming publication.
  - Chapter 6: This chapter outlines an improved exact diagonalization technique in Fock-space which incorporates the known information about the two-body interaction through the effective Hamiltonian approach. This requires a description of the effective Hamiltonian approach in general as well as a discussion of how to transform the two-body interaction integrals from the lab frame coordinate wavefunctions to the center-of-mass and relative coordinate frame wavefunctions. I will make a quantitative comparison with the basic exact diagonalization technique and qualitatively discuss how the method compares with other proposals for improved exact diagonalization performance. Finally I will briefly illustrate the method for an application to quench dynamics related to a future project.
  - Chapter 7: This chapter contains a discussion of my work in optomechanics and unlike the rest of the thesis is an example of open system dynamics. A method to experimentally engineer a position-modulated non-linear Kerr coupling is proposed and the resulting Hamiltonian is theoretically inves-

tigated. All of the results and their interpretation is to be found in the paper *Physical Review A*, **96**, 043832, 2017 [2] . The chapter itself will contain a brief summary of the results as well as a discussion of work by other researchers inspired by the paper.

Part I

General background, models and methods

Chapter 1

Quantum dynamics

The equilibrium properties of quantum-systems are well-studied and can yield much insight into diverse topics such as equilibrium thermodynamics, quantum phase diagrams and correlation properties [4, 5]. However, despite the many insights obtained from the equilibrium framework, out-of-equilibrium dynamics are a crucial aspect of natural processes and can yield further insight into the nature of quantum mechanics. Overall one can divide the topic of quantum dynamics into two categories. One category concerns isolated, closed systems governed by unitary dynamics, the other deals with open systems coupled to an environment governed by non-unitary dynamics. In this thesis the main focus is on the former. I will, however, also consider an example of an open quantum system related to optomechanical setups [18]. While this system yields interesting experimental insights, the results are semi-classical and pertain to the steady-state obtained through a balance of driven dynamics and dissipation. For a detailed description of the methods and results, see chapter 7.

Quantum dynamics for time-dependent Hamiltonians is a complicated topic and interesting for many purposes such as describing fundamental processes and quantum control [19, 20]. Dynamics driven by time-independent Hamiltonians, however, also offers unique insights into the properties of the driving Hamiltonian and the initial state $|\psi^I\rangle$. Such systems are often studied theoretically and experimentally utilizing quantum quenches in which the initial state is an eigenstate of some initial Hamiltonian H_I and the dynamics are driven by a final hamiltonian H_F where the difference between H_I and H_F corresponds to the change of some physical parameter. Quantum quenches have a wide array of applications for theoretical studies of few- and many-body physics. Quenches have been used to probe phase transitions [21–26], explore the orthogonality catastrophe [27–32] and investigate irreversibility, chaos and thermodynamic properties [12, 33]. While these are diverse areas, the same basic mathematical framework can be utilized to describe quench dynamics in all cases. Studying the dynamical response of a system to a sudden quench usually entails calculating the time-evolution of expectation values of observables such as the momentum distribution. However, one can also characterize a quench more broadly, for example through operator-independent (aside from the final Hamiltonian $\hat{H}_F$) quantities such as the diagonal ensemble (DE)

[10, 34] and the closely related experimentally measurable work probability distribution [33, 35–39].

1.1 Time-independent Hamiltonians and quantum quenches

Let us now consider the time-evolution of a state, the DE and the work statistics in some more detail. In the following treatment it is assumed for clarity (and since it corresponds to the cases of interest for my research) that the initial state is pure, but note that it is straightforward to generalize to mixed initial states. The dynamics of the state are then entirely characterized by the eigenbasis of the final Hamiltonian $\{|\psi_j^F\rangle, E_j^F\}$, where E_j^F are the final eigenenergies. Utilizing the overlap coefficients, obtained by projecting the initial state $|\psi^I\rangle$ onto this basis $c_j = \langle\psi_j^F|\psi^I\rangle$, the time-evolution of the quantum state is given by (utilizing natural units where $\hbar = 1$)

$$|\Psi(t)\rangle = \sum_j c_j e^{-iE_j^F}|\psi_j^F\rangle. \tag{1.1}$$

Utilizing this, the time-dependence of the expectation value for an observable $\hat{O}$ can be written as

$$\langle\hat{O}(t)\rangle = \sum_j |c_j|^2\langle\psi_j^F|\hat{O}|\psi_j^F\rangle + \sum_{j\neq k} e^{-i(E_k^F-E_j^F)t}c_j^*c_k\langle\psi_j^F|\hat{O}|\psi_k^F\rangle. \tag{1.2}$$

If the initial state is an eigenstate of the final Hamiltonian the time-evolution is trivial, corresponding to a simple phase shift in time which means that the expectation values of all observables remain unchanged. For an arbitrary initial state, however, interference of states with differently evolving phases complicates the time evolution and can lead to complex dynamics. An immediate consequence of Eq.(1.2) is that the infinite-time average of any observable in a non-degenerate system has zero contributions from the off-diagonal elements in the second term due to their oscillating nature, leaving only the diagonal contribution. For systems with degenerate energy levels, however, some off-diagonal terms will also contribute. The infinite-time average can therefore be written as

$$\langle\bar{\hat{O}}\rangle = \lim_{T\to\infty}\frac{1}{T}\int_0^T dt\langle\hat{O}(t)\rangle = \sum_j |c_j|^2\langle\psi_j^F|\hat{O}|\psi_j^F\rangle + \sum_{E_j=E_k} c_j^*c_k\langle\psi_j^F|\hat{O}|\psi_k^F\rangle. \tag{1.3}$$

which reduces to the first term for non-degenerate systems. This is known as the Extended Diagonal Ensemble (EDE) expectation value for degenerate systems and Diagonal Ensemble (DE) expectation value in non-degenerate systems. I will consider a non-degenerate system for the remainder of this discussion (and most of the thesis).

In a non-degenerate system the long-term average of any observable is described by the DE probabilities $|c_n|^2$. The most fundamental observable of interest for a quench is the work probability distribution defined as $P(W) = \langle\delta(W - (\hat{H}_I - \hat{H}_F)\rangle$. Note that

this contains information about the initial physical properties of the system through $\hat{H}_I$. As the energy is a constant of motion for a time-independent Hamiltonian this value is time-independent and given by the DE ensemble as

$$P(W) = \sum_j |c_j|^2 \delta(W - (E^I - E_j^F)), \tag{1.4}$$

under the assumption that $|\psi^I\rangle$ is an eigenstate of $\hat{H}^I$ with energy E_I. While the DE is more fundamental, the work probability distribution is a characterisation of the quench which takes into account the energy spectrum of the final Hamiltonian and the energy of the initial state and therefore contains further information about the physical process. Particularly, it allows one to connect quench properties with thermodynamic processes [33]. Additionally, the characteristic function of the work probability distribution is given by

$$\begin{aligned}\chi(t) &= \int dW e^{itW} P(W) \\ &= \langle \psi^I | e^{i\hat{H}_F t} e^{-i\hat{H}_I t} | \psi^I \rangle = \sum_j |c_j|^2 e^{i(E_j^F - E^I)t}.\end{aligned} \tag{1.5}$$

This is a measurable quantity in echo-type experiments [36–38] for cold gases, which means that the properties of the work probability distribution can be investigated experimentally in the systems of interest for this thesis. The moments of the work probability distribution are given by

$$\langle W^n \rangle = \int dW P(W) W^n = -\partial_t^n \chi(t)|_{t=0} = \sum_j |c_j|^2 (E_j^F - E_0^I)^n, \tag{1.6}$$

and are often used to quantify the amount of non-equilibrium excitations created during the quench. In particular, the irreversible work given by the difference between the average work $\langle W \rangle$ and the free energy ΔF, i.e. $\langle W_{\text{irr}} \rangle = \langle W \rangle - \Delta F = \langle W \rangle - (E_0^F - E_0^I)$, is often used to give an indication of the irreversibility of the quench process [33, 36, 39]. However, since it is an average of the dynamical excitations, it possesses less information about the nature of the irreversible dynamics than the full work probability distribution and its characteristic function. Similarly, the variance of the work probability distribution is given by $\Delta W^2 = \langle W^2 \rangle - \langle W \rangle^2$ which is of interest in the field of statistical quantum thermodynamics [12, 35, 40] and it has been suggested as a probe of critical behavior [41, 42].

In order to obtain further information about a system, beyond the DE and work statistics, an investigation of the time-dependence of relevant observables which do not commute with $\hat{H}_F$ is required. For such observables the DE contribution is still very important as it determines the infinite-time average, but the off-diagonal elements will determine the actual time-dependence. Depending on the structure of $\langle \psi_j | \hat{O} | \psi_k \rangle$ dephasing might ensure equilibration to the DE value, but in some cases of interest, such as the paradigmatic harmonic oscillator spectrum, perfect periodic revivals of the state prevent equilibration. The time-dependent behavior of observables is closely related

to the question of quantum integrability and chaos [9–12]. For integrable systems the DE can generally be described in terms of a generalised Gibbs Ensemble taking into account a number of locally conserved quantities [9, 11]. For chaotic systems, which are generally expected to obey the Eigenstate Thermalization Hypothesis (ETH), the diagonal ensemble can be shown to be equivalent to the microcanonical ensemble and the off-diagonal time-fluctuations can be shown to be small for large times [10, 12]. Such systems are said to thermalize. Another measure of quantum chaos, which has seen interest in the last 5 years, is operator scrambling [43]. Operator scrambling essentially describes the delocalisation of an operator in Hilbert space over time, after which it can no longer be reconstructed by local measurements. This measure turns out to be interesting, not just for chaotic systems, but for interacting quantum systems in general [44]. After a quench, it seems intuitive that this operator scrambling would be closely related to the non-equilibrium excitations described by the work probability distribution introduced in the previous section. One major topic of this thesis is connecting these two concepts for interacting particles in a harmonic oscillator which is presented in chapter 5.

Another avenue of interest is the dynamical study of phase transitions. Quenching the Hamiltonian parameters across a phase-transition will be reflected in the resulting dynamics. A major topic of this thesis is an investigation of what happens when one drives a quantum system possessing a non-trivial phase-diagram which is initially at rest. Specifically, in chapter 4 I will investigate what happens to strongly interacting bosons in a one-dimensional ring lattice when it is suddenly set in motion with a constant speed. By going to the co-moving frame this problem can be recast as a quench and the framework introduced above can be utilized. Indeed this work is partly inspired by similar investigations that probe superfluid properties of strongly interacting bosons by the sudden rotation of a delta-barrier utilizing the quench framework [45–47].

Chapter 2

Cold atomic gases

In this chapter I will give a brief outline of the field of cold atomic gases - what is experimentally achievable by today and how this can be utilized to engineer the Hamiltonians relevant for my theoretical studies.

2.1 Introduction

Over the last 20 years the field of cold atomic physics has become increasingly important - both with respect to fundamental physics and quantum engineering. This is in large part due to experimental progress that has made the cooling of neutral atoms to sub-μK temperatures and the precise control of such low-energy quantum systems possible. Chief amongst these are Doppler cooling [48], evaporative cooling [49], magneto-optical trapping [50] and purely optical traps [51]. Additionally the exploitation of Feshbach-resonances allows one to tune the s-wave two-body scattering length [52], which completely determines the interaction for low-energy processes. This makes these systems ideal for testing fundamental theories in very clean environments and it is possible to experimentally design systems corresponding to many different Hamiltonians. This allows one to test not just low-energy atomic physics, but also to investigate similarities to quantum phenomena in condensed matter systems [13, 15, 16], nuclear physics [14] and high-energy physics [53]. Since the first experimental realizations of a Bose-Einstein condensate (BEC) in 1995 [54, 55], a state of matter first proposed in 1925 by Bose and Einstein [56], experimental and theoretical progress in the field has exploded. This has lead to the development of a very diverse research area in which many ideas and theories originally proposed long ago, sometimes in other contexts, can finally be experimentally realized. One such example is the Tonks-Girardeau gas, an exactly solvable one-dimensional many-body model consisting of "fermionized" bosons, first proposed in 1960 [57] by Girardeau, which was observed experimentally for the first time in 2004/2005 [58, 59]. Cold atomic systems don't just allow for the experimental observation of old models, however, the high flexibility means that parameter regimes that were of little relevance in traditional fields, such as condensed matter and nuclear physics, can be realized as well, necessitating new developments on the theoretical side.

It turns out that cold atomic gases are also an ideal environment to study few-body physics. One example of that is the first experimental observation of the otherwise illusive three-body Efimov states first predicted in the context of nuclear physics in 1970 [60] by Vitaly Efimov, utilizing three-body recombination measurements of cold atomic gases [61, 62]. This is an example of how the field of cold atoms has lead to theoretical developments, as the three-body recombination became a relevant mechanism for observing the Efimov states, leading to new studies [63]. More recently experimental progress in the realm of few-body physics has made it possible to deterministically create small one-dimensional systems consisting of 2 to 5 particles [64], allowing for direct comparisons between experiment and analytically or numerically exact few-body predictions. Before discussing the specific focus of my research, which is one-dimensional models spanning both few- and many-body physics, I will introduce some of the relevant experimental techniques and fundamental theoretical assumptions for cold atomic gases. This is necessary, as it is these experimental techniques and theoretical simplifications that make cold atomic gases such a versatile tool and therefore suitable systems for investigating fundamental aspects of one-dimensional physics.

2.2 Optical trapping and lattices

In order to do any experiments with cold atomic systems the gases need to be confined in a trap. Additionally the specific shape of the trap determines many properties of the system. Some of the most relevant traps are harmonic potentials, double-wells and periodic lattices, all of which can be engineered by optical trapping [65–67]. The mechanism that underlies optical trapping is relatively straight forward. When an electric field, in this case in the form of an external laser, is applied to a neutral atom, an electric dipole moment is created. The interaction with the electric field in the dipole approximation can be written as [68]

$$U(x,t) = -\mu \mathbf{E}(x,t), \tag{2.1}$$

where μ is the magnetic dipole operator for the atom and $\mathbf{E}(x,t)$ is the electric field of the laser. For an off-resonant laser beam a shift in energy is created, a phenomenon commonly referred to as the AC Stark shift. In this case the dipole-interaction creates a conservative potential described by

$$V(x) = -\frac{1}{2}\alpha(\omega)|\overline{\mathbf{E}(x,t)}|^2, \tag{2.2}$$

where $\alpha(\omega)$ is the second-order contribution to the dipole moment at the laser frequency ω and $\overline{\mathbf{E}(x,t)}$ is the time-averaged electric field. In this way the atom can be trapped and due to the versatility of laser beams, many different trap geometries can be created. The optical lattice is of particular interest and can be achieved by using two counter-propagating laser beams. The electric field components are described by $\mathbf{E}(x,t) = e^{\pm ik_x x}$ and the interference pattern then gives a lattice potential described by

$$V(x) = V_x \cos^2(k_x x). \tag{2.3}$$

So far a one-dimensional spatial system has been assumed in order to ease the discussion. It is easy to generalize for three dimensions, whereby six counter-propagating laser beams are required to make a lattice. In two or three dimensions more complicated lattice structures are also possible, by changing the geometry of the lasers and their relative phases [67, 69]. In this research project, however, I am interested in one-dimensional systems, and since the physical world is three-dimensional by default, for this type of theory to be experimentally relevant the ability to effectively confine a gas to lower dimensions is required. Fortunately it is experimentally possible to freeze out spatial degrees of freedom using optical trapping. A simple example is to use a three-dimensional harmonic oscillator potential

$$V(x,y,z) = \frac{m}{2}(\omega_x^2 x^2 + \omega_\perp[y^2+z^2]), \tag{2.4}$$

where m is the mass of the particles and $\omega_x, \omega_y, \omega_z$ describe the trapping frequencies in the x, y, z directions. Increasing the confinement $\omega_\perp \gg \omega_x$ in the spatial directions y and z such that the energy associated with excitations in the x direction are smaller than the excitation energy required to excite from the ground state to the excited state in the transverse directions allows one to treat the system as effectively one-dimensional along the x-axis. One final advantage of optical trapping as opposed to magnetic trapping is that it allows for independent external magnetic fields which allow for tuning the two-body scattering properties of alkali atoms.

2.3 Two-body physics, scattering lengths and Feshbach resonances

In order to mathematically describe a cold atomic gas a good description of two-body interactions is needed, as these are the dominant interactions in dilute gases. Two-body scattering amounts to shooting one particle into another target particle. This means that all the properties are determined by a potential which depends only on the relative coordinate, $\mathbf{r}$, between the particles. This process can result in different outcomes, depending on the relative kinetic energy and the specific properties of the two-body potential. There is a continuum of scattering states, as well as the possibility of bound states. Neutral atoms interact via the van der Waals interaction, which is short-ranged. For low-energy scattering of bosons or distinguishable particles the process is dominated by s-wave scattering. In this limit the specific shape of the short-range potential is unimportant and the process exhibits a universal, model-independent character (intuitively the wavelength of the particles is too large to discern the details of the short-range potential). Therefore the simplest possible model is chosen for mathematical convenience. This is the zero-range model described by the Dirac-delta-function and all the scattering properties are now contained in one single parameter, the interaction strength g or equivalently the s-wave scattering length a. Mathematically the potential is described by the regularized delta-function in 3D as [70]

$$V(\mathbf{r}) = g_{3D}\delta_{\text{reg}}(\mathbf{r}) = g_{3D}\delta(\mathbf{r})\frac{d}{dr}(r,), \tag{2.5}$$

and the bare delta-function potential in 1D, i.e.

$$V(\mathbf{r}) = g_{1D}\delta(x), \tag{2.6}$$

with interaction strengths given by the parameters g_{3D} and g_{1D}. The relation between the strength, g_{3D}, and the scattering length a of the three-dimensional scattering process is given by

$$g_{3D} = \frac{2\pi\hbar^2 a}{\mu}. \tag{2.7}$$

Here $\mu = m_1 m_2/(m_1 + m_2)$ is the reduced mass of the two particles. In a quasi one-dimensional system a confinement potential similar to that described in the last section (2.2) must be involved. If the confining potential is given as a two-dimensional harmonic trap in the transverse directions, with no trapping potential along the 1D axis of interest, the interaction g_{1D} can be found in terms of a as [71]

$$g_{1D} = \frac{2\hbar^2 a}{\mu a_\perp^2}\left(1 - C\frac{a}{a_\perp}\right)^{-1}. \tag{2.8}$$

Here $a_\perp$ is the size of the single-atom ground state wavefunction in the transverse directions and $C = 1.4603$ is a constant. Note that this allows for a way to manipulate the 1D interaction strength, by changing transverse confinement properties, which is referred to as confinement-induced resonance.

This description of low-energy short-range scattering is equally valid for nuclei interacting via the strong interaction or cold atoms interacting via the van der Waals interaction due to its universal character. One crucial difference between nuclear and cold atomic systems, however, is that while the scattering length of a nuclear two-body interaction is a constant property of the system, the scattering length of neutral alkali atoms is experimentally tunable using the Feshbach resonance technique [52]. This technique utilizes the Zeeman-splitting to change the s-wave scattering length as a function of an applied external magnetic field B. While the underlying mechanism can be quite complicated, almost all experimental data can be fitted to the empirical relation [52]

$$a(B) = a_{bg}\left(1 - \frac{\Delta}{B - B_0}\right), \tag{2.9}$$

where a_{bg} is the background scattering length, B_0 is the resonant magnetic field and Δ is the width of the resonance. This means that the strength of the two-body interaction is a tunable parameter for neutral atoms, allowing for experimental investigations of few- and many-body properties as a function of the scattering length. Successful examples of this are the observations of Efimov states [61, 62] and the BEC-BCS crossover as a function of the scattering length [72, 73].

2.4 Models that can be investigated in cold atomic gases

Utilizing the zero-range interaction, the generic Hamiltonian for a N-particle cold atomic gas is given by

$$H(\mathbf{r}_1, ...\mathbf{r}_N) = \sum_{i=1}^{N} \left[-\frac{\hbar^2}{2m_i} \frac{\partial^2}{\partial \mathbf{r}_i^2} + V_{\text{ext}}(\mathbf{r}_i, t) \right] + \sum_{i<j}^{N} g_{ij} \delta_{\text{reg}}(|\mathbf{r}_i - \mathbf{r}_j|). \tag{2.10}$$

The first term corresponds to the kinetic energy of each particle with mass m_i, the second term can be any arbitrary position and time-dependent external potential, while the last term corresponds to the zero-range two-body interactions with an arbitrary strength g_{ij} for each two-body interaction. In general this remains a very difficult many-body problem, despite the simplification provided by the zero-range interaction. One particular advantage of cold atomic gases, however, is that they allow for the experimental realization of a variety of exactly solvable limits of Eq.(2.10) due to the degree of control obtainable through the ability to manipulate the external potential and the contact interactions. These solvable limits are often of experimental interest and contain interesting physics.

One example of this is the limit of weak two-body interactions for which quantum correlations become negligible. In this regime mean-field theory, which describes the many-body system in terms of an effective one-body theory, is very successful. For bosonic systems mean-field theory leads to the Gross-Pitaevskii equation (also known as the non-linear Schrödinger equation) which describes the macroscopically occupied classical field of a BEC with two-body zero-range interactions [74]. This equation has been extensively studied and many interesting phenomena emerge from its structure, a few examples being dark solitons [75] and quantum vortices [76], both phenomena that have been experimentally observed (see [77] and [78, 79] respectively). In order to understand the quantum nature of microscopic physics, however, models in which such correlations cannot be neglected must be investigated. The majority of these systems are not computationally tractable, but limiting ourselves to those that can be solved exactly - either analytically or numerically - should still yield insight into the nature of quantum correlations and dynamics. Particularly, the quench dynamics introduced in chapter 1 require knowledge of the full set of eigenstates and eigenvalues for the final Hamiltonian in order to be calculated and the investigation of unitary quantum quench dynamics in closed systems is therefore, in principle, dependent on obtaining the exact spectrum. In practice, not all states have a significant contribution to the dynamics for all initial states and exact solutions may therefore only be required for a limited number of eigenstates.

One physical limit of Eq.(2.10) which maintains strong interactions, but simplifies the problem is the limit in which the movement and location of particles are restricted by a tight external potential. Experimentally this can be engineered by imposing a lattice structure through the external potential. For a tight-binding lattice an effective discretization of space can be obtained and correspondingly the system can be

described in a finite-dimensional Hilbert-space as opposed to the continuum problem which is characterized by an infinite-dimensional Hilbert space. The resulting model is generally known as the Hubbard model and depending on the particles it can be either fermioninc or bosonic in character [15, 80]. Hubbard models are characterized by tunneling rates between the different sites corresponding to the kinetic energy term and two-body interaction terms. For short-range interactions, such terms can often be approximated as only having an effect for two particles at the same site. The minimal 2-site Bose-Hubbard model can be solved exactly utilizing the Bethe ansatz [81], while larger systems can be solved numerically utilizing exact diagonalization [82]. By engineering various lattice topologies and interactions a wide variety of interesting condensed matter phenomena can be investigated experimentally such as Mott-insulators and superfluidity [83, 84], frustrated magnetism [85] and topological phases [86]. These types of models, and the closely related spin chain models, are also widely used theoretically in statistical physics, non-equilibrium dynamics and quantum chaos [11, 12] which has made experimental investigations of these phenomena accessible as well [87, 88]. Common to all these areas is that the existence of exact solutions has helped pave the way for new and exciting insights.

A different way to simplify the problem, but one which can be used in conjunction with the discretization, is to consider lower spatial dimensionality. As discussed, it is possible to engineer this in cold gases and in particular effectively one-dimensional systems can be obtained. This offers a considerable simplification of the problem, but also allows for the investigation of physical features unique to 1D systems. Indeed, it is a well-established fact that physical systems behave differently depending on the dimensional degrees of freedom. This includes thermalization and critical behaviors such as phase transitions [89], where even for the simple classical Ising model a non-trivial phase-transition is only present in dimensions higher than one [4]. Lower dimensionality can also have a dramatic effect on the equilibration behaviour, which has been studied for cold quantum gases in recent years [9, 10, 90–92]. Staying in one dimension, a simple way to intuitively understand how dimensionality can affect the dynamics is to consider hard-core particles, where it is clear that unlike in higher dimensional-systems these cannot physically pass each other. The central model which will be under consideration for the majority of this thesis is a one-dimensional quantum gas consisting of N particles with two-body short-range interactions described by the zero-range formalism. The most general Hamiltonian for such a system is given by

$$H(x_1, ...x_N) = \sum_{i=1}^{N} \left[-\frac{\hbar^2}{2m_i} \frac{\partial^2}{\partial x_i^2} + V_{\text{ext}}(x_i, t) \right] + \sum_{i<j}^{N} g_{ij} \delta(|x_i - x_j|). \tag{2.11}$$

For indistinguishable bosons the overall wavefunction has to be symmetric with respect to particle exchange, while it must be anti-symmetric for indistinguishable fermions. Although this model is deceptively simple, it can yield a surprising amount of physical insight and is quite complex for arbitrary interaction strengths, meaning that it is only exactly solvable for relatively small N. In this regime interesting few-body properties can be exactly explored, which might yield insight into problems of a many-body character. For a one-component gas in an arbitrary external potential it is possible to

exactly solve this problem for any N in the case of vanishing interaction strength as this simply corresponds to a free Fermi or Bose-gas, while the Bose-Fermi mapping theorem allows one to solve the bosonic many-body system at infinitely repulsive interaction strength [57]. Another solvable limit is the famous Lieb-Liniger model, which corresponds to $V_{\text{ext}}(x) = 0$ with periodic boundary conditions, but arbitrary interaction strength g, which can be solved using the Bethe ansatz approach [93].

Chapter 3

Models and methods

In this chapter I will outline solution methods of the one-dimensional models studied in this thesis all corresponding to special cases of Eq.(2.11). I will attempt to go from the general to the specific, outlining the areas of broad applicability for each method, before describing specifics relevant to the physics I will investigate in the following chapters. The majority of this chapter outlines basic theoretical and numerical frameworks, while additional (original) analytical and numerical considerations required for my specific projects will be contained in their respective chapters.

The structure of this chapter is as follows. In section 3.1 I introduce the exactly solvable N-body Tonks-Girardeau gas which emerges in the limit of infinitely strong repulsive zero-range interactions [57]. In section 3.2 I look at a different limit in which analytic solutions are available, namely at the simplest non-trivial finitely-interacting system, that of two particles in a harmonic trap [94]. Finally in section 3.3 and 3.4 I consider the more general case of 3-5 finitely interacting (two-component) systems and how such systems can be treated numerically utilizing exact diagonalization approaches. In order to do this I first introduce some background material on second quantization.

3.1 The Bose-Fermi mapping theorem (Tonks-Girardeau gas)

For identical bosons in the regime of infinitely strong zero-range interactions, $g \to \infty$, solving the many-body Schrödinger equation

$$H(x_1, ..., x_N, t)\Psi(x_1, ..., x_N, t) = E\Psi(x_1, ..., x_N, t) \tag{3.1}$$

with H given by Eq.(2.11) reduces to solving for the non-interacting Hamiltonian

$$H(x_1, ..., x_N, t) = \sum_{i=1}^{N} \left[-\frac{\hbar^2}{2m}\frac{\partial^2}{\partial x_i^2} + V_{\text{ext}}(x_i, t) \right], \tag{3.2}$$

with the additional boundary condition

$$\Psi(x_1, ...x_N, t) = 0 \qquad \text{if} \qquad |x_i - x_j| = 0. \tag{3.3}$$

This boundary condition is equivalent to the Pauli exclusion principle in position space, which also forces the wavefunction to be zero when two particles are at the same position. The problem can therefore be mapped onto non-interacting spinless fermions [57] for which the many-body wavefunction can be written as a sum of single-particle product states utilizing the Slater determinant

$$\Psi_F(x_1, ..., x_N, t) = \frac{1}{\sqrt{N!}} \begin{vmatrix} \psi_0(x_1) & \psi_1(x_1) & \cdots & \psi_{N-1}(x_1) \\ \psi_0(x_2) & \psi_1(x_2) & \cdots & \psi_{N-1}(x_2) \\ \vdots & \vdots & \ddots & \vdots \\ \psi_0(x_N) & \psi_1(x_N) & \cdots & \psi_{N-1}(x_N) \end{vmatrix} \tag{3.4}$$

Here $\psi_n(x)$ are the single-particle eigenstates corresponding to Eq.(3.2) with $N = 1$. The Slater determinant is anti-symmetric with respect to particle exchange by construction, while the bosonic wavefunction has to be symmetric. It is possible to obtain a symmetric bosonic wavefunction obeying the same eigenvalue equation by multiplying the Slater determinant with the anti-symmetric unit function. The anti-symmetric unit function is defined by

$$A(x_1, ..., x_N) = \Pi_{1 \leq i < j \leq N} \mathrm{sgn}(x_i - x_j) \tag{3.5}$$

and the bosonic wavefunction is then written as

$$\Psi_B(x_1, ..., x_N, t) = A(x_1, ..., x_N)\Psi_F(x_1, ..., x_N, t). \tag{3.6}$$

One case of particular interest for my work is a Tonks-Girardeau gas confined to a ring geometry of circumference L, corresponding to the ring lattice model I investigate in chapter 4. To model this, one imposes periodic boundary conditions $\Psi_B(..., x_k + L, ..., t) = \Psi(..., x_k, ..., t)$ for all k.

With these constraints on the many-body wavefunction one can evaluate the effect of the anti-symmetric unit function and show that the periodic boundary condition is obtained when the fermionic many-body wavefunction obeys $\Psi_F(..., x_k + L, ...) = (-1)^{N-1}\Psi_F(..., x_k, ...)$. Imposing periodic boundary conditions for the bosonic TG gas therefore imposes periodic boundary conditions (PBC) for odd N and anti-periodic boundary conditions (A-PBC) for even N for the fermionic many-body wavefunction. Due to the orthogonality of the single particle eigenbasis $\{\psi_n(x, t)\}$ the two sums resulting from the Slater determinant are equal if and only if each term in the sum is

$$\psi_n(L, t) = (-1)^{N-1}\psi_n(0, t). \tag{3.7}$$

Therefore the single-particle eigenstates of the Hamiltonian have periodic boundary conditions for odd N and anti-periodic boundary conditions for even N.

This limit of infinitely strong interactions is known as the Tonks-Girardeau limit. The

system is often referred to as the TG gas in the continuum [95] and hard-core bosons [16] in discrete systems. It is one of the few examples of an exactly solvable, strongly-interacting N-body system. However, implicit in the solution method is that in many ways the system behaves like a non-interacting N-body Fermi gas. This generally holds true for density-density correlations, many-body overlaps and diagonal one-body operators in position space such as the single particle density which are all equivalent for the two systems. As such, the interesting physics due to the interplay between the bosonic symmetry and the strongly repulsive interactions are to be found elsewhere. Particularly, the reduced single particle density matrix, for which the off-diagonal terms contain information about the spatial self-correlations and therefore the coherence of the gas, will be very different for the two systems.

3.1.1 Reduced Single Particle Density Matrix and momentum distribution

The reduced single-particle density matrix (RSPDM) is defined by

$$\rho_1(x,y) = N \int \Psi(x,x_2,...x_N)\Psi(y,x_2,...x_N)dx_2...dx_N. \tag{3.8}$$

As mentioned above it measures the spatial self-correlation, giving the probability to find a particle at position y just after finding it at position x. Diagonalising the RSPDM leads to a set of eigenstates $\phi_i(x)$, known as the natural orbitals, with the corresponding eigenvalues λ_i giving the respective occupation numbers

$$\rho_1(x,y) = \sum_i \lambda_i \phi_i^*(x)\phi_i(y), \tag{3.9}$$

where $\sum \lambda_i = N$. For a non-interacting Fermi gas the reduced single particle density matrix is very simple. The natural orbitals are equal to the single-particle wavefunctions $\psi_n(x)$ with occupations $\lambda_1 = ... = \lambda_N = 1$ and $\lambda_{j>N} = 0$. This corresponds to a gas with no coherence. On the other hand, it is expected that the bosonic system has some degree of coherence. For a non-interacting Bose gas at zero temperature $\lambda_0 = N$ with all bosons occupying the ground-state. The presence of interactions will lower this coherence, but it seems unlikely that the system will become completely incoherent like the free Fermi gas. Indeed, inserting the TG many-body wavefunction into Eq.(3.8) the anti-symmetric unit function does not cancel out which means that the RSPDM sees the effect of the symmetrization requirement. Evaluating the full multi-dimensional integral is time-consuming, but fortunately an efficient algorithm to evaluate the RSPDM for the TG wavefunction in terms of one-dimensional integrals exists [96].

Further intuition about the difference between free fermions and the TG-gas can be obtained from the fact that the RSPDM is closely related to the single particle momentum distribution. This also connects the coherence properties of the gas to an experimental observable as the momentum distribution can be measured through time-of-flight experiments [16, 97]. The momentum distribution is given as the Fourier transform of

$\rho_1(x, y)$

$$n(k) = \int dx\, dy \rho_1(x, y) e^{-ik(x-y)}. \tag{3.10}$$

This can be recast in terms of the Fourier transform of the eigenstates of the RSPDM, $\widetilde{\phi}_i(k)$, using the same occupation numbers

$$n(k) = \sum_i \lambda_i \widetilde{\phi_i}^*(k) \widetilde{\phi}_i(k). \tag{3.11}$$

For non-interacting bosons in free space this will generally be described by a delta-peak at $n(k = 0)$ as the particles are entirely delocalised in space, while they are entirely localised in momentum space. Or, to put it differently, the bosons macroscopically occupy the $k = 0$ eigenstate. For non-interacting Fermions in free space, however, the Pauli-exclusion principle ensures that each momentum state beneath the Fermi momentum is equally occupied and the system is delocalised in momentum space. The TG gas, on the other hand will have a peak at $k = 0$, but the presence of interactions broadens the peak so that unlike the perfectly coherent non-interacting bosons, it is not completely localised. In summary the density distribution the TG-gas behaves exactly like free fermions, but the momentum distribution does not. This is because the constraints on the wavefunction in position space correspond to imposing the Pauli exclusion principle in position space, but unlike fermions the Pauli-exclusion principle is not imposed in momentum space.

3.2 Two interacting particles in a harmonic trap

The simplest possible non-trivial example of the one-dimensional model presented in chapter 2.4 is that of two interacting particles. This problem is numerically tractable for an arbitrary external potential and obtaining exact solutions is straightforward using simple finite-difference diagonalisation for an effectively two-dimensional system, corresponding to the two particle coordinates. Further insight, however, can be obtained through analytic solutions. One example of a trap for which an analytic solution is obtainable is the harmonic trap. The relevant Hamiltonian, scaled in terms of the natural oscillator length, is given by

$$\hat{H} = \sum_{n=1}^{2} \left[-\frac{1}{2m} \frac{\partial^2}{\partial x_n^2} + \frac{1}{2} \gamma^2 x_n^2 \right] + V_{\text{int}}(x_2 - x_1), \tag{3.12}$$

where γ is a non-dimensional scaling parameter that determines the width of the trap. This system is separable into a center-of-mass and relative coordinate Hamiltonian

$$\hat{H}_{\text{CM}} = -\frac{1}{2} \frac{\partial^2}{\partial X^2} + \frac{1}{2} \gamma^2 X^2 \tag{3.13}$$

$$\hat{H}_{\text{REL}} = -\frac{1}{2} \frac{\partial^2}{\partial x^2} + \frac{1}{2} \gamma^2 x^2 + V_{\text{int}}(\sqrt{2}x), \tag{3.14}$$

where $X = \frac{x_1+x_2}{\sqrt{2}}$ and $x = \frac{x_2-x_1}{\sqrt{2}}$ are the respective center of mass and relative position coordinates. The full wavefunction is a product of the center-of-mass wavefunction and the relative coordinate wavefunction $\psi(x_1, x_2) = \psi_{\mathrm{CM}}(X)\psi_{\mathrm{REL}}(x)$. Note that this solution can neatly be divided into the fermionic and bosonic symmetry sectors, as the latter forces the relative wavefunction to have even parity, while the former forces it to have odd parity. This is a massive simplification of the problem as it has been reduced to two independent single-particle problems. The center-of-mass Hamiltonian corresponds to the well-known non-interacting harmonic oscillator for which the analytic solution can be found in any quantum mechanics textbook. The solutions to the non-interacting harmonic oscillator (HO) scaled with γ are denoted by the eigenenergies and eigenfunctions $\{E_n, |\psi_n\rangle\}$ in this chapter. The relative Hamiltonian can be diagonalized using finite-difference diagonalization for any arbitrary interaction potential, but in the specific case of the zero-range interaction introduced in chapter 2.3 an analytic form of the eigenfunctions and eigenenergies can be obtained [94]. In this case the strength of the two-body interaction given by 2.6 is determined by g. The eigenfunctions and eigenenergies for a given g is therefore labelled by $\{E_j^g, |\psi_j^g\rangle\}$. Only the even parity eigenfunctions $\psi_{2j}^g(x)$ and eigenenergies E_{2j}^g are affected by the delta-function interactions. Indistinguishable fermions for which the relative part of the wavefunction is odd are therefore unaffected by the delta-function interaction which is a generic feature of the zero-range interaction as the Pauli-exclusion principle ensures that the wavefunction goes to zero whenever two particles are at the same position meaning that they can't see the potential.

There are multiple ways one can proceed to derive analytic expressions for the eigenenergies and eigenfunctions. I will proceed along a particular path which gives a useful representation of the eigenfunctions for the purposes of evaluating canonical operator matrix-elements. Let us first expand the eigenfunctions of $\hat{H}_{\mathrm{REL}}$ in terms of the basis of the non-interacting HO eigenfunctions $\psi_{2j}^g(x) = \sum_n c_{2n}^{2j}\psi_{2n}(x)$. As the interacting wavefunction has even parity it has zero overlap with odd parity HO eigenfunctions and the sum is therefore only given for even values $2n$. Inserting this expression in the eigenvalue equation for the interacting system, leads to

$$\sum_n c_{2n}^{2j}\psi_{2n}(x)\left[-\frac{1}{2}\frac{\partial^2}{\partial x^2} + \frac{1}{2}\gamma^2 x^2\right] + \frac{g}{\sqrt{2}}\delta(x)\psi_{2j}^g(x) = E_{2j}^g \sum_n c_{2n}^{2j}\psi_{2n}(x). \tag{3.15}$$

Next the inner product of this expression with $\langle\psi_{2k}|$ is taken, which in the position-basis is given by an integral. This results in $c_{2k}^{2j}E_{2k} + \frac{g}{\sqrt{2}}\psi_{2k}^*(0)\psi_{2j}^g(0) = c_{2k}^{2j}E_{2j}^g$ and the expansion can therefore be rewritten as

$$\psi_{2j}^g(x) = \frac{g}{\sqrt{2}}\psi_{2j}^g(0)\sum_n \frac{-\psi_{2n}^*(0)}{E_{2n} - E_{2j}^g}\psi_{2n}(x). \tag{3.16}$$

Evaluating this at $x = 0$ the energy quantization is obtained as

$$-\frac{\sqrt{2}}{g} = \sum_n \frac{|\psi_{2n}(0)|^2}{E_{2n} - E_{2j}^g}. \tag{3.17}$$

From the well-known analytic expressions of the harmonic oscillator eigenfunctions this infinite sum can be re-written in terms of Γ functions leading to the following transcendental equation

$$\frac{\Gamma(-\frac{E^g_{2j}}{2}+\frac{3}{4})}{\Gamma(-\frac{E^g_{2j}}{2}+\frac{1}{4})}=-\frac{g}{2}. \tag{3.18}$$

The energy of the $2j$'th state can also be expressed as

$$E^g_{2j}=(2j+\Delta_j)\gamma, \tag{3.19}$$

where $j=0,1,2...$ and Δ_j can be found from Eq.(3.18) and always gives a value $\Delta_j\in[0,1]$. For large j, $\Delta_j\propto j^{-1/2}$ (see [94]). Further manipulating the sums leads to the following expression of the $2j'th$ (even parity) eigenfunction of the interacting system ([98])

$$\psi^g_{2j}(x)=\Omega^g_{2j}\sum_n\frac{\psi^*_{2n}(0)}{E_{2n}-E^g_{2j}}\psi_{2n}(x), \tag{3.20}$$

where the normalization factor is given by

$$\Omega^g_{2j}=\sqrt{\frac{4\Gamma(\frac{3}{4}-E^g_{2j})}{\Gamma(-\epsilon_j)[\tilde{\Gamma}(\frac{3}{4}-E^g_{2j})-\tilde{\Gamma}(\frac{1}{4}-E^g_{2j})]}}. \tag{3.21}$$

Here Γ and $\tilde{\Gamma}$ are the gamma and di-gamma functions respectively. It is also possible to represent the interacting wavefunctions more succinctly using the parabolic cylinder functions [94], but this representation is not relevant in this thesis. In chapter 5 I will utilize the above representation of the wavefunction to derive analytic expressions for 4-point time-dependent correlation functions involving canonical operators.

3.3 Two-component many-body systems and second quantization

Moving from the two-body problem, the natural progression is to solve Eq.(2.11) with finite interactions for 3,4 or 5 particles.

Let us consider two special versions of Eq.(2.11), corresponding to identical particles and to a system with two species of distinguishable particles. These two cases are described by the following Hamiltonians respectively

$$\hat{H}_{1C}(x_1,...,x_N,t)=\sum_{n=1}^{N}\left[-\frac{\hbar^2}{2m}\frac{\partial^2}{\partial x_n^2}+V_{\text{ext}}(x_n,t)\right]+\sum_{i<j}^{N}g\delta(|x_i-x_j|), \tag{3.22}$$

and

$$\hat{H}_{2C}=\hat{H}_A+\hat{H}_B+\hat{H}_{\text{int}}, \tag{3.23}$$

where

$$\hat{H}_A = \sum_{n=1}^{N_A} \left[-\frac{\hbar^2}{2m_A} \frac{\partial^2}{\partial x_n^2} + V_{\text{ext}}(x_n, t) \right] + g_A \sum_{i<j}^{N_A} \delta(|x_i - x_j|), \tag{3.24}$$

$$\hat{H}_B = \sum_{n=1}^{N_B} \left[-\frac{\hbar^2}{2m_B} \frac{\partial^2}{\partial x_n^2} + V_{\text{ext}}(x_n, t) \right] + g_B \sum_{i<j}^{N_B} \delta(|x_i - x_j|), \tag{3.25}$$

$$\hat{H}_{\text{int}} = g_{AB} \sum_{i}^{N_A} \sum_{j}^{N_B} \delta(|x_i - x_j|). \tag{3.26}$$

The first case is essentially a special, simpler case of the second. There are many different ways of approaching such few-body problems. One approach that has seen success for three-dimensional three-body [99] and four-body systems [100] is the use of Jacobi-coordinates and the related hyper-spherical coordinates. These coordinates are also useful for the simpler case of one-dimensional problems [101]. The Jacobi-coordinates often allow for the center-of-mass coordinate to be decoupled from the system leading to a simpler treatment. Utilizing hyper-spherical coordinates the problem can be approximately separated into a hyper-radial and hyper-spherical part and approximate analytic results can be found based on geometrical considerations [102, 103] or utilizing variational approaches [104]. The separation of hyper-radial and hyper-spherical variables allows for a Born-Oppenheimer like approximation known as the adiabatic hyperspherical approximation [105] which can also be useful in one dimension [101]. In the same spirit an impurity in a gas (i.e. $N_A \gg N_B$) can be treated by separating the impurity coordinate from the other particle coordinates and applying a Born-Oppenheimer like approximation to the set of coordinates [102, 106]. A variety of schemes based on variational approaches, utilizing interpolations of known analytic limits have also been proposed [104, 107–109]. Some of these methods can even be extended to medium-sized or bigger systems, although whether or not the approximation breaks down depends to some extent on which parameter regime of the Hamiltonian is considered. For medium-sized systems other techniques exist as well. One proven technique is diffusion Monte Carlo simulations [110, 111]. The density matrix renormalization (DMRG) [112] expressed in terms of matrix product states is another technique which is very powerful for strongly correlated one-dimensional spin-systems on a lattice [113] and extensions to continuous space models have been developed [114].

While these and other methods can be powerful ways of solving the problem, they generally only gives access to the ground-state or a few excited states. In order to investigate the quench dynamics and correlations of interest in this thesis, however, a large number of eigenstates are required. A simple way to approach the few-body problem which gives access to the higher-lying states in the spectrum is simple brute-force diagonalization [115, 116], although it is limited to a small number of particles. One way to diagonalize the many-body problem is writing the wavefunction in terms of the second-quantized field operators and diagonalizing in Fock-space [115] which is the technique I will describe in this section and which has been successfully utilized for a variety of investigations in the recent past [115, 117–121]. An alternative way to

investigate dynamics, but one which is limited to strong interactions, is by mapping few-body systems to interacting spin models which can be done can be done to linear order in the inverse interaction strength [122–127].

In chapter 6 I will introduce an effective Hamiltonian approach which incorporates information about the two-body interactions into the many-body Hamiltonian allowing for more accurate exact diagonalization for larger particle numbers, but in this section an overview of the basic approach to exact diagonalization for the above Hamiltonians in Fock space is given. This method relies on the second quantized picture of the many-body system, which I will give a quick overview of first (more detailed discussions can of course be found in a number of standard textbooks, see for example chapter 2 in [5]).

3.3.1 Second quantization

The basic ingredients of second quantization are the creation and annihilation operators and the many-body Fock basis. The Fock basis is spanned by all possible state kets described by

$$|n_1, n_2, ..., n_k, ...n_M\rangle = |1\rangle^{n_1}|2\rangle^{n_2}...|k\rangle^{n_k}...|M\rangle^{n_M} \tag{3.27}$$

corresponding to the many-body state with n_k particles in the states $|k\rangle$. In order to keep vector representations of a consistent dimension one explicitly denotes $n_k = 0$ if there are zero particles in a state ket of interest. For fermions these numbers can't exceed 1 due to the anti-symmetrization condition, which provides a simple way to keep track of whether we are working with bosons or fermions. This Fock basis is only useful if relevant operators can be expressed in a form that can be simply applied to the Fock basis states. This can be achieved through the creation and annihilation operators defined by

$$\hat{a}_k^\dagger|n_1, n_2, ..., n_k, ...n_M\rangle = \sqrt{n_k + 1}|n_1, n_2, ..., n_k + 1, ...n_M\rangle \tag{3.28}$$

and

$$\hat{a}_k|n_1, n_2, ..., n_k, ...n_M\rangle = \sqrt{n_k}|n_1, n_2, ..., n_k - 1, ...n_M\rangle. \tag{3.29}$$

It is immediately clear why they are named like this as the creation operator $\hat{a}_k^\dagger$ creates a particle in the state $|k\rangle$, while the annihilation operator $\hat{a}_k$ annihilates a particle in the state $|k\rangle$. The Fock states are therefore not eigenstates of these operators. On the other hand, the Fock states are eigenstates of the number operator, defined by $\hat{n}_k = \hat{a}_k^\dagger\hat{a}_k$, wich has an eigenvalue corresponding to the number of particles in the state $|k\rangle$

$$\hat{n}_k|n_1, n_2, ..., n_k, ...n_M\rangle = n_k|n_1, n_2, ..., n_k, ...n_M\rangle. \tag{3.30}$$

For the number-operator to be well-defined when applied to all states (including the vacuum) the creation and annihilation operators must obey the following commutation and anti-commutation relations for bosons and fermions respectively

$$[\hat{a}_i, \hat{a}_j^\dagger] = \delta_{ij} \qquad , \qquad \{\hat{a}_i, \hat{a}_j^\dagger\} = \delta_{ij} \tag{3.31}$$

By applying creation operators successively to the vacuum state $|\Omega\rangle$ one gets the state

$$|n_1, ...n_k, ...n_M\rangle = (\hat{a}_1^\dagger)^{n_1}...(\hat{a}_n^\dagger)^{n_k}....(\hat{a}_M^\dagger)^{n_M}|\Omega\rangle \tag{3.32}$$

So exchanging two particles corresponds to changing the order of two creation operators $\hat{a}_i^\dagger$ and $\hat{a}_j^\dagger$. For bosons these two operators must therefore commute, while they have to anti-commute for fermions and by taking the Hermitian adjoint the same holds true for the annihilation operators

$$[\hat{a}_i, \hat{a}_j] = 0 \qquad , \qquad [\hat{a}_i^\dagger, \hat{a}_j^\dagger] = 0 \tag{3.33}$$

$$\{\hat{a}_i, \hat{a}_j\} = 0 \qquad , \qquad \{\hat{a}_i^\dagger, \hat{a}_j^\dagger\} = 0. \tag{3.34}$$

One of the major advantages of the second quantization approach is that by employing the correct commutation relations, the symmetrization requirement is automatically fulfilled. Note that I have already implicitly assumed a basis in the definition of these operators, namely the Fock basis consisting of all possible numbers of particles in all possible single-particle states (in real problems the Fock basis will be restricted to the relevant particle numbers and states). These operators are therefore implicitly given with respect to the states they create and destroy particles in. It is generally useful to be able to express states and the matrix elements of operators with respect to a different basis set. To do this in the second-quantized formalism one needs to find the transformation between creation/annihilation operators for different sets of states. Consider two single-particle basis sets $\{|\alpha_n\rangle\}, \{|\beta_n\rangle\}$ with creation operators $\hat{a}_{\alpha_n}^\dagger, \hat{a}_{\beta_n}^\dagger$ that creates particles in the states $|\alpha_n\rangle, |\beta_n\rangle$ respectively. The transformation between them can be obtained by inserting a complete set of states as

$$\hat{a}_{\alpha_n}^\dagger|\Omega\rangle = \sum_m |\beta_m\rangle\langle\beta_m|\alpha_n\rangle = \sum_m \hat{a}_{\beta_m}^\dagger|\Omega\rangle\langle\beta_m|\alpha_n\rangle, \tag{3.35}$$

which implies that

$$\hat{a}_{\alpha_n}^\dagger = \sum_m \langle\beta_m|\alpha_n\rangle\hat{a}_{\beta_m}^\dagger, \tag{3.36}$$

and by taking the adjoint one finds

$$\hat{a}_{\alpha_n} = \sum_m \langle\alpha_n|\beta_m\rangle, \hat{a}_{\beta_m} \tag{3.37}$$

where the inner products $\langle\alpha_m|\beta_n\rangle$ describe the transformation operators elements. Note that creation and annihilation operators transform like state-kets and not like typical operators in first-quantized QM. Considering creation and annihilation operators in the position basis leads to the important notion of field operators. In this basis the operators are commonly written as functions of the continuous position coordinate

$$\hat{\psi}(x) = \hat{\psi}_x \qquad , \qquad \hat{\psi}^\dagger(x) = \hat{\psi}_x^\dagger \tag{3.38}$$

where

$$\hat{\psi}^\dagger(x)|\Omega\rangle = |x\rangle. \tag{3.39}$$

Now consider the transformation of this operator to some discrete single-particle basis states $\{|\alpha_n\rangle\}$ with single-particle creation/annihilation operators $\hat{a}^\dagger_{\alpha_n}, \hat{a}_{\alpha_n}$ that correspond to creating or destroying particles in these states. Using Eqs.(3.36,3.37) one finds that

$$\hat{\psi}^\dagger(x) = \sum_n \langle \alpha_n | x \rangle \hat{a}^\dagger_{\alpha_n} = \sum_n \psi^*_{\alpha_n}(x) \hat{a}^\dagger_{\alpha_n} \tag{3.40}$$

$$\hat{\psi}(x) = \sum_n \langle x | \alpha_n \rangle \hat{a}_{\alpha_n} = \sum_n \psi_{\alpha_n}(x) \hat{a}_{\alpha_n} \tag{3.41}$$

which enables a connection between the creation and annihilation operators and the wavefunctions of first quantization. Indeed the creation and annihilation field operators as a function of position can be written as an expansion in a discrete set of basis states $\{|\alpha_n\rangle\}$ with respect to the position basis, where the expansion coefficients correspond to the field operators for creating and annihilating particles in the corresponding basis states. In other words, it is an expansion in terms of states described by single-particle wavefunctions that can easily be obtained using the methods of ordinary single-particle QM, while the action of the single-particle field operators $\hat{a}^\dagger_{\alpha_n}, \hat{a}_{\alpha_n}$ on the Fock-basis is straight-forward. As in the first quantized formalism one is often interested in transforming between the position basis $|x\rangle$ and the momentum basis $|p\rangle$ and this can be achieved by simply replacing the sums with integrals in Eqs.(3.36,3.37):

$$\hat{\psi}(p) = \int dx \langle p | x \rangle \hat{\psi}(x) \qquad , \qquad \hat{\psi}^\dagger(p) = \int dx \langle x | p \rangle \hat{\psi}^\dagger(x). \tag{3.42}$$

One advantage of the second-quantized language is the simple form few-body operators take when expressed in terms of anihilation and creation operators. A sum of one-body operators can be expressed in second quantized form as

$$\hat{K} = \sum_m k_m \hat{a}^\dagger_m \hat{a}_m = \sum_m \langle k_m | \hat{k} | k_m \rangle \hat{a}^\dagger_m \hat{a}_m \tag{3.43}$$

when the underlying single-particle basis set is the eigenstates of $\hat{k}$. No references to particle identification numbers are required in this expression, which is a major advantage of second quantization. It aligns with the intuition that a one-body operator is expressed by counting the number of particles in each eigenstate of that operator and multiplying by their respective eigenvalues. The lack of reference to particle identification numbers means that there is also no reference to the total number of particles in the operator, so evaluating for a specific number of particles N (corresponding to a given physical system) is done by restricting the Fock-space to the subspace corresponding to particle number N. Therefore describing a physical system in second quantization requires a specification of both the operators and the Fock-space on which they work. An operator often has to be represented with respect to a different basis than its single-particle diagonal states and transformations between different underlying basis states is therefore important. The operators are transformed using Eqs.(3.36,3.37) and the usual transformation rule for connecting the matrix-elements between single-particle

basis sets

$$\hat{K} = \sum_m \langle k_m|\hat{k}|k_m\rangle \hat{a}_m^\dagger \hat{a}_m = \sum_{m\mu\nu} \langle \alpha_\mu|k_m\rangle\langle k_m|\hat{k}|k_m\rangle\langle k_m|\beta_\nu\rangle \hat{a}_\mu^\dagger \hat{a}_\nu = \sum_{\mu\nu} \langle \alpha_\mu|\hat{k}|\beta_\nu\rangle \hat{a}_\mu^\dagger \hat{a}_\nu. \tag{3.44}$$

Similarly a sum of two-body operators can be expressed as

$$\hat{V} = \frac{1}{2}\sum_{mn} v_{mn}\hat{a}_m^\dagger \hat{a}_n^\dagger \hat{a}_m \hat{a}_n = \frac{1}{2}\sum_{mn} \langle v_m v_n|\hat{v}|v_m v_n\rangle \hat{a}_m^\dagger \hat{a}_n^\dagger \hat{a}_m \hat{a}_n, \tag{3.45}$$

where v_{mn} are the matrix-elements with respect to an underlying basis that is diagonal with respect to the two-body state $|v_n v_m\rangle$. One can now transform to an arbitrary basis in exactly the same way as for the one-body operator

$$\hat{V} = \frac{1}{2}\sum_{mn}\sum_{\mu\mu'\nu\nu'} \langle v_\mu v_{\mu'}|v_n v_m\rangle\langle v_m v_n|\hat{v}|v_m v_n\rangle\langle v_n v_m|v_\nu v_{\nu'}\rangle \hat{a}_\mu^\dagger \hat{a}_{\mu'}^\dagger \hat{a}_\nu \hat{a}_{\nu'} \tag{3.46}$$

$$= \frac{1}{2}\sum_{\mu\mu'\nu\nu'} \langle v_\mu v_{\mu'}|\hat{v}|v_\nu v_{\nu'}\rangle \hat{a}_\mu^\dagger \hat{a}_{\mu'}^\dagger \hat{a}_\nu \hat{a}_{\nu'}. \tag{3.47}$$

3.3.2 Second quantized Hamiltonians

All necessary ingredients for expressing the Hamiltonian operators of Eqs.(3.22,3.23) in their second quantized form have now been introduced. Using Eq.(3.44) the kinetic energy $\hat{K} = \sum_i k_i$ and the potential energy operators $\hat{U}_{\text{ext}} = \sum_i \hat{V}_{\text{ext},i}$ can be written with respect to the position basis (remembering that sums are now replaced by integrals) as

$$\hat{K} + \hat{U}_{\text{ext}} = \int dx_1 dx_2 \hat{\psi}(x)^\dagger [\langle x_1|\hat{k}|x_2\rangle + \langle x_1|\hat{V}_{\text{ext}}|x_2\rangle]\hat{\psi}(x) \tag{3.48}$$

$$= \int dx_1 dx_2 \hat{\psi}(x_1)^\dagger \left[-\frac{\hbar^2}{2m}\frac{\partial^2}{\partial x_1^2}\delta(x_1 - x_2) + V_{\text{ext}}(x_1)\delta(x_1 - x_2)\right]\hat{\psi}(x_2) \tag{3.49}$$

$$= \int dx \hat{\psi}(x)^\dagger \left[-\frac{\hbar^2}{2m}\frac{\partial^2}{\partial x^2} + V_{\text{ext}}(x)\right]\hat{\psi}(x) \tag{3.50}$$

where I have inserted the position-basis matrix elements of the single-particle Hamiltonian. The most general case of the interaction between two different components A and B is considered next, as the interaction between the same components can be obtained from this result by assuming that the two components are the same. For the two-component case the field operators of the two components are denoted by the subscripts A and B, i.e. $\hat{\psi}_A(x), \hat{\psi}_B(x)$. Writing down the two-body operator corresponding to $\langle x_1 x_2|\hat{v}_{\text{int}}|x_3 x_4\rangle = V(x_1 - x_2)\delta(x_2 - x_3)\delta(x_1 - x_4)$ (a more general case of

the zero-range delta-function of interest) in the position basis results in

$$\hat{V}_{\text{int}} = \frac{1}{2}\int dx_1 dx_2\ dx_3 dx_4 \hat{\psi}_A^\dagger(x_1)\hat{\psi}_B^\dagger(x_2)V(x_1-x_2)\delta(x_2-x_3)\delta(x_1-x_4)\hat{\psi}_A(x_3)\hat{\psi}_B(x_4) \tag{3.51}$$

$$= \frac{1}{2}\int dx_1 dx_2 \hat{\psi}_A^\dagger(x_1)\hat{\psi}_B(x_2)^\dagger V(x_1-x_2)\hat{\psi}_A(x_2)\hat{\psi}_B(x_1). \tag{3.52}$$

The full second quantized Hamiltonian corresponding to the one-component system Eq.(3.22) is therefore given by

$$\hat{H}_{1C} = \int dx \hat{\psi}^\dagger(x)\left(-\frac{\hbar^2}{2m}\frac{\partial^2}{\partial x^2} + V_{ext}(x,t)\right)\hat{\psi}(x) + \frac{1}{2}g\int dx \hat{\psi}^\dagger(x)\hat{\psi}(x)\hat{\psi}^\dagger(x)\hat{\psi}(x) \tag{3.53}$$

while the second quantized Hamiltonian corresponding to the two-component system Eq.(3.23) is given by

$$\hat{H}_{2C} = \hat{H}_A + \hat{H}_B + \hat{H}_{\text{int}}, \tag{3.54}$$

with

$$\hat{H}_A = \int dx \hat{\psi}_A^\dagger(x)\left(-\frac{\hbar^2}{2m_A}\frac{\partial^2}{\partial x^2} + V_{ext}(x,t)\right)\hat{\psi}_A(x) + \frac{1}{2}g_A\int dx \hat{\psi}_A^\dagger(x)\hat{\psi}_A(x)\hat{\psi}_A^\dagger(x)\hat{\psi}_A(x) \tag{3.55}$$

$$\hat{H}_B = \int dx \hat{\psi}_B^\dagger(x)\left(-\frac{\hbar^2}{2m_B}\frac{\partial^2}{\partial x^2} + V_{ext}(x,t)\right)\hat{\psi}_B(x) + \frac{1}{2}g_B\int dx \hat{\psi}_B^\dagger(x)\hat{\psi}_B(x)\hat{\psi}_B^\dagger(x)\hat{\psi}_B(x) \tag{3.56}$$

$$\hat{H}_{int} = \frac{1}{2}g_{AB}\int dx \hat{\psi}_A^\dagger(x)\hat{\psi}_B(x)^\dagger\hat{\psi}_A(x)\hat{\psi}_B(x) \tag{3.57}$$

3.4 Exact Diagonalization

In this section I will describe the theoretical background of the Exact Diagonalization (ED) scheme, as well as how to obtain the expectation values of relevant observables.

3.4.1 Mode Expansion and resulting Hamiltonians

The general idea utilized by the ED scheme is that the generic field operator $\hat{\Psi}(x,t)$ can be expressed exactly as a linear combination of basis states as in Eq.(3.41) using any complete basis for the corresponding Hilbert space. This allows for the problem to be expressed in terms of first-quantized eigenfunctions for the Hilbert space and annihilation and creation operators for the resulting Fock space. A natural choice of basis are the energy eigenfunctions $\psi_n(x)$ of the non-interacting single-particle (SP) Hamiltonian, corresponding to the many-body Hamiltonian of interest. In this case the eventual second-quantized Hamiltonian takes on a particularly simple form. The

expansion for the one-component case is given by

$$\hat{\Psi}(x,t) = \sum_{n=1}^{M} \hat{a}_n \psi_n(x), \tag{3.58}$$

where the expansion coefficients $\hat{a}_n^\dagger, \hat{a}_n$ now correspond to the creation and annihilation operators for particles in the eigenstate $\psi_n(x)$ and M is the number of energy modes (energy eigenstates) in the expansion. The expansion is only exact when the number of modes is infinite, but for the ground and lower-lying states of a given system the sum generally converges for a finite number of modes. A low temperature quantum gas will generally be filled up from the lowest energy levels and so we can improve the accuracy of the results simply by including more modes in the order determined by their energies (note that filling from the lowest Fock-state energies rather than the lowest SP mode energies is actually more logical [128], see chapter 6 for a brief discussion). The numerical feasibility of ED relies on the fact that a limited number of modes can describe the gas accurately. A numerical investigation of convergence as the number of modes is increased is therefore necessary to justify the use of the method for any particular problem. The two-component system is very similar to the one-component system, one just expands the many-body field operators for both components in the basis corresponding to their respective non-interacting single-particle Hamiltonians $H_{sp}^{A,B}$

$$\hat{\Psi}_A(x,t) = \sum_{n=1}^{M_A} \hat{a}_n \psi_n^A(x), \tag{3.59}$$

$$\hat{\Psi}_B(x,t) = \sum_{n=1}^{M_B} \hat{b}_n \psi_n^B(x). \tag{3.60}$$

Here $\hat{a}_n^\dagger, \hat{a}_n$ and $\hat{b}_n^\dagger, \hat{b}_n$ are the creation and annihilation operators for particles A and B in the energy state $\psi_n^{A,B}$ while M_A and M_B are the number of energy modes in the sum. By inserting Eq.(3.58) into Eq.(3.53), one gets the following form of the Hamiltonian for the one-component case

$$H_{1C} = \sum_{k,l} \hat{a}_k^\dagger \hat{a}_l H_{kl} + \frac{1}{2} \sum_{klmn} \hat{a}_k^\dagger \hat{a}_l^\dagger \hat{a}_m \hat{a}_n V_{klmn}, \tag{3.61}$$

where

$$H_{kl} = \int dx \phi_k^*(x) H_{sp} \phi_l(x), \tag{3.62}$$

$$V_{klmn} = g \int dx \phi_k^*(x) \phi_l^*(x) \phi_m(x) \phi_n(x). \tag{3.63}$$

The two-component Hamiltonian is obtained in exactly the same way, by inserting the two expansions into Eq.(3.54).

$$H_A = \sum_{k,l} \hat{a}_k^\dagger \hat{a}_l H_{kl}^A + \frac{1}{2} \sum_{klmn} \hat{a}_k^\dagger \hat{a}_l^\dagger \hat{a}_m \hat{a}_n V_{klmn}^A, \tag{3.64}$$

$$H_B = \sum_{k,l} \hat{b}_k^\dagger \hat{b}_l H_{kl}^B + \frac{1}{2} \sum_{klmn} \hat{b}_k^\dagger \hat{b}_l^\dagger \hat{b}_m \hat{b}_n V_{klmn}^B, \tag{3.65}$$

$$H_{int} = \sum_{klmn} \hat{a}_k^\dagger \hat{b}_l^\dagger \hat{b}_m \hat{a}_n V_{klmn}^{AB}, \tag{3.66}$$

where

$$H_{kl}^{A,B} = \int dx \phi_k^{*A,B}(x) H_{sp} \phi_l(x), \tag{3.67}$$

$$V_{klmn}^{A,B} = g_{A,B} \int dx \phi_k^{*A,B}(x) \phi_l^{*A,B}(x) \phi_m^{A,B}(x) \phi_n^{A,B}(x), \tag{3.68}$$

$$V_{klmn}^{AB} = g_{AB} \int dx \phi_k^{*A}(x) \phi_l^{*B}(x) \phi_m^{A}(x) \phi_n^{B}(x). \tag{3.69}$$

For the one-component case the Fock space consists of all possible states with the number of modes M and total number of particles N. The Hilbert space has a dimension of

$$D_{1C} = \frac{(N+M-1)!}{N!(M-1)!}. \tag{3.70}$$

The Fock-space of the two-component case is given as the Kronecker product of two sub-spaces corresponding to the one-component Fock-space with all possible states M_A (M_B) and a total number of particles N_A (N_B). The total dimension is then given by

$$D_{2C} = \frac{(N_A+M_A-1)!}{N_A!(M_A-1)!} \frac{(N_B+M_B-1)!}{N_B!(M_B-1)!}. \tag{3.71}$$

A more detailed discussion of the Fock-bases is contained in the next section when I consider how to numerically represent them. To implement the numerical diagonalization one finds the matrix representation of the Hamiltonians with respect to their respective Fock-basis, i.e.

$$H_{1C}^{\mu\nu} = \langle F_\mu | H_{1C} | F_\nu \rangle \tag{3.72}$$

and diagonalizes the resulting matrix. This leads to obtaining eigenstates $|\psi_n\rangle$ of the Hamiltonian with respect to the Fock basis

$$|\psi_n\rangle = \sum_\mu^D \langle F_\mu | \psi_n \rangle | F_\mu \rangle = \sum_\mu^D c_\mu^n | F_\mu \rangle. \tag{3.73}$$

3.4.2 Building the Fock-space Hamiltonian

In this section I will briefly outline how to implement the ED algorithm in practice. In order to implement the ED scheme, a numerical representation of the relevant Fock-

basis corresponding to N particles and M modes is needed. These can be represented by vectors with each entry corresponding to a specific mode and the value of each entry corresponding to the number of particles in that mode. So for example for $N = M = 3$ one possible vector is $(2, 1, 0)$. The general Fock-vector for an arbitrary state is then given by $F_\mu = (n_1^\mu, ..., n_M^\mu)$ with the number of particles $\sum_k n_k^\mu = N$. Generating these vectors efficiently is a standard problem and algorithms can be found in the literature [82]. Essentially one can define a total ordering of these states which allows for generating all the basis vectors using a simple algorithm. Additionally a unique number T_μ can be calculated based on each Fock-vector utilizing the formula $T_\mu = \sum_{k=1}^{M} \sqrt{100 \cdot k + 3} n_k^\mu$. This is important for the efficient evaluation of matrix elements, both for the Hamiltonian and other operators. The naive way to build the Hamiltonian is by explicitly calculating all the matrix elements using two `For`-loops over the dimension of the Hilbert space. The vast majority of the matrix-elements are zero, however, and this method is going to be very inefficient as the dimensionality of the Hilbert space grows. A smarter way of calculating the matrix elements is to consider the action of the Hamiltonian operator on each Fock-state and exploit the orthogonality of the Fock states. Due to the orthogonality the inner product between the resulting state after the Hamiltonian has been applied and an arbitrary Fock-state will only give non-zero results when they coincide. Each Fock-state can be given a unique tag as described above which allows for an efficient search algorithm to locate the relevant Fock-states that the Hamiltonian connects a given Fock-state to. This means that the matrix elements of the Hamltonian can be found by doing a single `For`-loop over the dimension of the Hilbert-space. Consider the Hamiltonian given by Eq.(3.61). This Hamiltonian has the one-body term given by

$$\sum_{k,l} \hat{a}_k^\dagger \hat{a}_l H_{kl} |n_1, ..., n_M\rangle. \tag{3.74}$$

In general this will only give a non-zero value whenever $n_l \neq 0$. Numerically one can therefore simply check the indices l for which $n_l \neq 0$ and the sum is than evaluated numerically by looping over those indices and a loop over the full set of k (this runs to M). In this case one obtains

$$\sum_{k,l|n_l \neq 0} \sqrt{n_k + 1} \sqrt{n_l} H_{kl} |n_1, ...n_l - 1, ..., n_k + 1, ...n_M\rangle. \tag{3.75}$$

It is important to remember that k and l can coincide in this sum. The square roots can be obtained by simply taking the square roots of the k'th or l'th values of the basis vector, but if k and l coincide one has to use the updated basis vector when extracting the k'th value. It therefore makes sense to define a temporary basis vector that can be manipulated as this allows general code, which is particularly useful when considering the two-body interaction terms. The tag of the new basis-vector after the application of each term is easily calculated and the values can be paired with the corresponding matrix elements $H_{\mu\nu}$. Using the eigenbasis of the single-particle part simplifies the problem considerably, as these diagonalize the single-particle Hamiltonian and $H_{kl} \neq 0$ only when $k = l$. A single loop over the number of modes M is therefore sufficient.

For the interaction-part (two-body term) things are slightly more complicated, but one proceeds along the same lines

$$\sum_{klmn} \hat{a}_k^\dagger \hat{a}_l^\dagger \hat{a}_m \hat{a}_n V_{klmn} |n_1, ..., n_M\rangle = \\ \sum_{klmn} \sqrt{n_k + 1}\sqrt{n_l + 1}\sqrt{n_m}\sqrt{n_n} V_{klmn} |n_1, ..., n_n - 1, ..., n_m - 1, ..., n_l + 1, ..., n_l + 1, ..., n_M\rangle. \tag{3.76}$$

Whenever $m \neq n$ this gives non-zero value only if $n_n, n_m \neq 0$. For $m = n$ on the other hand non-zero values are only obtained when $n_m > 1$. In practice I find all the operator combinations fulfilling these conditions and then generate a list of indices that contain all possible unique combinations of the other operators, while keeping the relevant operators constant. A `For`-loop over this list evaluating the matrix elements using a temporary basis as described above is then implemented. Duplicate elements (k and l, as well as m and n are interchangeable) are accounted for in this loop.

Building the two-component matrix is essentially the same. A Fock-basis is defined for each component and the full basis is then given by their Kronecker product. Unique numbers can still be calculated for each basis vector in the final basis. The Hamiltonian matrix elements can then be evaluated similarly to the one-component case, keeping track of which operators affect which component.

3.4.3 Some important observables within the ED approach

I have now shown how to obtain eigenstates of the second-quantized Hamiltonian in Fock-space. For quenches time-evolution can be straightforwardly implemented by diagonalizing the initial and final Hamiltonian in the same Fock-space and utilizing the formalism laid out in chapter 1. In this section I will take a closer look at the general structure of the eigenstates and how to obtain the expectation values of relevant observables utilizing these states. A generic quantum state can be expressed in terms of the eigenstates of the final Hamiltonian which can in turn be expressed in the Fock basis. An arbitrary state $|\psi\rangle$ is therefore given (utilizing Eq.(3.73)) by

$$|\psi\rangle = \sum_n^D \langle\psi|\psi_N\rangle|\psi_n\rangle = \sum_n^D \sum_\mu^D b_n c_\mu^n |F_\mu\rangle \tag{3.77}$$

In a quench the coefficients b_n would be time-dependent, but in order to ease the notation we just consider a generic, time-independent state. The time-evolution at any time t can be found using the exact same formulas. A fundamental quantity of importance are many-body correlations and the simplest such correlation is the one-body density matrix. I already discussed this quantity for the TG gas. In the language of second quantization the definition of the one-body density matrix is $\hat{\rho}_1(x, y) = \hat{\psi}^\dagger(x)\hat{\psi}(y)$ that is it is the field-field correlation at points x, y. The expectation value

of the one-body density matrix with respect to a given quantum state is given by

$$\langle\psi|\hat{\rho}_1(x,y)|\psi\rangle = \sum_{nm} b_n^* b_m \langle\psi_n|\hat{\rho}_1(x,y)|\psi_m\rangle \tag{3.78}$$

$$= \sum_{n,m}^{D} b_n^* b_m \sum_{\mu,\nu}^{D} \sum_{k,l}^{M} \phi_k^*(x)\phi_l(y)(c_\mu^n)^* c_\nu^m \langle F_\mu|\hat{a}_k^\dagger \hat{a}_l|F_\nu\rangle. \tag{3.79}$$

This means that one needs to consider the Fock-space matrix elements $\langle F_\mu|\hat{a}_n^\dagger \hat{a}_m|F_\nu\rangle$ of which a large number is zero. In fact, rather than using this sum directly it is more efficient to apply the density-matrix operator to the ket first and utilizing the same tricks as when building the Hamiltonian one only needs to evaluate its overlap for non-zero elements in the sum. Similarly one can define the two-body density-density correlations at points x,y as $\hat{\rho}_2(x,y) = \hat{\psi}^\dagger(x)\hat{\psi}^\dagger(y)\hat{\psi}(x)\hat{\psi}(y)$, for which the expectation value is given by

$$\langle\psi|\hat{\rho}_2(x,y)|\psi\rangle = \sum_{nm} b_n^* b_m \langle\psi_n|\hat{\rho}_2(x,y)|\psi_m\rangle \tag{3.80}$$

$$= \sum_{nm} b_n^* b_m \sum_{\mu,\nu}^{D} \sum_{k',l',k,l}^{M} \phi_{k'}^*(x)\phi_{l'}^*(y)\phi_k(x)\phi_l(x)(c_\mu^n)^* c_\nu^m \langle F_\mu|\hat{a}_{k'}^\dagger \hat{a}_{l'}^\dagger \hat{a}_k \hat{a}_l|F_\nu\rangle. \tag{3.81}$$

The evaluation of these quantities can take a lot of computational time and as they must be computed separately at every specific instant in time. It is one of the main bottlenecks time-wise in the evaluation of quench dynamics. The single particle density and the momentum distribution can be calculated much faster as the former simply corresponds to Eq.(3.79) with $x = y$, while the latter has the exact same structure, but with the momentum-space wavefunctions. The expectation value of any quantity which can be described in terms of the creation and annihilation operators are found the same way in the one- and two-component systems, one just needs to keep track of which operators corresponds to which type of particles. An alternative way to deal with the two-component system is by considering the reduced density matrices ρ_A and ρ_B rather than the full states $|\psi\rangle$. In this case one has to compute the matrix representation for operators of interest within the reduced fock space corresponding to A or B after which the trace of a simple matrix multiplication gives the desired expectation value. This is not a particular simplification, however, as the computation of the relevant matrix operator requires one to evaluate the same matrix elements considered above, such as $\langle F_\mu|\hat{a}_n^\dagger \hat{a}_m^\dagger \hat{a}_k \hat{a}_l|F_\nu\rangle$. In the case of the two-component system there are some additional quantities that are of interest, however. The reduced density matrices of the subsystems are themselves interesting and contain information about the mixedness of the subsystems for example.

Part II

Specific projects

In this second part of the thesis, I will present the results of various projects I have conducted throughout my PhD. First I will discuss strongly-interacting bosons in a lattice in chapter 4. This is solved using the Bose-Fermi mapping theorem introduced in chapter 3. In chapter 5 I will discuss information scrambling after a quench, utilizing the analytic solutions for two interacting particles in a trap introduced in chapter 3. In chapter 6 I will introduce an improved version of the ED scheme discussed in chapter 3, utilizing the effective Hamiltonian approach along with some early results of a project utilizing this method. Finally, chapter 7. contains an exposition of my work on nonlinear optomechanics and is an example of dynamics in an open quantum system.

Chapter 4

"Static and dynamic phases of a Tonks-Girardeau gas in an optical lattice" (originally published as [1])

4.1 Introduction

This project investigates the phases of strongly-interacting bosons in a continuum lattice and the non-equilibrium dynamics induced by a sudden rotation of the lattice. Within the framework of this thesis this represents an investigation of quench dynamics in a many-body system for which exact solutions exist and therefore complements the few-boy studies in the rest of the thesis. Particularly it showcases how quench dynamics can be used to probe many-body phases and how such many-body phases can result in interesting quench dynamics which can help further our understanding of the physics involved.

The motivation for studying this particular model is two-fold. It displays interesting many-body phases with a quantum phase transition [129] and it can be solved exactly utilizing the Bose-Fermi mapping theorem. Some investigations related to this model include [25, 130–133]. In the limit of strong interactions (the TG-gas) two distinct phases are known to exist which appear as a function of the ratio of number of bosons N to lattice sites M, $F = \frac{N}{M}$.

For incommensurate fillings ($F \neq \mathcal{N}$, with $\mathcal{N}$ a positive integer) in shallow lattices the system has superfluid-like characteristics with long-range coherence and good conductivity due to the delocalisation of the wavefunction over many lattice sites. However for commensurate filling ($F = \mathcal{N}$), the bosons become localised at individual lattice sites and the total system becomes *pinned* to the lattice. This pinned phase has no coherence, behaves as an insulator and is the hard-core continuum analogue of the Mott-insulator phase in the Bose-Hubbard model (BHM). In the continuum TG model the pinning happens at infinitesimally small lattice depths for $F = 1$. It was first theoretically proposed by Büchler *et al.* [129] and has been experimentally observed in

cold atom experiments [134, 135].

4.2 Publication

Mathias Mikkelsen, Thomás Fogarty and Thomas Busch, *Static and dynamic phases of a Tonks–Girardeau gas in an optical lattice*, New Journal of Physics, **20** 113011, 2018 [1].

4.3 Conclusion

In [1] I investigated the full phase-diagram as a function of the lattice depth and the filling ratio. Some attempts at investigating what happens for intermediate lattice depths had been undertaken previously, particularly it was suggested that intermediate lattice depths could be utilized to study the mechanism of defect-induced superfluidity [133]. In my work I did a systematic description in terms of the coherence and momentum distribution of the gas which helped elucidate the phase diagram. There are no phase-transitions outside the commensurate-incommensurate transition in shallow lattices, but as the lattice depth is increased a continuous crossover between the superfluid and a supersolid-like phase is observed for incommensurate particle numbers. Similarly, if the lattice depth is kept at a constant intermediate lattice depth, a continuous crossover from this supersolid-like phase for incommensurate particles numbers to the pinned phase for commensurate particle numbers is observed as a function of the filling ratio. The phases are well-characterized by their momentum distributions and auto-correlation functions. These quantities reveal the interplay between the external lattice breaking continuous spatial symmetry, imposing discrete spatial symmetry and the long-range order still present for incommensurate particle numbers.

The dynamics of Tonks-Girardeau gases, such as equilibration properties have seen extensive interest as well [25, 96, 131, 136–138] as the dynamical problem can be solved utilizing the Bose-Fermi mapping theorem as well. In the second part of our investigation I probed the phase-diagram by a sudden rotation. An optical lattice that is suddenly set in motion can be re-cast as a quench in terms of the solutions in the co-moving frame, similar to the solution for a delta-barrier suddenly set in motion, outlined in [45–47]. The dynamical properties of the coherence and momentum distribution contain information about the many-body phases, while the average momentum succinctly captures the amount of transport in the system. In the superfluid phase the particles don't react to the lattice moving through them, as they simply tunnel through the barriers. In the pinned phase, however, the transport becomes maximal (equal to the movement speed of the lattice) as the particles are pinned to the lattice sites and moved along with it. For deeper lattices maximal transport is also obtained in the incommensurate phase despite the existence of superfluid defects. However, an investigation of the momentum distribution reveals the microscopic origin of this transport to be different to that of the insulating phase.

The most interesting dynamical behaviour happens as the lattice is driven in the critical

region of the commensurate-incommensurate transition. Here the critical fluctuations manifest dynamically in the gas oscillating between a pinned and superfluid phase and hence between all particles moving together and standing still. This is very similar to the stick-slip behaviour observed in the classical Frenkel-Kontorova model of friction when driven close to commensurability [139].

Since the publication of this paper, some related works have come out. My co-authors Thomás Fogarty and Thomas Busch recently investigated a quantum heat engine utilizing cycles between the superfluid and pinned phase [140]. The existence of an energy gap between the phases and many-body cooperative effects leads to improved performance compared to a similar single-particle cycle. The characterization of many-body phases was an integral part of our project and quite recently a new simple algorithm for calculating the spectral function of a TG gas was developed and used to investigate the phases of a TG-gas in a lattice [141] as well. We are also considering some extensions of the ideas presented in the paper, for example a dynamic study of a disordered lattice which can be realized in the arbitrary Kronig-Penney model [142].

Chapter 5

Connecting information scrambling and work statistics for a harmonic trap

The response of quantum systems to sudden quenches in the Hamiltonian has been a topic of intense research interest in recent years as explained in chapter 1. In that chapter I introduced the diagonal ensemble (DE) [10, 34] and the closely related work probability distribution [33, 35–39] as a way to characterize the properties of a quench. These quantities essentially characterize the delocalisation of the initial state in the Hilbert space defined by the eigenstates of the final Hamiltonian and a natural extension of this characterization is to further investigate Hilbert-space delocalisation dynamics. This is often referred to as scrambling in the literature [43, 44] - the idea being that over time the initial state can no longer be reconstructed from local measurements.

One particular measure of scrambling - the squared commutator [43] and the closely related out-of-time-order correlation functions (OTOCs) have recently become the focus of intense research as a measure of information scrambling in quantum systems after it was proposed that they could be utilized as measures of quantum chaos [143–145]. Since this initial proposal, the squared commutator has also been shown to be a powerful tool for studying information scrambling in non-chaotic systems, for example near quantum critical points [146–148], in the presence of many-body entanglement and coherence [149, 150], and in quantum thermodynamics [151, 152].

In this chapter I will show that the squared commutator is a useful measure for characterizing different types of quantum quenches utilizing the paradigmatic cold atomic model of two interacting particles in a 1D harmonic trap. The focus of research into OTOCs so far has been limited to single-particle continuum models that are known to be chaotic in the semi-classical limit such as the quantum kicked rotor [144] and many-body lattice models in which interactions are expected to introduce information scrambling [43, 149] so this work is also a first step in considering such quantities in interacting continuum models. Finding a connection between information scrambling and other measures of irreversibility is important for connecting the abstract notion

of Hilbert space scrambling with physical measureables. While progress towards such an understanding has recently been made in chaotic systems [151, 153–155], the main result of this chapter is to connect the scrambling and work statistics for quenches in a non-chaotic system. Specifically I will connect the squared commutator with the diagonal ensemble and the work statistics describing the quench. At the same time I will elucidate the additional insights gained from the scrambling as opposed to the work statistics alone. Additionally measuring the OTOCs in a continuum system is exceedingly difficult as it requires a reversal of the time-evolution and connecting with the experimentally accessible work probability distribution is therefore important for practical reasons as well.

5.1 Basic definitions and characterizing the quantum quench

The most important and basic characterization of the quench is determined by the overlap of the initial state $|\psi_I\rangle$ with the eigenstates of the final Hamiltonian $|\psi_n^F\rangle$, $c_n = \langle\psi_n^F|\psi^I\rangle$. It is these overlap coefficients (in conjunction with the final Hamiltonian) that determine dynamical behavior as well as static quantities. Derived quantities such as the work probability distribution and its characteristic function were defined and discussed in chapter 1. As a reminder, these are defined in terms of the diagonal ensemble (DE) probabilities $|c_n|^2$ as

$$P(W) = \sum_n |c_n|^2 \delta(W - (E_n^F - E^I)), \tag{5.1}$$

and

$$\chi(t) = \int dW e^{itW} P(W) = \langle\psi^I|e^{i\hat{H}_F t} e^{-i\hat{H}_I t}|\psi^I\rangle = \sum_n |c_n|^2 e^{i(E_n^F - E^I)t}, \tag{5.2}$$

where W is the work, E^I the energy of the initial state and E_n^F the energy of the n'th state of the final Hamiltonian. As explained in chapter 1, the moments of this distribution can be used to characterize the irreversibility of the quench. However, in order to fully understand quench dynamics, one generally looks at some time-dependent dynamical quantities to understand the physical significance of the distribution. One measure of dynamical irreversibility is the survival probability $L(t) = |\chi(t)|^2$, which measures how much the quenched quantum state differs from the initial state over time. However, two quantum states being orthogonal doesn't necessarily tell us that they are significantly different since observables for the two states can be comparable. In addition, for finite systems the survival probability will simply oscillate around an average value and its long term behavior generally fails to characterize the irreversible dynamics in a meaningful way. The average value of the survival probability can be calculated as [156]

$$\bar{L} = \langle L(t)\rangle = \sum_n |c_n|^4, \tag{5.3}$$

which is also known as the inverse participation ratio. This quantity will be smaller if more states participate in the dynamics and it is therefore of interest for characterizing the delocalization in Hilbert space, but it contains no information about how the dynamics actually evolve in time. Additionally, both it and the survival probability can be almost identical for very different work probability distributions as the inverse participation ratio simply measures how far the system is from being described by one quantum state.

In order to overcome the drawbacks of these traditional measures I therefore propose to investigate an operator-related quantity to understand the irreversibility and delocalisation dynamics of the quench process, namely the expectation value of the squared commutator of two operators $\hat{A}$ and $\hat{B}$

$$C_{AB}(t) = \langle [\hat{A}(t), \hat{B}]^2 \rangle. \tag{5.4}$$

As mentioned in the beginning of this chapter, this quantity has been suggested as a good measure of information scrambling in quantum systems. It probes the delocalisation of the Heisenberg operator $\hat{A}(t)$ utilizing the operator $\hat{B}$. The larger $C_{AB}(t)$, the more the information about the initial value of $\hat{A}$ is spread in Hilbert-space and therefore the less accessible it is by local measurements. This process is commonly referred to as operator scrambling, and we expect that a more irreversible quench should introduce more operator scrambling. The squared commutator can be re-written in terms of time-dependent correlation functions as

$$C_{AB}(t) = D_{AB}(t) + I_{AB}(t) - 2\mathrm{Re}[F_{AB}(t)] \tag{5.5}$$

with

$$D_{AB}(t) = \langle \hat{B}^\dagger \hat{A}^\dagger(t) \hat{A}(t) \hat{B} \rangle \tag{5.6}$$

$$I_{AB}(t) = \langle \hat{A}^\dagger(t) \hat{B}^\dagger \hat{B} \hat{A}(t) \rangle \tag{5.7}$$

$$F_{AB}(t) = \langle \hat{A}^\dagger(t) \hat{B}^\dagger \hat{A}(t) \hat{B} \rangle. \tag{5.8}$$

Most work so far has focused on the 4-point out-of-time-ordered correlation function (4-OTOC) $F_{AB}(t)$ as $D_{AB}(t)$ is time-ordered and $I_{AB}(t) = \langle \hat{A}^\dagger \hat{B}^\dagger(-t) \hat{B}(-t) \hat{A} \rangle$ is anti-time-ordered for an eigenstate of the Hamiltonian. However, as was pointed out in [153] for initial non-eigenstates, a prominent physical example of which is quenched systems, $I_{AB}(t)$ is also an out-of-time-ordered correlation function, namely a 3-point out-of-time-ordered correlation function (3-OTOC). It was also shown that under certain circumstances $I_{AB}(t)$ is the most important contribution to the squared commutator. This is of interest as $I_{AB}(t)$ can readily be interpreted as a time-reversal test, i.e. it corresponds to taking the expectation value of $\hat{B}^\dagger \hat{B}$ with the quantum-state $e^{i\hat{H}t} \hat{A} e^{-i\hat{H}t} |\psi\rangle$ which measures how much the time-reversal symmetry is broken by the application of the operator $\hat{A}$. $F_{AB}(t)$ also involves a time-reversal, but it is more complicated and does not have the same physical interpretation in terms of a simple time-reversal protocol. For a generic initial state $|\psi^I\rangle$ the expectation values can be

explicitly written in terms of the overlap coefficients $c_n = \langle \psi_n^F | \psi^I \rangle$ as

$$D_{AB}(t) = \sum_{j,k,n,m} c_j^* c_k e^{-i(E_{mn})t} B_{jn}^\dagger \langle \hat{A}^\dagger \hat{A} \rangle_{nm} B_{mk}, \tag{5.9}$$

$$I_{AB}(t) = \sum_{j,k,n,m} c_j^* c_k e^{-i(E_{kj}+E_{nm})t} A_{jn}^\dagger \langle \hat{B}^\dagger \hat{B} \rangle_{nm} A_{mk}, \tag{5.10}$$

$$F_{AB}(t) = \sum_{j,k,n,m} c_j^* b_k e^{-i(E_{kj}+E_{nm})t} A_{jn}^\dagger B_{nm}^\dagger A_{mk}, \tag{5.11}$$

where $b_j = \langle \psi_j | \hat{B} | \psi^I \rangle$, $A_{mk} = \langle \psi_m | \hat{A} | \psi_k \rangle$, $\langle \hat{A}^\dagger \hat{A} \rangle_{nm} = \langle \psi_n | \hat{A}^\dagger \hat{A} | \psi_m \rangle$, and the other operator matrix elements are defined similarly. The energy differences are given by $E_{mn} = E_m - E_n$.

5.2 Model,coordinate frames and relevant OTOCs

To explore the scrambling dynamics and work statistics of an experimentally realizable system I consider a system of N interacting bosons confined to a one-dimensional harmonic trap with frequency ω

$$\hat{H} = \sum_{j=1}^{N} \left[-\frac{1}{2} \frac{\partial^2}{\partial x_j^2} + \frac{1}{2} \gamma^2 x_j^2 \right] + \sum_{k>j} g\, \delta(x_k - x_j) \, . \tag{5.12}$$

Here the Hamiltonian is rescaled in natural harmonic units with the length scale given by $a_\omega = \sqrt{\frac{\hbar}{m\omega}}$ and the energy scale by $\hbar\omega$. The strength of the short range interactions are parameterized by g which here has units of $\sqrt{\frac{\hbar^2\omega}{m}}$ and the trap width can be changed using the nondimensional parameter γ.

This problem is separable into a center-of-mass-coordinate $\sum_n x_n/N$ and a set of relative Jacobi-coordinates [157]. This basic property of the harmonic oscillator means that the squared commutator associated with the center-of-mass (CM) position and momentum operators are unaffected by the interaction, as the center-of-mass coordinate Hamiltonian commutes with the Jacobi coordinate Hamiltonians. The time-evolution is therefore entirely independent and the center-of-mass correlation functions reduce to the single-particle correlation functions multiplied by a factor N^2. The squared commutator for the stationary states of a single particle in a harmonic trap was calculated in [158] and I also consider it in some more detail (including for quenches) in section 5.5 and 5.6.1. Therefore, in order to see the effect of interactions, operators that involve the Jacobi coordinates are required. While finding solutions to this model becomes computationally intractable for large systems, few-body systems are readily solvable while retaining the physics stemming from the finite contact interactions [157]. In fact, for the minimal interacting system of $N = 2$ particles exact solutions can be found [94] as outlined in chapter 3.2. I therefore focus on the two particle problem due to its ubiquity in few-body physics and for the insights it offers into the quench dynamics of larger systems. This system can be separated in terms of the CM coordi-

nate $X = \frac{x_1+x_2}{\sqrt{2}}$ and the relative coordinate $x = \frac{x_2-x_1}{\sqrt{2}}$ with corresponding momentum operators $P = \frac{p_1+p_2}{\sqrt{2}}$ and $p = \frac{p_2-p_1}{\sqrt{2}}$. As per the above argument one needs to focus on the relative coordinate Hamiltonian to see the effect of the interaction.

In some cases one may only have access to the laboratory frame coordinates, and as this is a two-body system focusing exclusively on the relative coordinate could fail to capture the full problem. Let me therefore consider the relation between the correlation functions for the laboratory frame coordinate operators $A_i = x_i, p_i$, $B_i = x_i, p_i$ with $i, j = 1, 2$ and the relative/CM coordinate operators $A^R = x, p$ $B^R = x, p$ and $A^{CM} = X, P$, $B^{CM} = X, P$. To outline how the general results are obtained, I consider the form of one specific correlation function, namely $I_{x_1,x_1}(t)$ for an initial state with an even parity relative coordinate state and odd or even parity CM coordinate state (I use an even initial CM state in the example, but the derivation is the same for an odd one), corresponding to an eigenstate of the interacting bosonic system. This state can be described in terms of the eigenstates of the final Hamiltonian as $|\psi_I^{\rm CM}\rangle|\psi_I^{\rm REL}\rangle = \sum_{j,n} d_{2n}c_{2j}|\psi_{2n}\rangle|\psi^g_{2j}\rangle$ where the overlap coefficients $c_j = \langle\psi^g_j|\psi^{\rm REL}\rangle$ and $d_n = \langle\psi_n|\psi_I^{\rm CM}\rangle$ are zero for odd parity eigenstates. Here $|\psi_n\rangle$ are the eigenstates of a non-interacting harmonic oscillator, while $|\psi^g_j\rangle$ are the eigenstates given by Eq.(3.20) in chapter 3.2. $I_{x_1,x_1}(t)$ is then given by

$$I_{x_1,x_1}(t) = \sum_{j_1,n_1,j_2,n_2} \frac{1}{4} c_{2j_1} d_{2n_1} c_{2j_2} d_{2n_2} \langle\psi^g_{2j_1}|\langle\psi_{2n_1}|[\hat{x}(t)+\hat{X}(t)][\hat{x}+\hat{X}]^2[\hat{x}(t)+\hat{X}(t)]|\psi_{2n_2}\rangle|\psi^g_{2j_2}\rangle \tag{5.13}$$

Initially this looks quite complicated as one has to evaluate 16 terms. However, it can be simplified considerably by noticing that any term which involves an odd number of either relative or CM coordinate operators will be zero (due to the structure of the canonical operators, see also Eq.(5.20) in section 5.3). For example, for the relative coordinate, this combination will result in an odd parity state, which will have zero overlap with all the even parity states contained in the sum. Utilizing this knowledge the correlation functions can be calculated as (where $K = I, D$)

$$K_{A_jB_k}(t) = \frac{1}{4}(K_{A^RB^R}(t) + K_{A^{CM}B^{CM}}(t) + J_{B^{CM}}(0)J_{B^R}(t) + J_{A^R}(0)J_{A^{CM}}(t) \tag{5.14}$$

$$\pm 2[G^2_{A^RB^R}(t)G^1_{A^{CM}B^{CM}}(t) + G^1_{A^RB^R}(t)G^2_{A^{CM}B^{CM}}(t)]), \tag{5.15}$$

$$F_{A_jB_k}(t) = \frac{1}{4}(F_{A^RB^R}(t) + F_{A^{CM}B^{CM}}(t) + J_{B^{CM}}(0)J_{B^R}(t) + J_{A^R}(0)J_{A^{CM}}(t) \tag{5.16}$$

$$\pm 2[G^1_{A^RB^R}(t)G^2_{A^{CM}B^{CM}}(t) + G^2_{A^RB^R}(t)G^1_{A^{CM}B^{CM}}(t) + 2G^1_{A^RB^R}(t)G^1_{A^{CM}B^{CM}}(t)]), \tag{5.17}$$

where the second term is added for $j = k$ and subtracted for $j \neq k$. The functions in the above equations are given by

$$G^1_{AB} = \langle A(t)B\rangle \quad , \quad G^2_{AB} = \langle AB(t)\rangle \quad , \quad J_A(t) = \langle A^2(t)\rangle \tag{5.18}$$

where the expectation values are with respect to the relative wavefunction $|\psi_I^{\rm REL}\rangle = \sum_j c_{2j}|\psi^g_{2j+1}\rangle$ for relative coordinate operators and the CM wavefunction $|\psi_I^{\rm CM}\rangle =$

$\sum_n d_{2n+1}|\psi_{2n+1}\rangle$ for CM coordinate operators. The full squared commutator of the laboratory-frame coordinates is then given by

$$C_{A_j,B_j} = \frac{1}{4}[C_{A^R B^R}(t) + C_{A^{CM} B^{CM}}(t) \pm G^1_{A^R B^R}(t) G^1_{A^{CM} B^{CM}}(t)]. \tag{5.19}$$

The squared commutator of these operators are therefore given as the squared commutator of the relative coordinate plus the center-of-mass coordinate plus the product of two two-point correlation functions in the relative and CM coordinate respectively. As already argued, the CM coordinate does not see the interaction and the important contribution which determines the behaviour of the laboratory frame squared commutator is therefore the relative frame squared commutator, which will be the main focus of this chapter.

5.3 Analytic formulas for the correlation functions in the relative frame

The solution of the relative-coordinate frame Hamiltonian was introduced in chapter 3.2. Using the representation of the wavefunction given by Eq.(3.20) and their associated energies E^g_{2j} it is possible to calculate the constituent correlation functions that make up the squared commutator for position and momentum explicitly as it is known how these operators act on the harmonic-oscillator-states, i.e.

$$\hat{O}|\psi_n\rangle = \frac{\beta_O}{\sqrt{2}}[\sqrt{n+1}|\psi_{n+1}\rangle + \tilde{\beta}_O\sqrt{n}|\psi_{n-1}\rangle] \tag{5.20}$$

which reduces to the position operator for $\beta_O = 1, \tilde{\beta}_O = 1$ or the momentum operator for $\beta_O = i, \tilde{\beta}_O = -1$, using units scaled in terms of he oscillator length scale a_ω. Note that ω here refers to the trap frequency of the final Hamiltonian. One can now calculate the correlation functions by sequentially applying operators according to Eq.(5.6-5.8) and expressing the new state in terms of eigenstates of the final Hamiltonian in order to perform the time-evolution. Alternatively one can calculate the relevant matrix-elements in Eq.(5.9)-Eq.(5.11) and evaluate the sums. For any even parity initial state the correlation functions in an interacting system for momentum and position operators can be expressed as the sums

$$D_{AB}(t) = \sum_{j,k} c_{2j} c_{2k} K^{BA}_{jk} + \cos(2t) \sum_{j,k} c_{2j} c_{2k} J^{BA}_{jk} \tag{5.21}$$

$$I_{AB}(t) = \sum_j |c_{2j}|^2 [K_{jj}^{AB} + J_{jj}^{AB}\cos(2t)] + \sum_{j\neq k} c_{2j}c_{2k}\Big(K_{jk}^{AB}\cos[(E_{2j}^g - E_{2k}^g)t] + J_{jk}^{AB}\cos[(E_{2j}^g - E_{2k}^g + 2)t]\Big) \tag{5.22}$$

$$F_{AB}(t) = \sum_{j,k,n,m,l} c_{2j}c_{2k}e^{-i(E_{2n}^g - E_{2k}^g + 2l - 2m)t}\alpha_{m,n}^B\alpha_{m,k}^A\alpha_{l,n}^A\alpha_{l,j}^B \tag{5.23}$$

where

$$K_{jk}^{AB} = \sum_{m=0}^{\infty} \frac{|\beta_A|^2|\beta_B|^2\tilde{\beta}_B}{2}\alpha_{m,j}^A\alpha_{m,k}^A(4m+3) \tag{5.24}$$

$$J_{jk}^{AB} = \sum_{n=1}^{\infty} |\beta_A|^2|\beta_B|^2\sqrt{2n+1}\sqrt{2n}\alpha_{n,k}^A\alpha_{n-1,j}^A. \tag{5.25}$$

The coefficients c_{2j} and $\alpha_{m,j}^O$ are given by

$$c_{2j} = \langle\psi_{2j}^g|\Psi^I\rangle\ , \tag{5.26}$$

$$\begin{aligned}\alpha_{m,j}^O &= \langle\psi_{2m+1}|\hat{O}|\psi_{2j}^g\rangle/\beta_O \\ &= \sqrt{2m+1}\psi_{2m}(0)\frac{\Omega_{2j}^g}{\sqrt{2}}\left(\frac{1}{E_{2m}-E_{2j}^g} - \frac{\tilde{\beta}_O}{E_{2m+2}-E_{2j}^g}\right),\end{aligned} \tag{5.27}$$

where the energies E_{2m} are for the non-interacting harmonic oscillator and E_{2j}^g are the energies for finite interactions g, while Ω_{2j}^g is the normalization factor for the wavefunction defined in Eq.(3.21) in chapter 3.2. The structure of the position/momentum operator means only odd parity non-interacting states remain when applied to the sum of even parity non-interacting states given by Eq.(3.20), which is why these coefficients are only non-zero for $|\psi_{2m+1}\rangle$. These equations can give us an understanding of the behavior of the OTOCs. $I_{AB}(t)$ and $D_{AB}(t)$ are reducible to a relatively simple sum over 3 indices, while $F_{AB}(t)$ requires the evaluation of a sum over 5 indices. It is therefore harder to gain analytic insight into the dynamics of $F_{AB}(t)$, but it can still be calculated numerically.

In addition to these dynamical formulas, a simple expression for the infinite-time average of the squared commutator can be obtained. While it is easy to obtain this from the dynamical expressions above, it is illustrative to consider the generic infinite-time average as this allows us to identify which properties of the harmonic oscillator are important for obtaining the final result. For simplicity I consider a non-degenerate system [condition (i)], of which the harmonic oscillator is an example. From Eqs. (5.9-5.11) one can see that contributions to the long-time average of the squared commutator are only obtained when the complex exponential equals 1, which means that $D_{AB}(t)$ has

contributions whenever $E_m = E_n$. Similarly, the contributions to I_{AB} and F_{AB} can be split into 3 cases: the energy-differences can be pairwise zero in the case where $E_k = E_j$ and $E_m = E_n$ or the sum can be zero when $E_k = E_m$ and $E_n = E_j$. Finally, it is also possible that $E_k - E_j + E_n - E_m = 0$ for $j \neq k \neq n \neq m$. The resulting time-averages can then be written as

$$\bar{D}_{AB} = \sum_{j,k,n} c_j^* c_k B_{jn}^\dagger \langle \hat{A}^\dagger \hat{A} \rangle_{nn} B_{nk}, \tag{5.28}$$

$$\begin{aligned} \bar{I}_{AB} = &\sum_{j,n} |c_j|^2 A_{jn}^\dagger \langle \hat{B}^\dagger \hat{B} \rangle_{nn} A_{nj} \\ &+ \sum_{j \neq k} c_j^* c_k A_{jj}^\dagger \langle \hat{B}^\dagger \hat{B} \rangle_{jk} A_{kk} \\ &+ \sum_{j \neq k \neq n \neq m} c_j^* c_k A_{jn}^\dagger \langle \hat{B}^\dagger \hat{B} \rangle_{nm} A_{mk}, \end{aligned} \tag{5.29}$$

$$\begin{aligned} \bar{F}_{AB} = &\sum_{j,n} c_j^* b_j A_{jn}^\dagger B_{nn}^\dagger A_{nj} \\ &+ \sum_{j \neq k} c_j^* b_k A_{jj}^\dagger B_{jk}^\dagger A_{kk} \\ &+ \sum_{j \neq k \neq n \neq m} c_j^* b_k A_{jn}^\dagger B_{nm}^\dagger A_{mk}. \end{aligned} \tag{5.30}$$

The energies of the interacting states can be expressed as $E_{2j}^g = (2j + \Delta_j)\omega$, see Eq.(3.19) in chapter 3.2. Crucially, for any finite value of g one finds $\Delta_j \neq \Delta_k$ for $j \neq k$, which means that any finite interaction breaks the harmonicity of the energy spectrum for the even parity eigenstates. For even parity initial states, corresponding to those affected by the delta-function interaction, the only contributions to the dynamics come from the even parity eigenstates, while the odd parity eigenstates are completely decoupled. For the relevant eigenstates in the time-averages this means that $E_k - E_j + E_n - E_m \neq 0$ for $j \neq k \neq n \neq m$ [condition (ii)], which simplifies the calculation considerably. The canonical operators with respect to these eigenfunctions obey $B_{kk} = A_{kk} = 0$ [condition (iii)], as each eigenfunction is given as a sum of even parity non-interacting eigenfunctions via Eq. (3.20) which individually fulfill condition (iii). The time-averages for the interacting relative-coordinate Hamiltonian in the harmonic trap (and for any other system which fulfills conditions (i)-(iii)) therefore reduce to $\bar{F}_{AB} = 0$ and $\bar{C}_{AB} = \bar{D}_{AB} + \bar{I}_{AB}$, with

$$\bar{D}_{AB} = \sum_{j,k} c_{2j} c_{2k} K_{jk}^{BA}\,, \qquad \bar{I}_{AB} = \sum_{j} |c_{2j}|^2 K_{jj}^{AB}\,, \tag{5.31}$$

where $K_{jk}^{AB} = \sum_n A_{jn}^\dagger \langle \hat{B}^\dagger \hat{B} \rangle_{nn} A_{nk}$ in general and given by Eq.(5.24) for the harmonic oscillator. Any final Hamiltonian that is spatially symmetric with respect to the relevant canonical operators will obey these conditions, one example being the Jacobi coordinates for N interacting particles in a harmonic trap [103, 109, 157, 159–161], which allows us to extend some of our conclusions to larger systems.

The time-averaged scrambling has recently attracted attention, having been connected to the Loschmidt echo of time-reversal protocols [155] and the description of quantum phases [146, 148]. It describes the average scrambling in the system with a single number, although it lacks information about the dynamical process of the scrambling. Note that the infinite-time average for the laboratory frame coordinates as defined in Eq.(5.19) are simply given by the sum of the infinite time-average calculated above and the infinite-time average of the CM frame coordinates, i.e.

$$\bar{C}_{A_i,B_j} = \frac{1}{4}[\bar{C}_{A^R B^R} + \bar{C}_{A^{CM} B^{CM}}], \tag{5.32}$$

as $\bar{G}^1_{ab}(t) = \sum_{n,k} a_{nn} b_{nk} = 0$ by condition(iii).

The problem can also be solved numerically by obtaining the eigenspectrum of the final Hamiltonian using a finite-difference method. Specifically I utilize the DVR method [162] which gives accurate results for a delta-function potential allowing me to compare with the analytic results and to find the overlap coefficients for a trap quench in a system containing the delta-function interaction where no easily implementable analytic formula exists. The recipe for finding the correlation functions numerically is straightforward and exactly the same as in the analytic case, that is one applies the operators and time-evolution in the correct sequence to the initial state, performing the time-evolutions by expressing the relevant states in terms of the eigenstates of the final Hamiltonian. The results in the following sections for $[\hat{x}(t), \hat{x}]^2$ for the delta-function interaction are based on evaluating the analytic sums, but I have checked that the two methods give the same results.

5.4 General remarks about the analytic solutions

One thing which is immediately obvious from the structure of the infinite-time average is that it is closely related to the diagonal ensemble which determines the amount of non-equilibrium excitations and the infinite-time average of observables such as the momentum and density distribution. $\bar{I}_{AB}$ is given as the diagonal ensemble expectation value of an emergent operator and is therefore directly related to the DE probabilities with no dependence on the phase of the overlap coefficients. $\bar{D}_{AB}$ is given as a sum over all the off-diagonal values of a similar emergent operator, which means that the phase of the overlap coefficients matter and negative and positive contributions can interfere destructively.

For the dynamics it is clear that the time-ordered correlation function $D_{AB}(t)$ displays trivial harmonic oscillations with frequency 2ω. If the initial state is an eigenstate of $\hat{H}_F$, i.e. $c_{2j} = 1, c_{2k\neq 2j} = 0$ the off-diagonal terms in $I_{AB}(t)$ disappear and it displays trivial harmonic oscillations with frequency 2ω as well. This is because $I_{AB}(t)$ is anti-time-ordered for an eigenstate. In general, however, $I_{AB}(t)$ and $F_{AB}(t)$, both of which are out-of-time ordered for a non-eigenstate will have a more complicated time-dependence, although the latter will average to zero as shown above. These dynamics are investigated in more detail numerically in the upcoming sections.

So far the actual choice of canonical operators has not been important for the discussion. However, in order to move forward, one needs to analyse the matrix-elements of the emergent operators J^{AB}, K^{AB} which depend on the choice of A, B. The coefficients for $\hat{x}$ are given by

$$\alpha^x_{m,j} = \sqrt{2m+1}\psi_{2m}(0)\Omega^g_{2j}\frac{2}{(E_{2m}-E^g_{2j})(E_{2m+2}-E^g_{2j})}. \tag{5.33}$$

This means that the terms in the sum in Eq.(5.24) and Eq.(5.25) scale as $\propto m^{-2}\psi^2_{2m}(0) = m^{-5/2}$ (see appendix A.1 for the scaling of $\psi_{2m}(0)$) in sums involving these coefficients and therefore converge. For the coefficients $\hat{p}$, however, such a reduction of the coefficients is not possible and the terms in the sum scale like $\propto \psi^2_{2m}(0) = m^{-1/2}$ which means that the sums diverge. The squared commutator involving the momentum operators is therefore problematic, essentially because we attempt to twice-differentiate a function which is not twice-differentiable due to the non-analytic cusp in the single particle solutions for the zero-range delta-function pseudo-potential. Using a Gaussian interaction, this divergence disappears, but the results now depend on the finite range of the Gaussian. Similar results can be obtained by cutting off the divergent sum at some m which means that a system-dependent regularization parameter is required to calculate the squared commutator involving momentum operators. The focus of this chapter is therefore on $\hat{A} = \hat{x}, \hat{B} = \hat{x}$, where the analytic expressions of J^{xx}, K^{xx} for the delta-function interaction are convergent. In appendix A.2 an investigation of momentum operators is contained, while a further analysis of the x, x matrix elements can be found in appendix A.1. Here I will present a short summation of those results and their consequences for the infinite-time average as well as the dynamics. Both J^{xx} given by Eq.(5.25) and K^{xx} given by Eq.(5.24) can effectively be described by a tri-diagonal matrix $K^{xx}_{j,j+1} = K^{xx}_{j,j-1} = -J^{xx}_{j,j} = J^{xx}_{j,j+2} = -\xi_1 j^2$ and $K^{xx}_{j,j} = -J^{xx}_{j,j+1} = \xi_2 j^2$, while all other matrix elements are of insignificant size in comparison. Here ξ_1 and ξ_2 are constants determined by the interaction strength g and obtained by calculating the matrix elements and fitting to the quadratic functions.

Combined with the fact that $(E^g_{2j})^2 \propto (2j)^2$, this form of the matrix elements leads to an interesting realization which is a major result of this investigation. The second moment of the work probability distribution is given as $\langle W^2\rangle \propto \sum_j |c_{2j}|^2(2j)^2$ while $\bar{I}_{xx}$, which only has the diagonal contribution, is given by $\bar{I}_{xx} \propto \sum_j |c_{2j}|^2(2j)^2$. These two values are therefore proportional to each other. In fact it is found that this proportionality holds for the variance of the work probability distribution $\Delta W^2 = \sum_j |c_{2j}|^2(E^g_{2j})^2 - \left(\sum_j |c_{2j}|^2 E^g_{2j}\right)^2$ as well, as $\langle W^2\rangle \propto \langle W\rangle$. D_{xx} on the other hand can effectively be described as a sum over the tri-diagonal matrix $K^x x$. This means that the off-diagonal negative contributions $K^{xx}_{j,j+1} = K^{xx}_{j,j-1} = -\xi_1 j^2$ are either subtracted or added to the diagonal positive contribution $K^{xx}_{j,j} = \xi_2 j^2$ depending on the signs of the overlap coefficients. In the next sections I will consider different quenches which will lead to different overlap coefficients and therefore to different behaviours of $\bar{D}_{xx}$. When the off-diagonals are consistently subtracted it suppresses this contribution, while adding them leads to an overall value which is also proportional to the work fluctuations. The infinite time-average of the squared commutator $\bar{C}_{xx}$ is therefore proportional to the variance

of the work probability distribution as well. Investigating $\hat{C}_{AB}$ for other combinations of canonical operators reveals similar results (see appendix A.2). The main takeaway is that while $\bar{I}_{AB}$ is always proportional to ΔW^2, the time-ordered contribution $\bar{D}_{AB}$ can have constructive interference for one set of A, B making it proportional to ΔW^2, but destructive interference for a different set A, B making it effectively zero for the same quench.

5.5 Analytic results for a generic quench in the non-interacting system

For the special case of non-interacting particles for which the relative part of the wave-function is given by the non-interacting harmonic oscillator the squared commutator has been calculated for eigenstates in earlier works, such as [158], but in this section an arbitrary initial state is considered. For the non-interacting harmonic oscillator the full Heisenberg equations of motion for position and momentum operators are known and given by (still in units of the oscillator length a_ω)

$$\hat{x}(t) = \hat{x}(0)\cos(t) + \hat{p}(0)\sin(t) \tag{5.34}$$
$$\hat{p}(t) = \hat{p}(0)\cos(t) - \hat{x}(0)\sin(t). \tag{5.35}$$

These can be utilized to calculate the time-dependent correlation functions by simple multiplication and taking the expectation-value of the time-independent correlation functions with respect to the initial state. As an example the position-position correlation functions are given by

$$\begin{aligned} D_{xx}(t) = &\langle\psi_I|\hat{x}^4(0)|\psi_I\rangle\cos^2(t) \\ &+ \langle\psi_I|\hat{x}^2(0)\hat{p}(0)\hat{x}(0)|\psi_I\rangle\cos(t)\sin(t) \\ &+ \langle\psi_I|\hat{x}(0)\hat{p}(0)\hat{x}^2(0)\ |\psi_I\rangle\cos(t)\sin(t) \\ &+ \langle\psi_I|\hat{x}(0)\hat{p}^2(0)\hat{x}(0)|\psi_I\rangle\sin^2(t) \end{aligned} \tag{5.36}$$

$$\begin{aligned} I_{xx}(t) = &\langle\psi_I|\hat{x}^4(0)|\psi_I\rangle\cos^2(t) \\ &+ \langle\psi_I|\hat{x}^3(0)\hat{p}(0)|\psi_I\rangle\cos(t)\sin(t) \\ &+ \langle\psi_I|\hat{p}(0)\hat{x}^3(0)|\psi_I\rangle\cos(t)\sin(t) \\ &+ \langle\psi_I|\hat{p}(0)\hat{x}^2(0)\hat{p}(0)|\psi_I\rangle\sin^2(t) \end{aligned} \tag{5.37}$$

$$\begin{aligned} F_{xx}(t) = &\langle\psi_I|\hat{x}^4(0)|\psi_I\rangle\cos^2(t) \\ &+ \langle\psi_I|\hat{x}^2(0)\hat{p}(0)\hat{x}(0)|\psi_I\rangle\cos(t)\sin(t) \\ &+ \langle\psi_I|\hat{p}(0)\hat{x}^3(0)|\psi_I\rangle\cos(t)\sin(t) \\ &+ \langle\psi_I|\hat{p}(0)\hat{x}(0)\hat{p}(0)\hat{x}(0)|\psi_I\rangle\sin^2(t). \end{aligned} \tag{5.38}$$

No choice of initial state will introduce a more complicated time-dependence than ω and 2ω oscillations. This result is unsurprising since the Heisenberg equations for

position and momentum are given for any initial state with the only time-dependence being the sines and cosines. Different initial states can, however, introduce different amplitudes and in principle constructive or destructive interference between the terms in the correlation functions.

5.6 Trap quench and harmonic limits

For the initial exploration of nonequilibrium scrambling in this system I will consider a sudden change of the trapping frequency $\omega_I \to \omega_F$ while keeping the interaction fixed. The ground-state of the initial Hamiltonian will be considered as the initial state. This allows me to clearly identify the effects of finite interactions on the information scrambling and work statistics after the quench by comparing with the same quench in the harmonic limits. By scaling all relevant quantities in units of the final Hamiltonian the results only depend on the frequency ratio $\gamma = \omega_I/\omega_F$, which also quantifies the strength of the quench. Therefore Eq. (3.14) describes the Hamiltonian of the initial state, while setting $\gamma = 1$ describes the quenched Hamiltonian.

5.6.1 Analytic results in the harmonic limit

In the TG-limit $g = \infty$ the even parity states becomes two-fold degenerate with the non-interacting odd parity states, that is $\Delta_j = 1$ for all j and $E^g_{2j} = 2j + 1$ [94], and the corresponding eigenfunctitons can be obtained as $\psi^g_{2j}(x) = |\psi_{2j+1}(x)|$. Therefore, both the TG-limit $g = \infty$ and the non-interacting limit $g = 0$ ($\Delta_j = 0$ for all j) have a harmonic spectrum and solutions can be obtained by considering Eqs.(5.36-5.38) with the relevant initial state. For $g = 0$, $|\psi_I\rangle = |\psi^I_0\rangle$, while for $g = \infty$, $|\psi_I\rangle = ||\psi^I_1\rangle|$. General expressions in terms of $\hat{A}, \hat{B}$ can be found. $I_{AB}(t) = D_{AB}(t)$ and expressions for the $g = 0$ quench are given by

$$\begin{aligned}
I_{AA}(t) =& \frac{3}{4}[G_A \cos^2(t) + \sin^2(t)], \\
\mathrm{Re}\,[F_{AA}(t)] =& \frac{3}{4}[G_A \cos^2(t) + \sin^2(t)] - \frac{1}{2}\sin^2(\omega_F t), \\
I_{AB}(t) =& \frac{3}{4}[\cos^2(t) + G_A \sin^2(t)], \\
\mathrm{Re}\,[F_{AB}(t)] =& \frac{3}{4}[\cos^2(t) + G_A \sin^2(t)] - \frac{1}{2}\cos^2(t),
\end{aligned}$$

with the squared commutators given by

$$\begin{aligned}
[\hat{A}(t), \hat{A}]^2 &= \sin^2(t), \\
[\hat{A}(t), \hat{B}]^2 &= \cos^2(t).
\end{aligned}$$

Here $G_x = \frac{1}{\gamma^2}$ and $G_p = \gamma^2$, leading to an operator-dependent difference between squeezing and opening the trap. For the $g = \infty$ quench the formulas are given by

$$\begin{aligned} I_{AA}(t) =& \frac{1}{4}[15G_A\cos^2(t) + 7\sin^2(t)], \\ \mathrm{Re}\,[F_{AA}(t)] =& \frac{1}{4}[15G_A\cos^2(t) + 7\sin^2(t)] - \frac{1}{2}\sin^2(\omega_F t), \\ I_{AB}(t) =& \frac{1}{4}[15\cos^2(t) + 7G_A\sin^2(t)], \\ \mathrm{Re}\,[F_{AB}(t)] =& \frac{1}{4}[15\cos^2(t) + 7G_A\sin^2(t)] - \frac{1}{2}\cos^2(t), \end{aligned}$$

with the squared commutators given by

$$\begin{aligned} [\hat{A}(t), \hat{A}]^2 &= \sin^2(t), \\ [\hat{A}(t), \hat{B}]^2 &= \cos^2(t). \end{aligned}$$

These all display simple harmonic oscillations reflecting the harmonic spectrum, which leads to perfect periodic revivals. The amplitude of these oscillations (and therefore the infinite-time average) depends on the quench strength γ for the individual correlation functions, but the amplitude of the full squared commutator is completely independent of γ with $\bar{C}_{AB} = \frac{1}{2}$. This implies that no significant scrambling takes place independent of the amount of non-equilbirium excitations generated by the quench. Indeed, the work fluctuations, which were already argued to be proportional to the infinite-time average of the squared commutator in the interacting case, can be calculated analytically for these limiting cases (utilizing the analytic expressions for the overlap coefficients $c_j = \langle\psi_j|\psi^I\rangle$ [163]) as $\Delta W^2 = \lambda(g)\left(\gamma - \frac{1}{\gamma}\right)^2$, with $\lambda(0) = \frac{1}{8}$ and $\lambda(\infty) = \frac{3}{8}$. This is clearly proportional to the strength of the quench squared which is in stark contrast to the average scrambling and something is therefore fundamentally different when compared to the interacting system which will be investigated in detail in the next section.

Finally, it should be noted that the squared commutator for the center-of-mass part of the two-body problem after a trap quench corresponds to the $g = 0$ results.

5.6.2 Scrambling properties for the interacting system

In this section I will consider the scrambling properties as a function of the finite interaction g and the quench strength γ. In Fig. 5.1 an example of the dynamics for opening and squeezing the trap is shown. For these finite interactions the harmonicity of the energy spectrum is broken and therefore the correlation functions can possess complex dynamics. Indeed, $I_{xx}(t)$ and $F_{xx}(t)$ possess irregular oscillations as they are not time-ordered. It is clear that the time average of $F_{xx}(t)$ quickly vanishes, with the long time behaviour of the squared commutator determined solely by $D_{xx}(t)$ and $I_{xx}(t)$. Additionally the time-ordered $D_{xx}(t)$ displays the same qualitative behaviour as the correlation functions did in the harmonic limits, that is the amplitude depends on whether the trap is opened or closed in exactly the same ways as in the harmonic

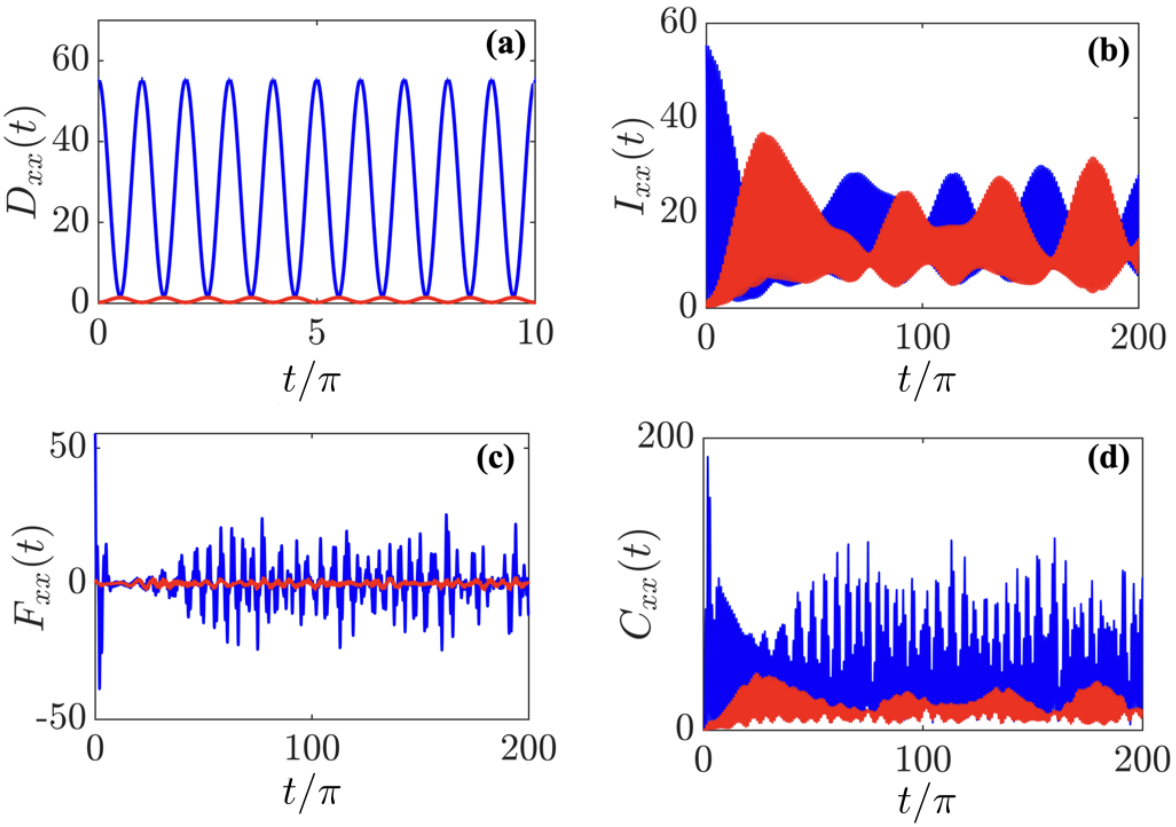

Figure 5.1: $D_{xx}(t)$ (a), $I_{xx}(t)$ (b), $F_{xx}(t)$ (c) and $C_{xx}(t)$ (d) as a function of time for $g = 10$. The blue lines correspond to a quench with $\gamma = \frac{1}{4}$, while the red lines correspond to a quench with $\gamma = 4$.

limit. Moving forward it will be clear that this is a general trend, $D_{xx}(t)$ and the work statistics tend to have a smooth crossover between the interacting and harmonic limits, while the OTOCs do not.

In Figs. 5.2(a) and (b) the infinite time-averages of the correlation functions (full lines) and the variance of the work probability distribution (yellow dotted line) as a function of the interaction strength for $\gamma = 4$ and $\gamma = \frac{1}{4}$ are shown. ΔW^2 has a similar functional form to $\bar{I}_{xx}$ and in Fig. 5.2(c) it is shown that these two quantities are linearly related through $\bar{I}_{xx} = b_I(g)\Delta W^2$, allowing us to extract the fitting parameter for each value of the interaction g (see panel (d)). Note that this is simply a confirmation of the general relationship uncovered in section 5.4. The values for $\bar{I}_{xx}(t)$ are almost identical for opening or squeezing the trap, making its behavior fully equivalent to ΔW^2 which measures the amount of non-equilibrium excitations. The 3-OTOC, which corresponds to a time-reversal test, is therefore a good quantifier of irreversibility.

In contrast to $\bar{I}_{AB}$ one can show that $\bar{D}_{AB}$ is operator dependent, which leads to a markedly different behaviour of the time-ordered contribution $\bar{D}_{xx}$ for squeezing or opening of the trap. In particular one can see that $\bar{D}_{xx}$ remains small whenever $\gamma > 1$ and therefore does not contribute much to $\bar{C}_{xx}$, whereas for $\gamma < 1$ we find

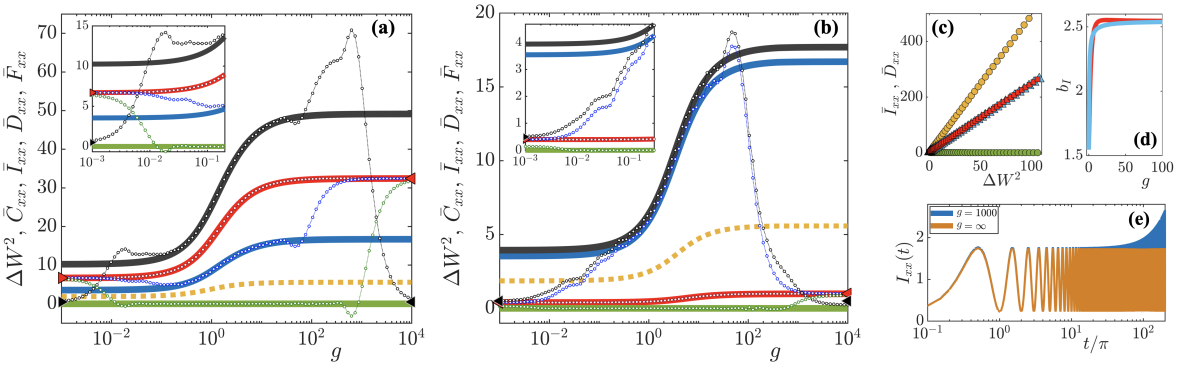

Figure 5.2: (a-b) The full lines show $\bar{D}_{xx}$ (red), $\bar{I}_{xx}$ (blue), $\bar{F}_{xx}$ (green), $\bar{C}_{xx}$ (black) as a function of g for (a) $\gamma = \frac{1}{4}$ and (b) $\gamma = 4$. The circles show the time-averages of the same quantities in an interval $t \in [0, 200\pi]$. The variance of the work probability distribution function ΔW^2 is given by the dotted yellow line. The triangles correspond to the $g = 0$ and $g = \infty$ values of $\bar{C}_{xx}$ (black) and $\bar{I}_{xx} = \bar{D}_{xx}$ (red). Insets: zoom of correlation functions in main panel at weak interactions. (c) $\bar{I}_{xx}$ as a function of ΔW^2 at fixed interaction $g = 10$, with each data point representing a quench of the trap frequency for $\gamma > 1$ (red squares) and $\gamma < 1$ (blue triangles). The blue and red markers are essentially on top of each other. Similarly, yellow circles correspond to $\bar{D}_{xx}$ for $\gamma < 1$ while green circles are $\gamma > 1$. (d) b_I for $\gamma > 1$ (red) and $\gamma < 1$ (blue) as a function of g. All fits are accurate with $R^2 > 0.99$. (e) $I_{xx}(t)$ as a function of time for $g = 1000$ (blue) and $g = \infty$ (orange) with $\gamma = 4$.

that $\bar{D}_{xx} = b_D \Delta W^2$ (see Fig. 5.2(c)). The full squared commutator $\bar{C}_{xx} = \bar{D}_{xx} + \bar{I}_{xx}$ is therefore also proportional to ΔW^2 for both squeezing and opening of the trap, showing that the scrambling in this system is closely related to the irreversible non-equilibrium excitations created by the quench. Mathematically the difference between opening and closing the trap is related to the signs of the overlap coefficients as explained in section 5.4. Indeed, for opening the trap we find that the coefficients are all positive (numerically and for the analytic [163] non-interacting case) which means that the off-digaonal negative values are subtracted from the diagonal giving the overall small value observed, while for squeezing the trap they alternate between positive and negative values. This adds an overall contribution that also scales as approximately j^2, explaining why these values are also proportional to ΔW^2 with a larger proportionality constant than for $\bar{I}_{xx}$.

The proportionalities uncovered above mean that information about the scrambling in the system is therefore also contained in ΔW^2 for the interacting system. For finite values of g one can show that ΔW^2 is related to γ in the same functional form as in the harmonic limits by fitting the parameter $\lambda(g)$ numerically and obtaining excellent accuracy. The work fluctuations and the scrambling therefore grow with the strength of the quench with the functional dependence $\left(\gamma - \frac{1}{\gamma}\right)^2$.

These results also hold if one investigates the full two-body problem, not just for the relative coordinate part. The work fluctuations of the CM coordinate Hamiltonian are given by $\Delta W^2_{CM} = \frac{1}{8}\left(\gamma - \frac{1}{\gamma}\right)^2$ based on the solutions outlined in section 5.6.1 and the work fluctuations of the full system are therefore given by $\Delta W^2 + \Delta W^2_{CM} =$

$[1+\frac{1}{\lambda}]\Delta W^2 \propto \bar{C}_{xx}$. Utilizing the same solutions in section 5.6.1 and Eq.(5.32), the lab frame-coordinate operators for a trap quench is given by $\bar{C}_{x_j,x_j} = \frac{1}{4}\bar{C}_{xx} + \frac{1}{8}$ and is therefore proportional to the work fluctuations as well.

Note that these results are in stark contrast to the harmonic limits where scrambling is independent of ΔW^2. This difference in the infinite-time averages can be partly understood by noting that for $g = 0$ and $g = \infty$ the system violates condition (ii) and the expressions for $\bar{F}_{AB}$, $\bar{I}_{AB}$ and therefore $\bar{C}_{AB}$ (see Eq. 5.31) are no longer valid. In fact, $\bar{I}_{AB}$ and $\bar{F}_{AB}$ have off-diagonal contributions and the long-time average of the squared commutator ends up being given by $\bar{C}_{AB} = \frac{1}{2}$ as reported in section 5.6.1. The squared commutator for the non-interacting system reflects the simple breathing dynamics induced by the quench, which due to the equidistance of the energy spectrum results in perfect periodic revivals of the initial state and therefore no scrambling of the state on average. Scrambling in these limits is therefore not solely a reflection of the non-equilibrium excitations and we need to bridge the gap between them and finite g.

In Fig. 5.2(a) and (b) the values in the harmonic limits are represented by the triangles. Each correlation function (except $\bar{F}_{xx}$ which vanishes) grows with increasing interactions. When approaching the TG limit ($g \to \infty$) the known limiting values for infinite interactions, $\bar{C}_{xx} = 1/2$ (black triangles in the figures), are not reached. In fact, only the time ordered function $\bar{D}_{xx}$ reaches the asymptotic values, while the out-of-time ordered functions $\bar{I}_{xx}(t)$ and $\bar{F}_{xx}(t)$ do not. A similar observation can be made for $g \to 0$.

The difference between the asymptotic value of the OTOCs and their value in the harmonic limit shows that the scrambling (through the OTOCs) is very sensitive to small deviations from harmonicity on infinitely long timescales. In Fig. 5.2(a) and (b) I also plot the time-average taken in a range $t \in [0, 200\pi]$ for comparison. For intermediate values of $g \in [0.1, 70]$ these are indistinguishable from the infinite-time average, but as the extremal interaction limits are approached this finite-time average goes towards the harmonic cases. This reflects the fact that on short timescales the correlation functions are initially similar to the $g = \{0, \infty\}$ cases, but on long time-scales the behaviour becomes qualitatively different owing to the infinitesimal anharmonicity of the spectrum (see Fig. 5.2(e)). This can be explained explicitly for $I_{xx}(t)$ in terms of Eq.(5.22). Most terms will oscillate with a frequency closely related to a multiple of the harmonic frequency, but the terms $j, j+1$ can give rise to small frequency oscillations in the dynamics as they result in the term $\cos[(2 + E^g_{2j} - E^g_{2j+2})t] = \cos[(\Delta_j - \Delta_{2j+2})t]$ with $\Delta_j \to 0$ for all j as the harmonic limits are approached. The long time-scale required for observing scrambling is therefore due to the proximity to the harmonic limits and not due to higher-order excitations becoming important on longer timescales. Investigating the full work probability distribution confirms this as only the first couple of states enter into the dynamics (see Fig. 5.5 in section 5.8). The discontinuity between the average scrambling in the finite strongly interacting system ($g \to \infty$) and the infinite limit ($g = \infty$) is therefore only observable in the long-time limit as the timescale required to actually observe the average scrambling diverges (similar for the $g = 0$ case).

5.7 Interaction quench

The trap quench helps illuminate the scrambling properties of the interacting system versus the non-interacting system, but despite the finite interaction creating a complex pattern of phase interference, it is still related to the breathing mode dynamics of relatively few excited states. Investigating a quench which is expected to introduce more complicated dynamics and higher-order excitations is therefore of interest. The natural choice is to quench the interaction strength, which corresponds to a local change in position-space. We consider a system which is initially in the ground-state ψ_0^I of a Hamiltonian with g_I. At some finite time $t = 0$ the interaction strength is suddenly changed from g_I to g_F and the system evolves with the new Hamiltonian. Note that the center-of-mass part is unaffected by this quench and the contribution to the squared commutator from the CM part is therefore given by the solutions outlined in section 5.6.1 with $\gamma = 1$. The overlap coefficients for the relative part of the wavefunction for an interaction quench are known analytically [98] and in fact display a higher degree of non-equilibrium excitations, with coefficients that scale as $c_{2j} \propto j^{-\frac{5}{4}}$ (see section appendix A.1 for the scaling of Ω_{2j}^g),

$$c_{2j} = \langle \psi_0^I | \psi_{2j}^{g_F} \rangle = \frac{\Omega_{2j}^{g_F} \Omega_0^{g_I}}{g_I g_F} \frac{g_I - g_F}{E_0^{g_I} - E_{2j}^{g_F}}, \tag{5.39}$$

while for $g_I = 0$ they are given as

$$c_{2j} = \langle \psi_0^I | \psi_{2j}^{g_F} \rangle = \Omega_{2j}^{g_F} \frac{\psi_0^*(0)}{E_0 - E_{2j}^{g_F}} \, . \tag{5.40}$$

$D_{xx}(t)$ is unaffected by the interaction quench, that is it has exactly the same dynamics as if we were time-evolving with the initial Hamiltonian. One can express the coefficients in the final state $\alpha_{m,j}^{O,F}$ in terms of the coefficients for the initial state $\alpha_{m,j}^{O,I}$ since

$$\begin{aligned} \alpha_{m,k}^{O,I} \beta_O^I &= \langle \psi_{2m+1} | \hat{O} | \psi_{2k}^{g_I} \rangle = \sum_j \langle \psi_{2m+1} | \hat{O} | \psi_{2j}^{g_F} \rangle \langle \psi_{2j}^{g_F} | \psi_{2k}^{g_I} \rangle \\ &= \sum_j \beta_O^F \alpha_{m,j}^{O,F} c_{2j}. \end{aligned}$$

By inserting this into Eq.(5.21) it reduces to $D_{xx}(t)$ with respect to the initial state. Additionally, the time-average will always be small as all the overlap coefficients have the same sign per the argument in section 5.4. Finally for the special case of $g_F = 0$ the overlap coefficients are given by

$$c_{2j} = \langle \psi_0^I | \psi_{2j}^{g_F} \rangle = \Omega_0^{g_I} \frac{\psi_{2j}^*(0)}{E_{2j} - E_0^{g_I}} \tag{5.41}$$

and the 4-point correlation functions are given by Eq.(5.36-5.38).

In Fig. 5.3 the correlation functions for two interaction quenches, going from interacting

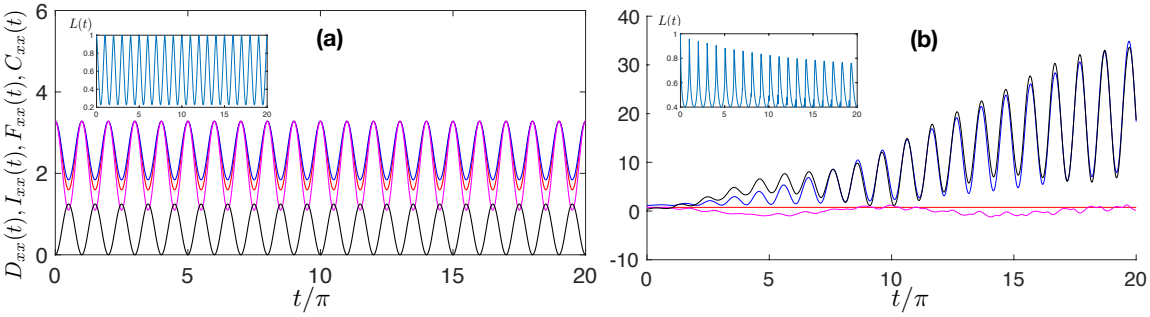

Figure 5.3: $D_{xx}(t)$ (red line), $I_{xx}(t)$ (blue line), $F_{xx}(t)$ (magenta line), $C_{xx}(t)$ (black line) and survival probability $L(t)$ (inset) as a function of time for $g_I = 10, g_F = 0$ (a) ($\langle W_{\rm irr}\rangle = 0.53$, $\bar{L} = 0.569$) and $g_I = 0, g_F = 10$ ($\langle W_{\rm irr}\rangle = 4.5, \bar{L} = 0.5417$) (b).

to non-interacting, $g_I = 10$ to $g_F = 0$, and from non-interacting to interacting, $g_I = 0$ to $g_F = 10$, in the time-period $t \in [0, 20\pi]$, are shown. The survival probability is plotted in the insets. As per Eq.(5.36-5.38) the only periodicity for quenching off the interactions ($g_F = 0$) is 2ω. The only effect of choosing different initial values of g_I is a slight change in the amplitude of the correlation functions. For the opposite case of quenching to strong interactions, $I_{xx}(t)$ exhibits clear growth. On this time-scale it seems as though this growth is actually concurrent with a fall-off in the survival probability, but in order to see whether these are related the long-term behavior of both quantities must be investigated. Indeed, the fidelity is not expected to showcase any long-term decay as this quench has a finite average value of the survival probability of $\bar{L} = 0.5417$.

In Fig. 5.4(a) a log-log plot of $I_{xx}(t)$ for a range of interaction quenches with $g_F \neq 0$ on a much longer time-scale $t \in [0, 10^4\pi]$ is shown, which shows that $I_{xx}(t)$ continues to grow at larger time-scales. In comparison, the survival probability $L(t)$ has no long-term decay and oscillates around an average value equal to the inverse participation ratio (see inset). Here, I focus solely on $I_{xx}(t)$ as $C_{xx}(t) \approx I_{xx}(t)$, since $D_{xx}(t)$ and $F_{xx}(t)$ become negligible at long times. Therefore, the information scrambling is essentially all due to $I_{xx}(t)$ which measures the irreversibility of the time-evolution after the application of the position operator. There are two clearly distinct regimes of $I_{xx}(t)$ visible in panel (a): *(i)* For quenches with a high degree of non-equilibrium excitations, one can see an initial growth that is highly dependent on the specific interaction quench, being faster for those that do more irreversible work, followed by a slow growth which seems almost independent of the quench. *(ii)* For quenches with very few non-equilibrium excitations there is essentially no growth in this initial regime, but at some later time, $I_{xx}(t)$ shows slow growth with a rate similar to the asymptotic growth seen for the stronger quenches. The time-scale at which this happens depends on the quench (particularly the amount of non-equilibrium excitations as measured through the irreversible work), and for a small quench $g_i = 9$ to $g_F = 10$ there is essentially no growth on the time-scale considered.

A much clearer understanding of these behaviors are obtained by comparing with the work probability distributions in Fig. 5.4(c). While all the work probability distribu-

tions have a tail that decays as $j^{-5/2}$, their amplitudes are distinct, and consequently the distribution of the first 10 states are very different. This is why a different growth rate is obtained for intermediate time-scales, while a similar growth-rate (but not absolute value) is obtained for the different quenches on long time-scales. The more higher-lying state dynamics are initially suppressed, the less growth is seen on relevant time-scales (for $g_i = 9$, $g_F = 10$, $c_0 \approx 1$ which is why no long-term growth is observed on the time-scale considered). Additionally one observes that the work probability distributions are not symmetric for $g_I = 2$ to $g_F = 10$ and $g_I = 10$ to $g_F = 2$, although their inverse participation ratio is essentially the same. This is reflected in both the irreversible work and $I_{xx}(t)$. As $I_{xx}(t)$ measures the delocalisation of the position operator dynamically this suggests that the moments of the work probability distribution might be a better measure of delocalisation than the inverse participation ratio, which only measures the delocalisation by how different the initial state is from a single eigenstate of the Hamiltonian. The moments of the work probability distribution and $I_{xx}(t)$, however, both depend on the energy spectrum of the final Hamiltonian in addition to the overlap coefficients.

All of the observed behavior can be understood analytically by considering the scaling of c_{2j}, the matrix elements analysed in section 5.4 (for detials see appendix A.1) and a further investigation of Eq.(5.22). In the limit of large j one can combine the $K_{j,k}$ and $J_{j,j+1}$ terms as $K_{j,j} + J_{j,j+1} = \xi_2 j^2 c_{2j}^2 [2\sin^2(\frac{j^{-3/2}}{2}t)] + \xi_2 j^2 c_{2j}\Delta c_j$, since c_{2j} and c_{2j+2} have the same sign for the interaction quench. Here $\Delta c_j = c_{2j} - c_{2j+2}$. Utilizing the scaling of the overlap coefficients ($c_{2j} \propto j^{-5/4}$) one obtains that $K_{j,j} + J_{j,j+1}$ scales as $j^{-1/4}[2\sin^2(\frac{j^{-3/2}}{2}t)] + j^{-3/2}$. For a constant value of j there will be a time t for which the sine term becomes important and the value of the term will increase. For constant t the small angle approximation of the sine function results in an overall scaling $\frac{j^{-13/4}}{2}t^2$ at large values of j, which means that the sum is convergent at any finite time. $I_{xx}(t)$ will therefore be finite at any time t, but grow as t increases due to the participation of increasingly excited states. In fact, due to the peculiarity of the delta-function interaction quench which has a very long tail for the diagonal ensemble probabilities, this growth continues forever. Evaluating the infinite-time average Eq.(5.31), the terms in the sum scale as $j^{-1/2}$ which means that it diverges. This holds true for the second moment of the work probability distribution as well and the work fluctuations also diverge. This is why I have so far discussed the work probability distribution in terms of its first moment, more specifically the irreversible work, rather than the fluctuations which have already been shown to be proportional to the average scrambling.

This divergence is obviously not a physical effect, but related to the same pathology of the delta-function which requires regularisation for the calculation of squared commutators involving the momentum operator. Indeed, by introducing an effective range regularisation the divergence disappears. In this work this is simply done by replacing the delta-function interaction with a Gaussian interaction given by

$$V(x_2 - x_1) = \kappa \frac{1}{\sigma\sqrt{2\pi}} e^{-(x_2-x_1)^2/\sigma^2}, \tag{5.42}$$

where σ determines the width of the Gaussian, while κ determines its height.

In Fig. 5.4(b) $I_{xx}(t)$ is shown for interactions described by a finite-range Gaussian potential with $\sigma = 0.07$ and $\sigma = 0.04$. The κ is chosen such that the energy levels are close to the $g = 10$ delta-function interaction (with which I compare) and are given as $\kappa = 10$ and $\kappa = 11$ respectively. For the Gaussian interaction the growth of $I_{xx}(t)$ saturates. The saturation time-scale is related to the finite range of the interaction, as the saturation happens at a later time for a narrower Gaussian. Looking at the work probability distributions in Fig. 5.4(d) the Gaussian interaction is hard to distinguish from the delta-function interaction at low energies, but the high energy tails of the Gaussian interaction decay faster than the $j^{-5/2}$-behaviour of the delta-function interaction. The narrower the Gaussian the larger the energy at which this discrepancy occurs. This explains the saturation observed in $I_{xx}(t)$. The variance of the work probability distribution is therefore not uniquely determined by the delta-function as its terms, similarly to the time-average of $I_{xx}(t)$, scale as $j^{-1/2}$, but requires a finite-range regularization parameter which determines the saturation time and value. For cold atoms the relevant the short-range interaction is the van der Wahls interaction from which a non-universal regularisation parameter can be determined for a given atom. As discussed in section 5.4 a similar regularization is required for squared commutators involving the momentum-operators and these values (regardless of the quench type) are therefore non-universal and determined by the same short-range parameter. Once such a parameter has been chosen, everything about the system is fixed (see appendix A.2 for more details on the other correlation functions). The simplest way to regularize is to impose an energy cutoff at some j_{cut}, but relating a possible cut-off value to the non-universal physical features of a given system is beyond the scope of this chapter.

5.8 Comparison of the quenches and concluding remarks

In summary, I have shown that for harmonically trapped interacting atoms, which are a fundamental building block in many cold atom experiments, the time-average of the irreversibility measure $I_{AB}(t)$ and the full operator scrambling $C_{AB}(t)$ for canonical operators are proportional to the work fluctuations. It was also shown that finite interactions that break the harmonicity of the spectrum are required for scrambling to occur, as the harmonic spectrum display trivial breathing dynamics for any initial state. The times-scales required to observe scrambling diverge as these non-scrambling harmonic limits are approached ($g \to 0, g \to \infty$), highlighting the importance of intermediate interactions to be able to achieve meaningful scrambling time-scales. Additionally the dynamics of the operator scrambling has been connected to the diagonal ensemble probabilities - the distribution of which determines whether operators delocalise to more and more highly excited states as the post-quench time increases.

This allows one to explain the different scrambling behaviour of the trap and interaction quenches in terms of the work probability distribution. The dynamical behaviour of the squared commutator and particularly the 3-OTOC $I_{xx}(t)$ clearly shows qualitatively different behavior for the two. For an interaction quench, the work probability

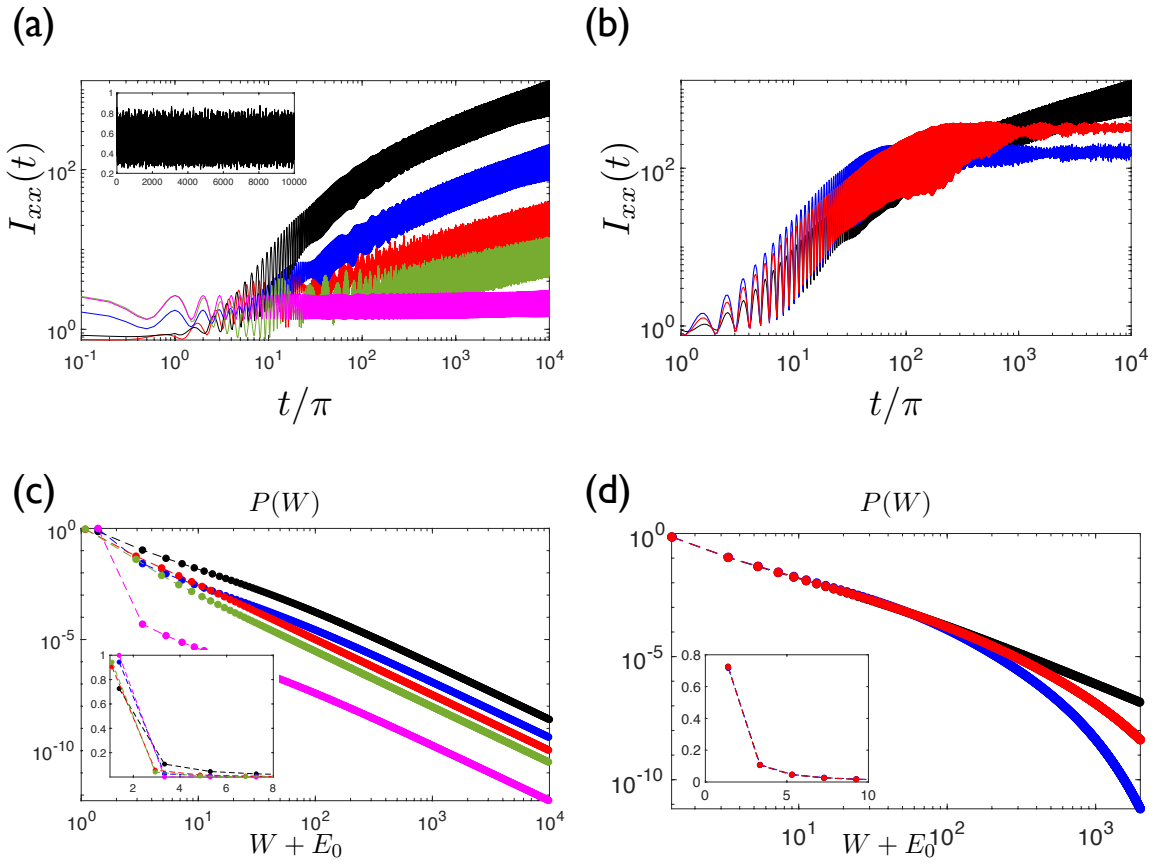

Figure 5.4: $I_{xx}(t)$ as a function of time and $P(W)$ for the same quenches are depicted respectively in (a) and (c) with black corresponding to $g_I = 0, g_F = 10, \langle W_{\text{irr}} \rangle = 4.74, \bar{L} = 0.5417$, red corresponding to $g_I = 0, g_I = 2, \langle W_{\text{irr}} \rangle = 0.54, \bar{L} = 0.8228$, blue corresponding to $g_I = 2, g_I = 10, \langle W_{\text{irr}} \rangle = 0.75, \bar{L} = 0.8917$, green corresponding to $g_I = 10, g_I = 2, \langle W_{\text{irr}} \rangle = 0.22, \bar{L} = 0.8926$ and magenta corresponding to $g_I = 9, g_F = 10, \langle W_{\text{irr}} \rangle = 0.0011, \bar{L} = 0.9998$. (b) and (d) also depict $I_{xx}(t)$ as a function of time and $P(W)$, but for different Guassian interaction quenches from non-interacting to $\sigma = 0.07, \kappa = 10, \langle W_{\text{irr}} \rangle = 3.08, \bar{L} = 0.5287$ (blue line) and $\sigma = 0.04, \kappa = 11, \langle W_{\text{irr}} \rangle = 3.49, \bar{L} = 0.5389$ (red line). The black line shows the $g_I = 0, g_F = 10$ delta-function interaction quench for reference as these all have similar energy eigenvalues.

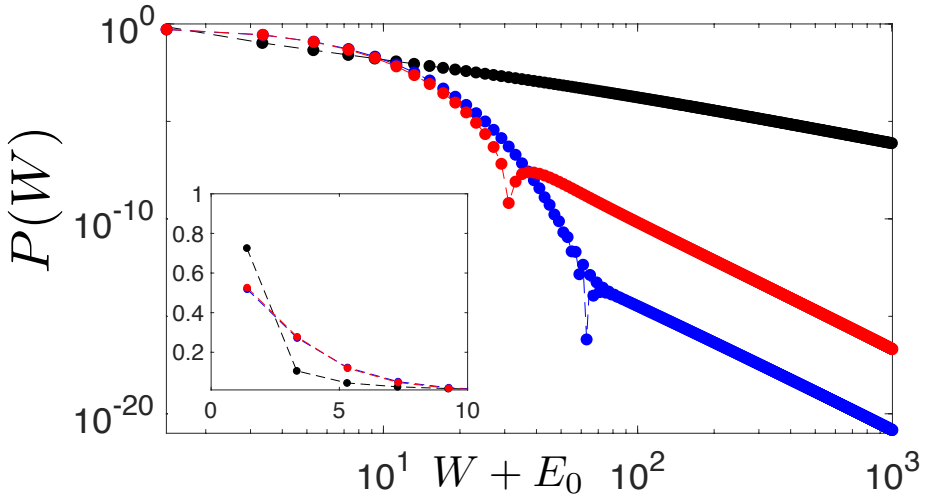

Figure 5.5: The work probability distribution for $g = 10, \gamma = 4$ (red line), $g = 10, \gamma = \frac{1}{4}$ (blue line) and $g_I = 0, g_F = 10$ (black line).

distribution involves more highly excited states of the final Hamiltonian, due to the slow decay of the DE probabilities as $|c_{2j}|^2 \propto j^{-5/2}$ (see Fig. 5.5), and the squared commutator will eventually have contributions from all excited states on long enough time-scales. These long time-scales are required because the energies of the high-lying states become closer and closer to the non-interacting harmonic energies, which leads to a larger time-scale required in order to see them in the dynamics. In physical systems a finite range parameter sets an upper limit to the number of excited states that can participate in the dynamics and therefore determines a saturation time-scale. For a trap quench on the other hand, only the first few states contribute to the dynamics, as seen from the corresponding work probability distribution in Fig. 5.5, which means that highly excited states do not contribute on any time-scale. The scrambling properties can therefore be determined by looking at relatively short time-scales for intermediate interaction strengths. That the trap and interaction quench is fundamentally different is obvious by comparing the full work probability distributions which are qualitatively very different (see Fig. 5.5), but the investigation in this chapter has shown that the important difference between them in terms of the post-quench scrambling is their different variances, which is generally larger for the interaction quench, which will therefore display more scrambling.

Post-quench operator scrambling in Hilbert space is therefore intimately linked to the work probability distribution, which is an experimentally accessible thermodynamic measure [36–38] of the non-equilibrium excitations induced by the quench. While our results are of relevance for modern few-body cold atom experiments [65], these insights should also hold in larger systems where the structure of the relative Jacobi-coordinates ensure that the relevant asymptotic criteria are still obeyed.

Chapter 6

Fock-space diagonalization using effective one- and two-body Hamiltonians

In this chapter I will apply the effective Hamiltonian approach to the Fock space exact diagonalization method explained in chapter 3.4. The main idea of the effective Hamiltonian approach is to incorporate information obtained from exact solutions of the external and interaction potentials in position space into the many-body Hamiltonian through the matrix elements H_{kl} and V_{klmn} (see Eq.(3.62 ,3.63) in chapter 3.4). If the mode expansion is done in terms of single-particle eigenstates for the external potential information about the former is already incorporated. However, in some cases of interest such as for a change in the external potential during a quench one has to choose a single-particle basis corresponding to the final Hamiltonian, which worsens the convergence properties of the initial state. Additionally, the presence of two-body interactions cause slow convergence with respect to basis size, even using the respective single-particle basis [164]. This is partly because the delta-function interactions of interest creates cusps in the many-body wavefunctions that are difficult to accurately represent using a smooth basis. In the case of contact interactions in a harmonic trap the exact analytic solutions are known as described in chapter 3.2 and it is possible to incorporate the knowledge of the exact two-body solution and the exact one-body solution in a different basis by utilizing the effective Hamiltonian approach. This approach allows us access to exact solutions in a restricted part of the solution space, employing a finite basis set.

The content of this chapter is a synthesis of various known methods for which the basic idea goes back to the 50'ies, suggested in the context of nuclear physics [165–167]. I will utilize the simple formula for the effective Hamiltonian first presented in [168], which was first used in the context of cold atomic gases in [169] and extended to two-component systems (with zero intra-particle interactions) in [116] (in both cases for a harmonic oscillator potential). Note that in these previous works the exact diagonalization was generally done in configuration space, while I will do the exact diagionalization

in Fock-space. I will present a general overview and application to two-component systems with arbitrary interaction strengths and external potentials.

Other methods for improving convergence properties exist, including renormalisation of the interaction constant utilizing the TG-energies [170], a different unitary transformation approach to build an effective Hamiltonian (not based on the interaction potential solution) [171] and variationally optimizing the basis in order to obtain more accurate results for a target state [172]. An improvement method, which can be used in conjunction with other methods is to choose the reduced Fock-basis in ordered by lowest non-intracting many-body energies rather than simply the lowest M single particle energy modes [128]. This last approach dramatically reduces the Hilbert space required to accurately represent intermediate excited states, as the usual selection takes very high energy non-interacting states into account while ignoring lower energy non-interacting states that matter more at the relevant energies. In fact, I have implemented this basis choice in conjunction with the effective Hamiltonian approach, leading to even better convergence, however, to keep the focus on the effective Hamiltonian I will compare the bare and effective Hamiltonians using the conventional choice of Fock-basis in this chapter.

6.1 Effective Hamiltonians in a model-space

The effective Hamiltonian approach, which has its roots in nuclear physics, is a general procedure which is useful for diagonalizing complicated Hamiltonians that do not necessarily have nice convergence properties for simple basis sets. Consider the solution of the eigenvalue equation

$$\hat{H}|\psi\rangle = E|\psi\rangle. \tag{6.1}$$

The Hilbert space can be split into two subspaces, a (small) model-space P and the complement Q corresponding to the remaining Hilbert-space. The projection operators $\hat{P}, \hat{Q}$ project onto these subspaces respectively. Deriving an effective Hamiltonian which acts within the restricted model-space and yields the same eigenvalues as the original Hamiltonian is the goal. This can be done by finding a way to transform the Hamiltonian $\hat{H}$ with a unitary transformation such that the solutions to the P and Q spaces decouple and the solutions in P-space are the same as those in the original system. Consider the Hamiltonian after a unitary transformation $\hat{H}' = \hat{U}^\dagger \hat{H} \hat{U}$ (note that this doesn't change the eigenvalues). Utilizing the projection operators the Hamiltonian equation of this system can be written as

$$\begin{pmatrix} \hat{P}\hat{H}'\hat{P} & \hat{P}\hat{H}'\hat{Q} \\ \hat{Q}\hat{H}'\hat{P} & \hat{Q}\hat{H}'\hat{Q} \end{pmatrix} \begin{pmatrix} \hat{P}|\psi'\rangle \\ \hat{Q}|\psi'\rangle \end{pmatrix} = E \begin{pmatrix} \hat{P}|\psi'\rangle \\ \hat{Q}|\psi'\rangle \end{pmatrix} \tag{6.2}$$

It is clear that the P and Q-space equations decouple when $\hat{Q}\hat{H}'\hat{P} = \hat{P}\hat{H}'\hat{Q} = 0$ in which case the P-space operator $\hat{P}\hat{H}'\hat{P}$ is an effective Hamiltonian, i.e.

$$\hat{H}_{eff}(\hat{P}\hat{U}|\psi\rangle) = \hat{P}\hat{U}^\dagger \hat{H} \hat{U} \hat{P}(\hat{P}\hat{U}|\psi\rangle) = E(\hat{P}\hat{U}|\psi\rangle) \tag{6.3}$$

that has the same eigenvalues as the original equation in the P-space. The general idea is to determine the unitary transformation that fulfills the decoupling condition. In the case where one can actually solve the full problem for some Hamiltonian $\hat{H}_2$ the effective Hamiltonian in the model space which fulfills the decoupling condition can explicitly be written in a simple form [168]:

$$\hat{H}_{eff} = \frac{\hat{U}^{\dagger}_{2,P}}{\sqrt{\hat{U}^{\dagger}_{2,P}\hat{U}_{2,P}}} E_{2,P} \frac{\hat{U}_{2,P}}{\sqrt{\hat{U}^{\dagger}_{2,P}\hat{U}_{2,P}}} \tag{6.4}$$

where U_2 is the unitary transformation that diagonalizes H_2 and E_2 are the corresponding eigenvalues

$$E_2 = \hat{U}^{\dagger}_2 \hat{H}_2 \hat{U}_2. \tag{6.5}$$

The P-subscripts then signify the projection of these onto the P-model space.

This holds true for any generic Hamiltonian. Now I want to apply this approach not to a full Hamiltonian, but to the one-body and two-body interaction terms in a many-body model. This is achieved by replacing these terms with an equivalent effective Hamiltonian when evaluating the matrix elements. For the interaction potential the full solution can also be found in terms of a one-body problem in the relative coordinate, but the interaction integrals are given in terms of the laboratory frame coordinate eigenfunctions. A transformation between these two frames in terms of the eigenfunctions is therefore required. As with the effective interaction, this is an old problem which has been addressed in nuclear physics [173, 174].

6.2 The Talmi Transformation (interaction integrals)

The most general interaction integral is given by

$$V^{AB}_{klmn} = \int dx_1 dx_2 \phi^{*A}_k(x_1) \phi^{*B}_l(x_2) V(x_2 - x_1) \phi^{A}_m(x_1) \phi^{B}_n(x_2). \tag{6.6}$$

As the two-body interaction only depends on the relative coordinate, it is possible to simplify this integral by transforming to the CM and relative coordinate frame. To do this one needs to expand the coordinate frame eigenfunctions in terms of the relative and center-of-mass eigenfunctions. The coordinate transformation between the lab frame coordinates and relative/center of mass coordinates are defined as

$$x = \frac{1}{\mu_x}(x_2 - x_1) \quad , X = \frac{1}{\mu_x}(x_2 + x_1) \tag{6.7}$$

where the constants μ_r, μ_R can be chosen in whichever way is most convenient for solving the problem at hand. Labeling the eigenstates of the laboratory frame as $\phi_{n_1}(x_1), \phi_{n_2}(x_2)$ and the eigenstates of the relative/center of mass frame as $\phi_n(x), \phi_N(X)$

this expansion can be formally written as

$$\phi^A_{n_1}(x_1)\phi^B_{n_2}(x_2) = \sum_{n,N} M^{n,N}_{n_1,n_2}, \phi_n(x)\phi_N(X) \tag{6.8}$$

where $M^{n,N}_{n_1,n_2}$ are the expansion coefficients. The integral can then be transformed to these new coordinates as(this is known as the Talmi transformation [173, 175])

$$V_{klmn} = \det(J) \sum_{j,j',N} \left(M^{j,N}_{k,l}\right) M^{j',N}_{m,n} v_{jj'} \tag{6.9}$$

where J is the Jacobian of the coordinate transformation between the lab an CM/relative frame and

$$v_{jj'} = \int dx dx' \phi^*_j(x) V(x\mu_x, x'\mu_x)\phi_{j'}(x'). \tag{6.10}$$

or

$$v_{jj'} = \int dx \phi^*_j(x) V(x\mu_x)\phi_{j'}(x). \tag{6.11}$$

for a local potential $\langle xx'|\hat{V}|xx'\rangle = V(x)\delta(x-x')$. Here I have utilized that the center-of-mass coordinate integral decouples from the rest and therefore only terms with $N = N'$ have non-zero values in the sum reducing the task to the evaluation of a single integral. This becomes even simpler for the zero-range interaction which is the main topic of interest in this thesis. Here one can evaluate

$$v_{nn'} = \int dx \phi^*_n(x) g/\mu_x \delta(x)\phi_{n'}(x) = g/\mu_x \phi^*_n(0)\phi_{n'}(0) \tag{6.12}$$

which means that analytic formulas for the interaction integrals can be found in cases where analytic formulas for the coefficients (and single-particle eigenstates) exist. At first glance, however, this does not seem like much of an improvement, as one now needs to evaluate an infinite sum for each state one wishes to express in the relative/center-of-mass eigenbasis. However, there are some single-particle bases for which this sum is finite and for which simple expressions of the coefficients can be obtained, namely free space (plane-waves) and harmonic oscillator eigenfunctions. The finite sum is a consequence of the separability of the Hamiltonians describing these two-particle systems, which means that only states with the same energy as the lab-frame eigenstate enters the sum. For the harmonic oscillator the coefficients are called the Talmi-Brody-Moshinsky coefficients and I will utilize the HO basis as the computational basis for ED in the rest of this chapter. Simple analytic expressions of these coefficients exist for identical particles [175, 176], mass-imbalanced particles [177] and even particles in different external trapping frequencies [178]. Note that Eq.(6.12), while simple, does not incorporate any information about the two-body solution which was the motivation for applying this transformation. So let us now consider, how to use the effective Hamiltonian in conjunction with this interaction integral.

6.3 Application of Effective Hamiltonians for ED

I will be utilizing the harmonic oscillator eigenstates and consider the model-space consisting of all oscillator states ϕ_n with a quantum number smaller than $n_{\max}$. The effective Hamiltonian for a system with eigenfunctions ψ_n can then be obtained from Eq.(6.4) in terms of the matrix representation of $U_{2,P}$ which is given as

$$U_{2,P} = \begin{pmatrix} \langle\phi_1|\psi_1\rangle & \phi_1|\psi_2\rangle & \cdots & \langle\phi_1|\psi_{n_{\max}}\rangle \\ \langle\phi_2|\psi_1\rangle & \phi_2|\psi_2\rangle & \cdots & \langle\phi_2|\psi_{n_{\max}}\rangle \\ \vdots & \vdots & \ddots & \vdots \\ \langle\phi_{n_{\max}}|\psi_1\rangle & \langle\phi_{n_{\max}}|\psi_2\rangle & \cdots & \langle\phi_{n_{\max}}|\psi_{n_{\max}}\rangle \end{pmatrix}. \tag{6.13}$$

If ψ_n are the eigenfunctions of the interacting relatice coodinate part, an effective interaction can then be obtained simply by subtracting the HO single-particle energy H_0, i.e. $\hat{V}_{eff} = hat H_{eff} - \hat{P}\hat{H}_0\hat{P}$. So far I have constructed an effective two-body interaction in a model-space consisting of a restricted basis of HO eigenfunctions, which essentially means that one can get exact two-body results utilizing this model-space as our basis. The next step is to relate this to the many-body diagonalization. A formal relation can be obtained by considering the cluster expansion of the many-body Hamiltonian and demanding that the correlation operator be chosen such that the effective two-body interaction in the expansion corresponds to the hermitian effective interaction derived above [167]. I will not do this explicitly, instead I will simply replace the bare two-body interaction with the effective two-body interaction in the many-body Hamiltonian. In practice this means that

$$V_{klmn} = \det(J) \sum_{j,j',N} \left(M^{j,N}_{k,l}\right) M^{j',N}_{m,n} \langle j|\hat{V}_{eff}|j'\rangle. \tag{6.14}$$

Note that the sum is finite and completely determined for any interaction integral V_{klmn} once $n_{\max}$ has been chosen. For any value of $\langle j|U_{2,P}|j'\rangle$ the only non-zero contribution to a given V_{klmn} is determined by $N = (k+l+n+m-j-j')/2$. Since the effective interaction gives exact two-body results in the model-space, it is expected that the convergence properties of the many-body Hamiltonian using the same basis-states will be significantly improved with respect to the bare interaction and this is borne out in the numerics.

A similar mapping is possible for the one-body integral, but this one is much simpler as no coordinate transformation is required. Indeed in this case the matrix elements are simply given by

$$H_{kl} = \langle k|H_{eff}|l\rangle. \tag{6.15}$$

One thing to note is that it is not possible to choose n_{max} independently of the number of modes M used for the exact diagonalization for the one-body potential, with $n_{max} = M$ always being true. Using this method it should also be possible to get accurate results for species-dependent external potentials as the effective one-body Hamiltonians can be calculated separately for the two species.

6.4 Advantages (and disadvantages) of the effective Hamiltonian approach

There exists a variety of methods for improving exact diagonalization results. For example in [170] it was shown that a dramatic improvement in convergence properties could be achieved by rescaling the interaction strength. In [172] an auxiliary parameter which can be used to optimize the basis was introduced which likewise led to dramatic improvement. The latter method, however, targets a specific state, nominally the ground-state, while the former improves convergence of low-lying states as well, but less so the higher one goes in the spectrum. This makes such methods less useful for investigating the properties of the spectrum, as higher-lying states are not necessarily more accurate than for the bare interaction approach. The effective interaction approach on the other hand, improves the results of excited states in addition to the ground-state as can be seen in Fig. 6.1 and is therefore more suitable for quench dynamics which requires access to a large part of the final Hamiltonian spectrum. In the following sections I will show that the effective interaction approach leads to more accurate results for a smaller number of modes M in general, which enables the study of larger and more strongly interacting systems, since the size of the Fock-space Hamiltonian sets a hard limit beyond which full diagonalization is not feasible. The method is therefore more about accuracy and pushing the limits than time-efficiency. Indeed, building the Fock space Hamiltonian for the effective interactions is slower than for the bare interaction with the evaluation of interaction integrals taking longer as $n_{\max}$ is increased. However, this evaluation is only required once and the time required is insignificant compared with the time required to calculate dynamical quantities. In so far as the same accuracy can be obtained for a smaller Hilbert-space the method therefore also leads to faster numerical evaluation of dynamics.

6.4.1 Identical particles in a harmonic trap

For two particles, the effective interaction trivially gives the exact results, as it is build into the model-space, and a minimum of three particles is therefore required to gauge whether or not the effective interaction actually improves convergence. I focus on three particles as this allows me to go to a large number of modes M, while still retaining a relatively small Hilbert space, but similar improvement of convergence is seen for $N = 4$ and in section 6.4.2 I will investigate the more complicated 2+2 case. In Fig. 6.1 the different energies of 3 particles with $g = 100$ is plotted as a function of the number of modes for the bare interaction and a variety of values for $n_{\max}$. I have chosen the strongly interacting value for two reasons. The first is that getting good convergence for strongly interacting systems is more difficult than for weaker interactions and this is therefore a good test of how well the method performs when pushed to the limit. The second is that it enables a comparison with the TG-limit for which the energies are known. Note that the numerical system is not actually in the TG-limit and the relative difference between the calculated energy and the TG-energy plotted in Fig. 6.1 is not the relative error from the exact solution at $g = 100$. Nevertheless, it is illustrative and clearly shows that the bare interaction for the ground-state is not converged even

at $M = 40$ ($D = 11480$) and overestimates the energy, which is known to be slightly smaller than 4.5ω (the TG energy). This is unsurprising as it has been shown that the error scales with $M^{-\frac{1}{2}}$ in this case [164]. The effective interaction gives better results, including for excited states. In fact the same accuracy for the ground state can be obtained for $D = 220$ ($M = 10$) as for the bare interaction at $D = 11480$ ($M = 40$). For the $n = 100$ excited state on the other hand, $D = 1540$ ($M = 20$) is required to have roughly the same accuracy as the bare interaction at $D = 11480$ ($M = 40$), but this is still a dramatic reduction in Hilbert space size.

One potential drawback of the method is also clear from the figure. Namely, the dependence on $n_{\max}$ makes the question of convergence slightly more complicated. It is clear that for a small model-space $n_{\max} = 20$ the results converge quickly with M. However, as can be seen from the results for the ground-state, this value does not correspond to the converged values for larger $n_{\max}$. The model with $n_{\max} = 20$ is converged, but this does not correspond exactly to the original Hamiltonian. As $n_{\max}$ increases, however, their values at $M = 40$ start to converge to the same value. This means that there is a trade-off between convergence in terms of M and convergence in terms of $n_{\max}$, requiring an optimal choice of the latter parameter. For $n_{\max} \to \infty$ the bare interaction model would be recovered.

6.4.2 Two-component systems in harmonic trap

The method also works quite well for two-component systems. In this case, the effective interaction must be implemented separately for each interaction term. Let us check the convergence properties of the 2+2 system. For reasons similar to above I consider the strongly interacting case of $g_A = g_B = g_{AB} = 100$. Compared to the 3-particle system, the amount of modes that can reasonable be dealt with is much smaller. I investigate with a maximum of $M_A = M_B = 18$ corresponding to $D = 29241$. This in turn limits the values of $n_{\max,\mathrm{A}}, n_{\max,\mathrm{B}}, n_{\max,\mathrm{AB}}$ for which improved convergence can be achieved. The results are displayed in Fig. 6.2. It turns out that the convergence properties are particularly sensitive to $n_{\max,\mathrm{AB}}$ and keeping this smaller than the other two generally leads to better numerical results. Compared with the bare interaction, it is clear that the results for these (relatively small) model spaces are still much closer to the real values of the energy as the bare interaction overestimates the energy compared to the TG-limit. Indeed, the bare interaction performs worse relative to the bare interaction for the $N = 3$ case, although it should be noted that the error is not quite as large for smaller values of g_A, g_B, g_{AB}. The effective interaction energies are converging to a similar value as n_{max}-values are slowly increased. Clearly, the 2+2 case is more complicated than $N = 3, 4$ and one needs to be careful about the choice of model-space, but improved accuracy can be achieved. Let me also note that mass-imbalanced systems can be solved using the same method, utilizing the Talmi-Brody-Moshinsky coefficents for mass-imbalanced systems [177] for the required Talmi transformation and the HO basis sets for the different masses for the two species.

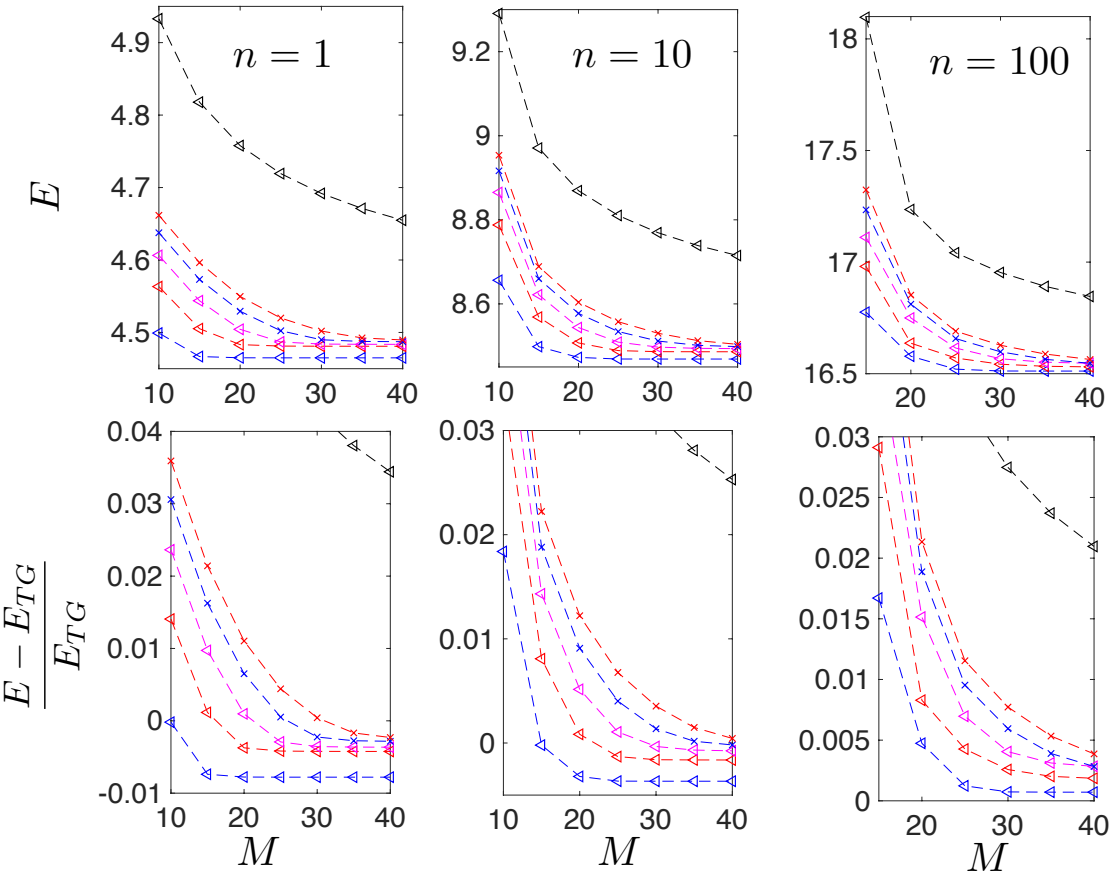

Figure 6.1: The energies as well as the relative difference with the respective Tonks-energies for the $n = 1, 10, 100$ states, as a function of the number of modes M for $N = 3$ particles in a harmonic trap with $g = 100$. The black triangles correspond to the ED scheme with no effective interaction. The remaining plots correspond to the effective interaction with $n_{\max} = 20$ (blue triangles), $n_{\max} = 30$ (red triangles),$n_{\max} = 40$ (magenta triangles), $n_{\max} = 50$ (blue crosses) and $n_{\max} = 60$ (red crosses).

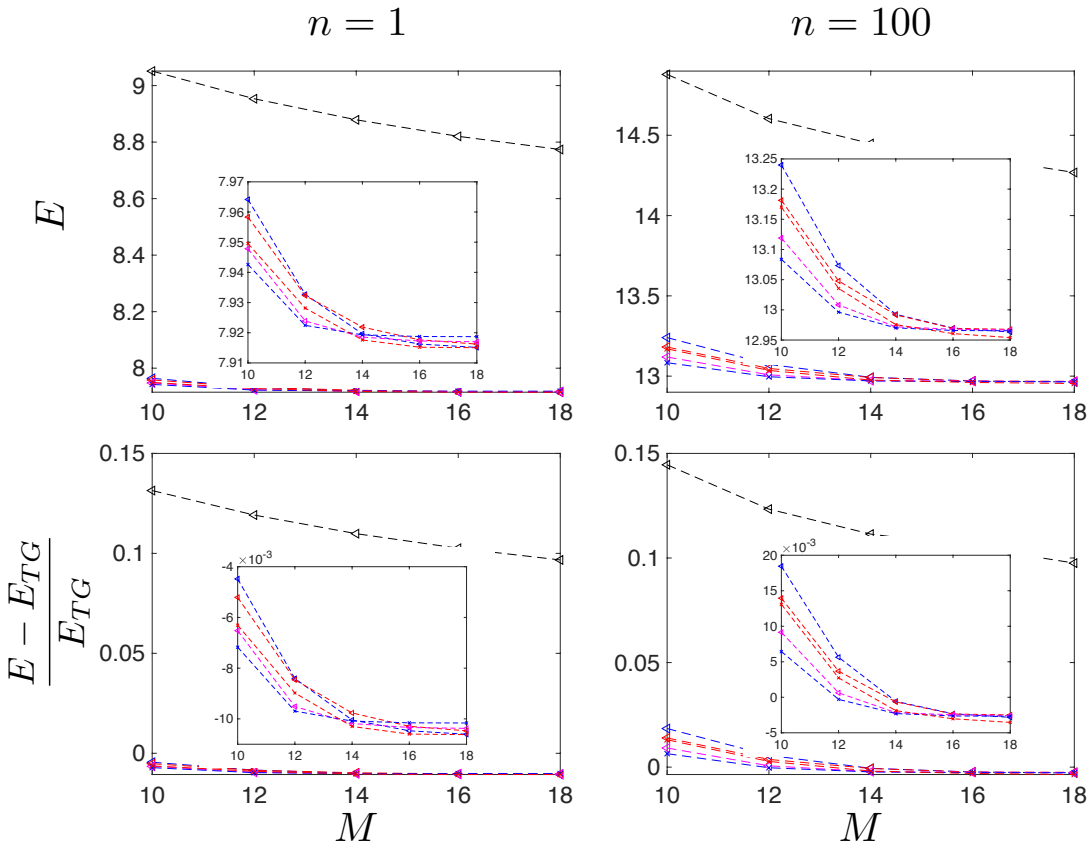

Figure 6.2: The energies as well as the relative difference with the respective Tonks-energies for the $n = 1, 100$ states, as a function of the number of modes M for $N_A = 2, N_B = 2$ particles in a harmonic trap with $g_A = g_B = g_{AB} = 100$. The black triangles correspond to the ED scheme with no effective interaction. The remaining plots correspond to the effective interaction with $n_{\mathrm{max,A}} = n_{\mathrm{max,B}} = 20, n_{\mathrm{max,AB}} = 12$ (blue triangles), $n_{\mathrm{max,A}} = n_{\mathrm{max,B}} = 20, n_{\mathrm{max,AB}} = 10$ (red triangles),$n_{\mathrm{max,A}} = n_{\mathrm{max,B}} = 16, n_{\mathrm{max,AB}} = 10$(magenta triangles), $n_{\mathrm{max,A}} = n_{\mathrm{max,B}} = 14, n_{\mathrm{max,AB}} = 10$(blue crosses) and $n_{\mathrm{max,A}} = n_{\mathrm{max,B}} = n_{\mathrm{max,AB}} = 14$(red crosses). The insets show the same, but zoomed in on the relevant range for the effective interaction values.

6.4.3 Identical particles in a double-well potential

So far I have investigated the properties in a harmonic oscillator for which the effective interaction approach is particularly well-suited since it relies on the HO basis which in this case coincides with the SP basis of the external potential. It is therefore also relevant to investigate how well the method performs in a different potential compared with the bare interaction utilizing the SP eigenfunctions of that external potential in its basis. To do this I incorporate the effective Hamiltonian approach for the external potential part as described in section 6.3. I consider $N = 3$ particles in a double well potential described by $V_{\text{ext}}(x) = -\frac{1}{2}x^2 + 0.0225x^4$ in the strongly interacting limit of $g = 100$. As can be seen from Fig. 6.3 the effective interaction approach utilizing the HO basis still converges much faster than the bare interaction utilizing the SP basis of $V_{\text{ext}}(x)$. The results for the bare interaction for the $n = 100$ state is omitted as the code runs into numeric problems for higher-lying states for this particular potential. This shows another advantage of the effective interaction, it is seemingly more stable towards such problems. One caveat to keep in mind is that for the mapping onto the model-space to work, a HO basis with eigenfunctions that have a comparable spatial extent as the eigenfunctions for $V_{\text{ext}}(x)$ is required.

6.5 Quench dynamics in two-component systems and quantum speeds

This project is still in its early stages, but I include a few preliminary results in this thesis as an example of an application of the improved ED technique. Note that while the code utilized for these calculations was written by me, the actual calculations were performed on the OIST cluster in collaboration with Tai Tran, another PhD student in my unit.

The main aim of this project is to dynamically investigate the consequence of quenching between the different correlation regimes described in [119]. Towards this end, an investigation of post-quench dynamical observables such as the densities, momentum-distribution and reduced density matrices is performed. Further characterization in terms of derived quantities such as the coherence, the von Neuman entropy and survival probabilities is also considered. Finally an attempt at establishing a link between the instantaneous speed of the reduced density matrix time-evolution and the coherence properties, similar to that proposed in [179], will be made. In this section I will briefly note a few intriguing properties of one particular quench, namely going from the phase-separated BEC-TG regime $g_A = g_{AB} = 20, g_B = 0$ to the fully fermionized regime $g_A = g_B = g_{AB} = 20$.

In Fig. 6.4 the quantities related to the reduced single particle density matrix of the two components are shown. There is a clear separation of time-scales visible for the speed and the von Neuman entropy, both of which change dramatically within the first five oscillator periods, but are relatively constant afterwards. However, the system has not equilibrated in any meaningful sense as is clear from the single particle densities which display large oscillations after this initial time-scale. However, a periodic oscillation is

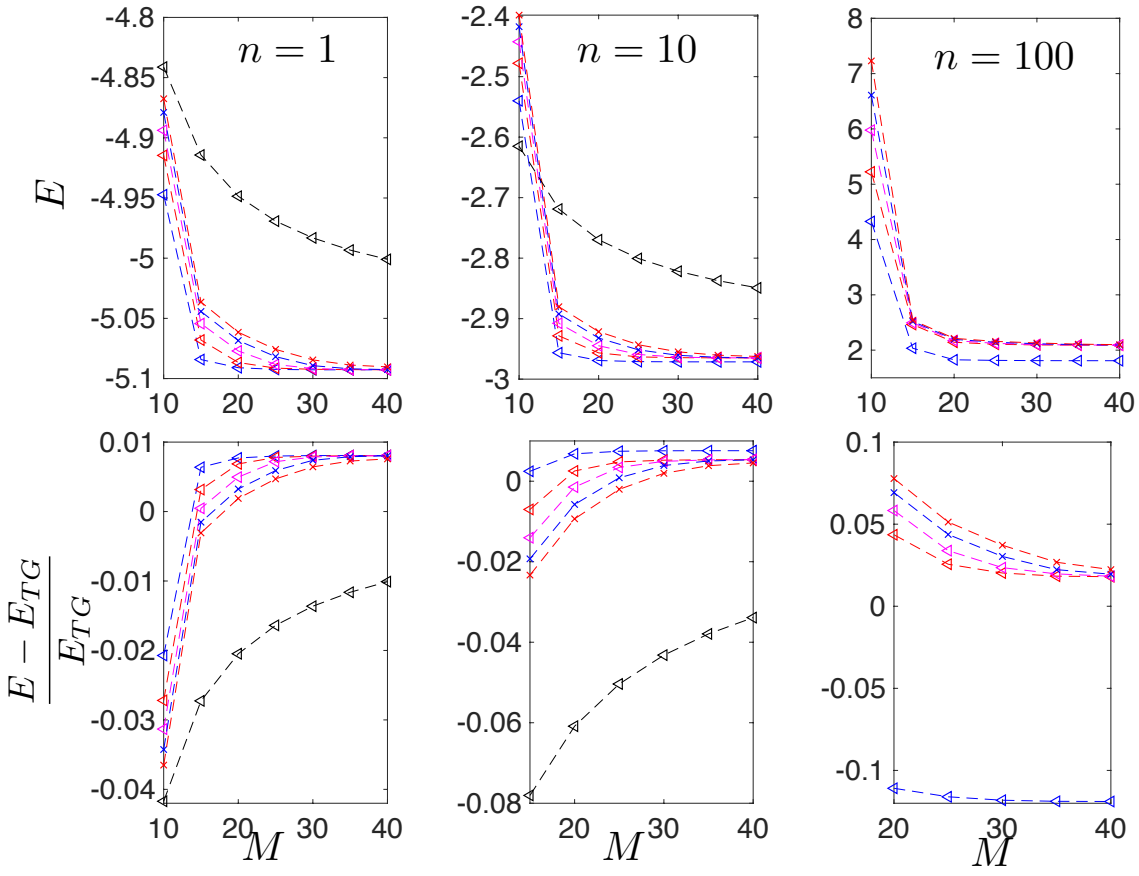

Figure 6.3: The energies as well as the relative difference with the respective Tonks-energies for the $n = 1, 10, 100$ states, as a function of the number of modes M for $N = 3$ particles in a double well trap with $g = 100$. The black triangles correspond to the ED scheme with no effective interaction. The remaining plots correspond to the effective interaction with $n_{\max} = 20$ (blue triangles), $n_{\max} = 30$ (red triangles),$n_{\max} = 40$ (magenta triangles), $n_{\max} = 50$ (blue crosses) and $n_{\max} = 60$ (red crosses).

obtained after an initial reorganization in the first five oscillator periods corresponding to the time-scale at which the speed and von Neuman entropies become constant. Looking at the natural orbitals it is clear that for the coherence (the first orbital) the equilibration-like behaviour of the speed and von Neuman entropy is not observed and that this is therefore an effect that comes from taking into account multiple natural orbital occupations as is required in both of these measures. A further understanding of this separation of time-scales and how it can be understood is one of the current aims of the project.

Additionally, it is observed that the speed with which the two subsystems evolve oscillates with respect to each other during the initial five oscillator periods. This is not observed for the von Neuman entropy and is therefore a consequence of the natural orbitals, the time evolution of which is important for the speed. A further understanding of the physical meaning of this is an interesting topic as well. Finally, quenches between different regimes are of interest. For the quench showcased here the final Hamiltonian is symmetric with respect to A and B which is why both the speeds and the entropies go towards the same value at longer times. This is no longer true for different final Hamiltonians.

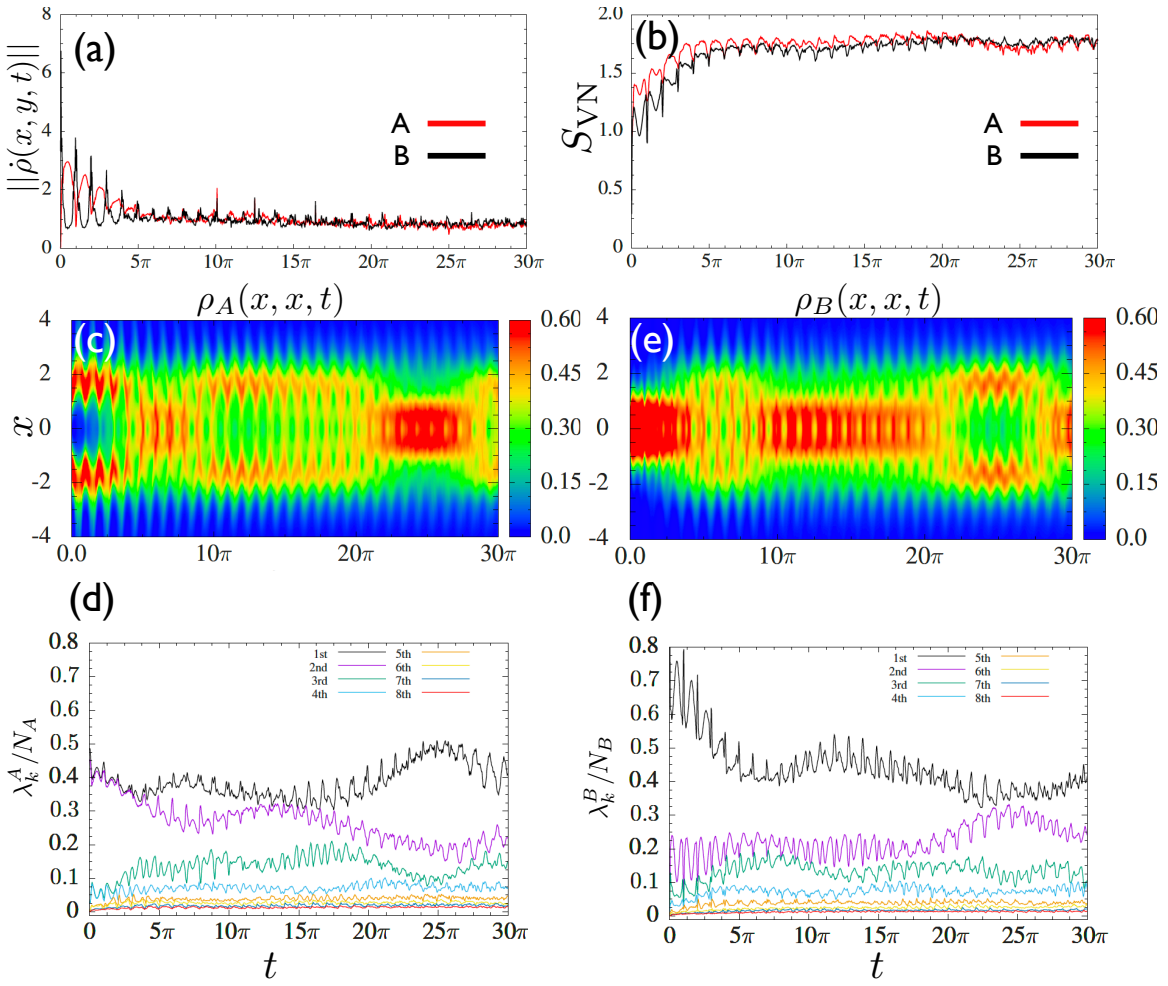

Figure 6.4: Postquench dynamics of quantities related to the RSPDM of the two components. (a) shows the quantum speed, while (b) shows the von Neuman entropy. (c) and (d) show the single particle density and the occupation of the first 8 natural orbitals respectively for component A, while (e) and (f) show the same for component B.

Chapter 7

"Optomechanics with a position-modulated Kerr-type nonlinear coupling" (originally published as [2])

7.1 Introduction

This project deals with an open quantum system as opposed to the closed unitary dynamics that has been the focus so far and it is related to the experimental platform of solid-state nano-nodevices and cavity QED rather than cold atoms. Conceptually, it therefore complements these other works by extending the concerns with dynamics to open quantum systems, however a price has to be paid. Namely, the system can no longer be treated exactly in the quantum regime and the main focus is on the semi-classical limit. The choice of platform, however, ensures that the semi-classical limit is experimentally relevant as many optomechanical experiments are performed in this regime [18]. The details of the investigation are reported in [2]. Here I will briefly summarise the study and results as well as discuss a few developments since the publication of the paper.

The motivation for this study is the consideration of nonlinear light-matter interactions. In general, much interest in optomechanical systems is that they provide a coupling of a macroscopic mechanical element to the electromagnetic field of a cavity [18]. This allows for many interesting features, such as red side-band cooling of the mechanical element [180, 181], lasing [182] and precision sensing [183–186]. The mechanical element and the cavity interact via radiation pressure, which pushes the mechanical element and therefore changes the resonance frequency, making it dependent on the displacement of the center-of-mass motion of the mechanical element q, i.e. $\omega(\hat{q})$. Since the harmonic oscillator is described by $\hbar\omega(\hat{q})\hat{a}^\dagger\hat{a}$ this gives rise to a position-dependent interaction

which is linear in the optical-field operators.

$$\omega(\hat{q}) \approx \omega(0) + \left.\frac{d\omega(\hat{q})}{d\hat{q}}\right|_{\hat{q}=0} \hat{q} = \omega_0 - g_{\mathrm{L}}\hat{q} \tag{7.1}$$

In [2] I suggest and conceptualize a position-coupling that is nonlinear in the field operators. Such a coupling can be obtained from a $\chi^{(3)}$ material described by $H_{\mathrm{Kerr}} = \eta\hbar\hat{a}^\dagger\hat{a}^\dagger\hat{a}\hat{a}$, i.e. a two-photon process. A position-dependent interaction is obtained if the nonlinear coefficient depends on q, ie. $\eta(\hat{q})$. If this can be engineered the nonlinear coefficient will be given similarly to the linear coefficient as

$$\eta(\hat{q}) \approx \eta(0) + \left.\frac{d\eta(\hat{q})}{d\hat{q}}\right|_{\hat{q}=0} \hat{q} = \eta_0 - g_{\mathrm{NL}}\hat{q}. \tag{7.2}$$

In [2] I make some suggestions for how a position-dependence can be experimentally engineered. The majority of the paper is concerned with a thorough analysis of the consequences of this interaction, particularly in the resolved red sideband regime where the mechanical element can be cooled down. This analysis is done utilizing the Quantum Langevin formalism (see for example [187]) for which the Heisenberg equations are modified to contain photonic losses in the cavity and mechanical dissipation associated with the finite temperature of the mechanical element. Steady state classical solutions are derived while linearised quantum fluctuations around these are investigated semi-analytically.

7.2 Publication

Mathias Mikkelsen, Thomás Fogarty, Jason Twamley and Thomas Busch, *Optomechanics with a position-modulated Kerr-type nonlinear coupling*, Physical Review A, **96**, 043832, 2017

7.3 Conclusion

The main takeaway of this analysis is that the effective non-linear coupling scales with the square of the photon number which means that effects associated with the strong-coupling regime can be seen even for small nonlinearites and at relatively low laser powers. This means that efficient cooling can be obtained at lower laser powers. Additionally the interplay between the nonlinear and linear interactions when they have opposite sign leads to three stable solutions with associated jumps and hysteresis behaviour.

The main result of this paper is the introduction of the position-modulated nonlinear Kerr coupling and the investigation into its fundamental behaviour. Since its publication, some further investigations based on the Hamiltonian I proposed in [2] have been undertaken by other researchers. In [188] an investigation of the photon blockade effect utilizing the nonlinear coupling was undertaken. They found that it can greatly enhance the photon blockade effect. In [189] they studied the blue sideband regime,

where phonon lasing can be achieved [182], rather than the red side-band regime which is optimal for cooling and was the main focus of our investigation. Due to the strong scaling of the nonlinear interaction with the number of photons in the cavity, large effective interactions required for phonon lasing can be achieved at very low powers. Finally, a recent proposal for a precision measurement of the gravitational acceleration g [190] is also based on the effective strong coupling obtained from the nonlinear coupling. They found that improved accuracy for the same measurement time is obtained in comparison with a scheme based solely on the linear optomechanical coupling as proposed in [186].

The common theme of these investigations is the utilization of the strong effective interaction which scales with the square of the photon number to achieve strong coupling. Further investigations utilizing this might be proposed in the future. On the other hand, a further analysis of the multi-stability obtained when the linear and nonlinear interactions are in competition has yet to be undertaken and might also be an interesting project.

Conclusion

Throughout this thesis I have investigated the dynamics of a variety of quantum systems. A short summary of the conclusions for each project is contained in this chapter, for more detailed conclusions please see the conclusions at the end chapters 4,5 and 7.

I showed how quenching to a moving lattice allowed for probing the phases of the many-body T-G gas in the lattice and how the critical region resulted in interesting dynamical fluctuations of the order parameter. I have also shown how there is an intimate connection between the non-equilibrium excitations created by a quench and the post-quench information scrambling as measured by the squared commutator of canonical operators for two interacting particles in a harmonic trap. Particularly I have shown that the time-averaged scrambling is proportional to the work fluctuations. In a continuum system such as the one under investigation it is very difficult to directly measure the operator scrambling and this connection therefore establishes a way to experimentally probe the scrambling for the harmonic trap with interacting particles which is a fundamental and important model in cold atom physics. I have also developed an improved method for exact diagonalization of few-boy continuum systems in chapter 6, which generally improves the convergence properties of even highly excited states and enables the investigation of quench dynamics for $N = 4, 5$ particles with finite interactions. This is important for further investigations of the topics considered in chapter 4 and particularly chapter 5 as well as other investigations of quench dynamics for interacting systems.

In chapter 7 I introduced and showed how to engineer a coupling between a Kerr nonlinear medium and the position of a mechanical element coupled to a cavity. I showed that this nonlinear Kerr coupling gives a much larger effective light-matter coupling than the usual linear optomechancial coupling, allowing one to enter the strong coupling regime at lower laser powers. This was shown by investigating the classical steady-state solutions and the dynamics associated with the quantum fluctuations. This large effective coupling is a useful resource for quantum engineering.

Overall I have shown how quenched and driven dynamics can be utilised to probe the properties of few- and many-body Hamiltonians utilizing three examples. In chapter 4 and 5 the unitary dynamics of few- and many-body cold atomic gases was considered, while the driven-dissipative mechanics of a light-matter coupled optomechanical system was considered in chapter 7.

Bibliography

[1] M. Mikkelsen, T. Fogarty, and T. Busch, *Static and dynamic phases of a Tonks–Girardeau gas in an optical lattice*, New J. Phys. **20**, 113011 (2018).

[2] M. Mikkelsen, T. Fogarty, J. Twamley, and T. Busch, *Optomechanics with a position-modulated Kerr-type nonlinear coupling*, Phys. Rev. A **96**, 043832 (2017).

[3] H. Kragh. *Quantum Generations: A History of Physics in the Twentieth Century.* Princeton University Press, (1999).

[4] M. Plischke and B. Birger, *Equilibrium Statistical Physics 3rd Edition*, World Scientific (2006).

[5] A. Altland and B. D. Simons. *Second quantization.* Cambridge University Press, 2nd edition, (2010).

[6] M. A. Nielsen and I. L. Chuang, *Quantum Computation and Quantum Information: 10th Anniversary Edition*, Cambridge University Press, USA, 10th edition (2011).

[7] C. Gardiner and P. Zoller, *Quantum Noise*, Springer-Verlag Berlin Heidelberg (2004).

[8] I. Rotter and J. P. Bird, *A review of progress in the physics of open quantum systems: theory and experiment*, Rep. Prog. Phys. **78**, 114001 (2015).

[9] M. Rigol, V. Dunjko, V. Yurovsky, and M. Olshanii, *Relaxation in a Completely Integrable Many-Body Quantum System: An Ab Initio Study of the Dynamics of the Highly Excited States of 1D Lattice Hard-Core Bosons*, Phys. Rev. Lett. **98**, 050405 (2007).

[10] M. Rigol, V. Dunjko, and M. Olshanii, *Thermalization and its mechanism for generic isolated quantum systems*, Nature **452**, 854–858 (2008).

[11] L. Vidmar and M. Rigol, *Generalized Gibbs ensemble in integrable lattice models*, J. Stat. Mech. **2016**, 064007 (2016).

[12] L. D'Alessio, Y. Kafri, A. Polkovnikov, and M. Rigol, *From quantum chaos and eigenstate thermalization to statistical mechanics and thermodynamics*, Adv. Phys. **65**, 239–362 (2016).

[13] I. Bloch, J. Dalibard, and W. Zwerger, *Many-body physics with ultracold gases*, Rev. Mod. Phys. **80**, 885 (2008).

[14] N. T. Zinner and A. S. Jensen, *Comparing and contrasting nuclei and cold atomic gases*, J.Phys.G **40**, 5 (2013).

[15] M. Lewenstein, A. Sanpera, V. Ahufinger, B. Damski, A. Sen(De), and U. Sen, *Ultracold atomic gases in optical lattices: mimicking condensed matter physics and beyond*, Adv. Phys. **56**, 243–379 (2007).

[16] M. A. Cazalilla, R. Citro, T. Giamarchi, E. Orignac, and R. M., *One dimensional bosons: From condensed matter systems to ultracold gases*, Rev. Mod. Phys. **83**, 1405 (2011).

[17] M. Mikkelsen, T. Fogarty, and T. Busch. *Connecting scrambling and work statistics for short-range interactions in the harmonic oscillator*, (2020).

[18] M. Aspelmeyer, T. J. Kippenberg, and F. Marquardt, *Cavity optomechanics*, Rev. Mod. Phys. **86**, 1391–1452 (2014).

[19] J. Werschnik and E. K. U. Gross. *Quantum Optimal Control Theory*, (2007).

[20] D. Guéry-Odelin, A. Ruschhaupt, A. Kiely, E. Torrontegui, S. Martínez-Garaot, and J. G. Muga, *Shortcuts to adiabaticity: Concepts, methods, and applications*, Rev. Mod. Phys. **91**, 045001 (2019).

[21] A. Silva, *Statistics of the Work Done on a Quantum Critical System by Quenching a Control Parameter*, Phys. Rev. Lett. **101**, 120603 (2008).

[22] C. Karrasch and D. Schuricht, *Dynamical phase transitions after quenches in nonintegrable models*, Phys. Rev. B **87**, 195104 (2013).

[23] S. Campbell, *Criticality revealed through quench dynamics in the Lipkin-Meshkov-Glick model*, Phys. Rev. B **94**, 184403 (2016).

[24] M. Heyl, *Dynamical quantum phase transitions: a review*, Rep. Prog. Phys. **81**, 054001 (2018).

[25] T. Fogarty, A. Usui, T. Busch, A. Silva, and J. Goold, *Dynamical phase transitions and temporal orthogonality in one-dimensional hard-core bosons: from the continuum to the lattice*, New J. Phys. **19**, 113018 (2017).

[26] N. Fläschner, D. Vogel, M. Tarnowski, B. S. Rem, D.-S. Lühmann, M. Heyl, J. C. Budich, L. Mathey, K. Sengstock, and C. Weitenberg, *Observation of dynamical vortices after quenches in a system with topology*, Nat. Phys. **14** (2018).

[27] A. del Campo, *Long-time behavior of many-particle quantum decay*, Phys. Rev. A **84**, 012113 (2011).

[28] J. Goold, T. Fogarty, N. Lo Gullo, M. Paternostro, and T. Busch, *Orthogonality catastrophe as a consequence of qubit embedding in an ultracold Fermi gas*, Phys. Rev. A **84**, 063632 (2011).

[29] M. Cetina, M. Jag, R. S. Lous, J. T. M. Walraven, R. Grimm, R. S. Christensen, and G. M. Bruun, *Decoherence of Impurities in a Fermi Sea of Ultracold Atoms*, Phys. Rev. Lett. **115**, 135302 (2015).

[30] M. M. Parish and J. Levinsen, *Quantum dynamics of impurities coupled to a Fermi sea*, Phys. Rev. B **94**, 184303 (2016).

[31] M. Cetina, M. Jag, R. S. Lous, I. Fritsche, J. T. M. Walraven, R. Grimm, J. Levinsen, M. M. Parish, R. Schmidt, M. Knap, and E. Demler, *Ultrafast many-body interferometry of impurities coupled to a Fermi sea*, Science **354**, 96–99 (2016).

[32] R. Schmidt, M. Knap, D. A. Ivanov, J.-S. You, M. Cetina, and E. Demler, *Universal many-body response of heavy impurities coupled to a Fermi sea: a review of recent progress*, Rep. Prog. Phys. **81**, 024401 (2018).

[33] M. Á. García-March, T. Fogarty, S. Campbell, T. Busch, and M. Paternostro, *Non-equilibrium thermodynamics of harmonically trapped bosons*, New J. Phys. **18**, 103035 (2016).

[34] A. Polkovnikov, *Microscopic diagonal entropy and its connection to basic thermodynamic relations*, Ann Phys (N Y) **326**, 486 – 499 (2011).

[35] M. Campisi, P. Hänggi, and P. Talkner, *Colloquium: Quantum fluctuation relations: Foundations and applications*, Rev. Mod. Phys. **83**, 771–791 (2011).

[36] L. Fusco, S. Pigeon, T. J. G. Apollaro, A. Xuereb, L. Mazzola, M. Campisi, A. Ferraro, M. Paternostro, and G. De Chiara, *Assessing the Nonequilibrium Thermodynamics in a Quenched Quantum Many-Body System via Single Projective Measurements*, Phys. Rev. X **4**, 031029 (2014).

[37] T. B. Batalhão, A. M. Souza, L. Mazzola, R. Auccaise, R. S. Sarthour, I. S. Oliveira, J. Goold, G. De Chiara, M. Paternostro, and R. M. Serra, *Experimental Reconstruction of Work Distribution and Study of Fluctuation Relations in a Closed Quantum System*, Phys. Rev. Lett. **113**, 140601 (2014).

[38] F. Cerisola, Y. Margalit, S. Machluf, A. J. Roncaglia, J. P. Paz, and R. Folman, *Using a quantum work meter to test non-equilibrium fluctuation theorems*, Nat. Commun. **8** (2017).

[39] T. Keller and T. Fogarty, *Probing the out-of-equilibrium dynamics of two interacting atoms*, Phys. Rev. A **94**, 063620 (2016).

[40] M. Esposito, U. Harbola, and S. Mukamel, *Nonequilibrium fluctuations, fluctuation theorems, and counting statistics in quantum systems*, Rev. Mod. Phys. **81**, 1665–1702 (2009).

[41] J. D. Jaramillo, J. Deng, and J. Gong, *Quantum work fluctuations in connection with the Jarzynski equality*, Phys. Rev. E **96**, 042119 (2017).

[42] D. Nigro, D. Rossini, and E. Vicari, *Scaling properties of work fluctuations after quenches near quantum transitions*, J. Stat. Mech. **2019**, 023104 (2019).

[43] B. Swingle, *Unscrambling the physics of out-of-time-order correlators*, Nat. Phys. **14**, 988–990 (2018).

[44] R. Lewis-Swan, A. Safavi-Naini, A. Kaufman, and A. Rey, *Dynamics of quantum information*, Nat. Rev. Phys. **1**, 627–634 (2019).

[45] D. W. Hallwood, T. Ernst, and J. Brand, *Robust mesoscopic superposition of strongly correlated ultracold atoms*, Phys. Rev. A **82**, 063623 (2010).

[46] C. Schenke, A. Minguzzi, and F. W. J. Hekking, *Nonadiabatic creation of macroscopic superpositions with strongly correlated one-dimensional bosons in a ring trap*, Phys. Rev. A **84**, 053636 (2011).

[47] C. Schenke, A. Minguzzi, and F. W. J. Hekking, *Probing superfluidity of a mesoscopic Tonks-Girardeau gas.*, Phys. Rev. A **85**, 053627 (2012).

[48] T. W. Hänsch and A. L. Schawlow, *Cooling of gases by laser radiation.*, Opt. Commun. **13**, 68–69 (1975).

[49] W. Ketterle and N. J. V. Druten, *Evaporative Cooling of Trapped Atoms.*, Adv. At. Mol. Opt. Phy. **37**, 181–236 (1996).

[50] E. L. Raab, M. Prentiss, A. Cable, S. Chu, and D. E. Pritchard, *Trapping of Neutral Sodium Atoms with Radiation Pressure.*, Phys. Rev. Lett. **59**, 2631 (1987).

[51] S. Chu, J. E. Bjorkholm, A. Ashkin, and A. Cable, *Experimental Observation of Optically Trapped Atoms.*, Phys. Rev. Lett. **57**, 314 (1986).

[52] C. Chin, R. Grimm, P. Julienne, and E. Tiesinga, *Feshbach resonances in ultracold gases*, Rev. Mod. Phys. **82**, 1225 (2010).

[53] E. Zohar, J. I. Cirac, and B. Reznik, *Quantum simulations of lattice gauge theories using ultracold atoms in optical lattices*, Rep. Prog. Phys **79**, 1 (2015).

[54] M. H. Anderson, J. R. Ensher, M. R. Matthews, C. E. Wieman, and E. A. Cornell, *Observation of Bose-Einstein Condensation in a Dilute Atomic Vapor.*, Science **2699**, 52211 (1995).

[55] K. B. Davis, M. O. Mewes, M. R. Andrews, N. J. van Druten, D. S. Durfee, D. M. Kurn, and W. Ketterle, *Bose-Einstein Condensation in a Gas of Sodium Atoms.*, Phys. Rev. Lett. **75**, 3969 (1995).

[56] W. Ketterle, *Nobel lecture: When atoms behave as waves: Bose-Einstein condensation and the atom laser*, Rev. Mod. Phys. **74**, 1131 (2002).

[57] M. Girardeau, *Relationship between Systems of Impenetrable Bosons and Fermions in One Dimension*, J. Math. Phys. **1**, 516 (1960).

[58] B. Paredes, A. Widera, V. Murg, O. Mandel, I. Fölling, S. Cirac, G. V. Shlyapnikov, T. W. Hänsch, and I. Bloch, *Tonks-Girardeau gas of ultracold atoms in an optical lattice*, Nature **429**, 277–281 (2004).

[59] T. Kinoshita, T. Wenger, and W. D. S., *Local Pair Correlations in One-Dimensional Bose Gases*, Phys. Rev. Lett. **95**, 190406 (2005).

[60] V. Efimov, *Energy levels arising from resonant two-body forces in a three-body system*, Phys. Lett. B **33**, 563 (1970).

[61] T. Kraemer, M. Mark, P. Waldburger, J. G. Danzl, C. Chin, B. Engeser, A. D. Lange, K. Pilch, A. Jaakkola, H.-C. Nägerl, and R. Grimm, *Evidence for Efimov quantum states in an ultracold gas of caesium atoms.*, Nature **440**, 315–318 (2006).

[62] B. Huang, L. A. Sidorenkov, R. Grimm, and J. M. Hutson, *Observation of the Second Triatomic Resonance in Efimov's Scenario.*, Phys. Rev. Lett. **112**, 190401 (2014).

[63] E. Nielsen and J. H. Macek, *Low-Energy Recombination of Identical Bosons by Three-Body Collisions*, Phys. Rev. Lett. **83**, 1566 (1999).

[64] F. Serwane, G. Zürn, T. Lompe, T. B. Ottenstein, A. N. Wenz, and S. Jochim, *Deterministic Preparation of a Tunable Few-Fermion System*, Science **332**, 6027 (2011).

[65] G. Zürn, F. Serwane, T. Lompe, A. N. Wenz, M. G. Ries, J. E. Bohn, and S. Jochim, *Fermionization of Two Distinguishable Fermions*, Phys. Rev. Lett. **108**, 075303 (2012).

[66] S. Murmann, A. Bergschneider, V. M. Klinkhamer, G. Zürn, T. Lompe, and S. Jochim, *Two Fermions in a Double Well: Exploring a Fundamental Building Block of the Hubbard Model*, Phys. Rev. Lett. **114**, 080402 (2015).

[67] I. Bloch, *Ultracold quantum gases in optical lattices*, Nat. Phys. **1**, 23–30 (2005).

[68] H. Friedrich, *Theoretical Atomic Physics*, Springer (2003).

[69] L. Santos, M. A. Baranov, J. I. Cirac, H.-U. Everts, H. Fehrmann, and M. Lewenstein, *Atomic Quantum Gases in Kagomé Lattices*, Phys. Rev. Lett. **93**, 030601 (2004).

[70] K. Huang and C. N. Yang, *Quantum-Mechanical Many-Body Problem with Hard-Sphere Interaction*, Phys. Rev. **105**, 767 (1957).

[71] M. Olshanii, *Atomic Scattering in the Presence of an External Confinement and a Gas of Impenetrable Bosons*, Phys. Rev. Lett. **81**, 938 (1998).

[72] Y. Ohashi and A. Griffin, *BCS-BEC Crossover in a Gas of Fermi Atoms with a Feshbach Resonance*, Phys. Rev. Lett. **89**, 130402 (2002).

[73] M. Greiner, C. A. Regal, and D. S. Jin, *Probing the Excitation Spectrum of a Fermi Gas in the BCS-BEC Crossover Regime*, Phys. Rev. Lett. **94**, 070403 (2005).

[74] C. J. Pethick and S. H., *Bose-Einstien Condensation in Dilute Gases 2nd Edition*, Cambridge (2008).

[75] P. A. Ruprecht, M. J. Holland, K. Burnett, and M. Edwards, *Time-dependent solution of the nonlinear Schrödinger equation for Bose-condensed trapped neutral atoms*, Phys. Rev. A **51**, 4704 (1995).

[76] F. Dalfovo and S. Stringari, *Bosons in anisotropic traps: Ground state and vortices*, Phys. Rev. A **53**, 2477 (1996).

[77] S. Burger, K. Bongs, S. Dettmer, W. Ertmer, K. Sengstock, A. Sanpera, G. V. Shlyapnikov, and M. Lewe, *Dark Solitons in Bose-Einstein Condensates*, Phys. Rev. Lett. **83**, 5198 (1999).

[78] K. W. Madison, F. Chevy, W. Wohlleben, and J. Dalibard, *Vortex Formation in a Stirred Bose-Einstein Condensate*, Phys. Rev. Lett. **84**, 806 (2000).

[79] J. R. Abo-Shaeer, C. Raman, J. M. Vogels, and W. Ketterle, *Observation of Vortex Lattices in Bose-Einstein Condensates*, Science **292**, 5516 (2001).

[80] O. Dutta, M. Gajda, P. Hauke, M. Lewenstein, D.-S. Lühmann, B. A. Malomed, T. Sowiński, and J. Zakrzewski, *Non-standard Hubbard models in optical lattices: a review*, Rep. Prog. Phys. **78**, 066001 (2015).

[81] J. Links, A. Foerster, A. P. Tonel, and G. Santos, *The Two-Site Bose–Hubbard Model*, Annales Henri Poincaré **7**, 1591–1600 (2006).

[82] J. M. Zhang and R. X. Dong, *Exact diagonalization: the Bose–Hubbard model as an example*, Eur. J. Phys. **31**, 591–602 (2010).

[83] M. Greiner, O. Mandel, T. Esslinger, T. W. Hänsch, and I. Bloch, *Quantum phase transition from a superfluid to a Mott insulator in a gas of ultracold atoms*, Nature **415**, 39–44 (2002).

[84] R. Jördens, N. Strohmaier, K. Günter, H. Moritz, and T. Esslinger, *A Mott insulator of fermionic atoms in an optical lattice*, Nature **455**, 204–207 (2008).

[85] J. Struck, C. Ölschläger, R. Le Targat, P. Soltan-Panahi, A. Eckardt, M. Lewenstein, P. Windpassinger, and K. Sengstock, *Quantum Simulation of Frustrated Classical Magnetism in Triangular Optical Lattices*, Science **333**, 6045 (2011).

[86] N. R. Cooper, J. Dalibard, and I. B. Spielman, *Topological bands for ultracold atoms*, Rev. Mod. Phys. **91**, 015005 (2019).

[87] T. Kinoshita, T. Wenger, and D. S. Weiss, *A quantum Newton's cradle*, Nature **440**, 900–903 (2006).

[88] A. M. Kaufman, M. E. Tai, A. Lukin, M. Rispoli, R. Schittko, P. M. Preiss, and M. Greiner, *Quantum thermalization through entanglement in an isolated many-body system*, Science **353**, 794 (2016).

[89] L. D. Landau and E. M. Lifschitz, *Statistical physics 1*, Pergamon Press (1980).

[90] M. Rigol, *Breakdown of Thermalization in Finite One-Dimensional Systems*, Phys. Rev. Lett. **103**, 100403 (2009).

[91] A. C. Cassidy, C. W. Clark, and M. Rigol, *Generalized Thermalization in an Integrable Lattice System*, Phys. Rev. Lett. **106**, 140405 (2011).

[92] E. Kaminishi, T. Mori, T. N. Ikeda, and M. Ueda, *Entanglement prethermalization in a one-dimensional Bose gas*, Nature Phys. **11**, 1050–1056 (2015).

[93] E. H. Lieb and W. Liniger, *Exact Analysis of an Interacting Bose Gas. I. The General Solution and the Ground State*, Phys. Rev. **130**, 1605–1616 (1963).

[94] T. Busch, B.-G. Englert, K. Rzazewski, and M. Wilkens, *Two Cold Atoms in a Harmonic Trap*, Found. Phys. **28**, 549 (1998).

[95] M. D. Girardeau, E. M. Wright, and J. M. Triscari, *Ground-state properties of a one-dimensional system of hard-core bosons in a harmonic trap*, Phys. Rev. A **63**, 033601 (2001).

[96] R. Pezer and H. Buljan, *Momentum Distribution Dynamics of a Tonks-Girardeau Gas: Bragg Reflections of a Quantum Many-Body Wave Packet*, Phys. Rev. Lett. **98**, 240403 (2007).

[97] F. Gerbier, S. Trotzky, S. Fölling, U. Schnorrberger, J. D. Thompson, A. Widera, I. Bloch, L. Pollet, M. Troyer, B. Capogrosso-Sansone, N. V. Prokof'ev, and B. V. Svistunov, *Expansion of a Quantum Gas Released from an Optical Lattice*, Phys. Rev. Lett. **101**, 155303 (2008).

[98] L. Budewig, S. I. Mistakidis, and P. Schmelcher, *Quench dynamics of two one-dimensional harmonically trapped bosons bridging attraction and repulsion*, Molecular Physics **117**, 2043–2057 (2019).

[99] E. Nielsen, D. V. Fedorov, A. S. Jensen, and E. Garrido, *The three-body problem with short-range interactions*, Phys. Rep. **347**, 373 (2001).

[100] S. T. Rittenhouse, J. von Stecher, J. P. D'Incao, N. P. Mehta, and C. H. Greene, *The hyperspherical four-fermion problem*, J. Phys. B **44**, 172001 (2011).

[101] A. G. Volosniev, D. V. Fedorov, A. S. Jensen, and N. T. Zinner, *Hyperspherical treatment of strongly-interacting few-fermion systems in one dimension*, Eur. Phys. J. Spec. Top. **224**, 585–590 (2015).

[102] A. S. Dehkharghani, A. G. Volosniev, E. J. Lindgren, J. Rotureau, C. Forssén, D. Fedorov, A. Jensen, and N. T. Zinner, *Quantum magnetism in strongly interacting one-dimensional spinor Bose systems*, Sci. Rep. **5**, 10675 (2015).

[103] A. S. Dehkharghani, A. G. Volosniev, and N. T. Zinner, *Impenetrable mass-imbalanced particles in one-dimensional harmonic traps*, J. Phys. B **49**, 085301 (2016).

[104] B. Wilson, A. Foerster, C. Kuhn, I. Roditi, and D. Rubeni, *A geometric wave function for a few interacting bosons in a harmonic trap*, Phys. Lett. A **378**, 1065 – 1070 (2014).

[105] J. Macek, *Properties of autoionizing states of He*, J. Phys. B **1**, 831–843 (1968).

[106] A. S. Dehkharghani, A. G. Volosniev, and N. T. Zinner, *Quantum impurity in a one-dimensional trapped Bose gas*, Phys. Rev. A **92**, 031601(R) (2015).

[107] D. Rubeni, A. Foerster, and I. Roditi, *Two interacting fermions in a one-dimensional harmonic trap: Matching the Bethe ansatz and variational approaches*, Phys. Rev. A **86**, 043619 (2012).

[108] N. J. S. Loft, A. S. Dehkharghani, N. P. Mehta, A. G. Volosniev, and N. T. Zinner, *A variational approach to repulsively interacting three-fermion systems in a one-dimensional harmonic trap*, Eur. Phys. J. D **69**, 65 (2015).

[109] R. E. Barfknecht, A. S. Dehkharghani, A. Foerster, and N. T. Zinner, *Correlation properties of a three-body bosonic mixture in a harmonic trap*, J. Phys. B **49**, 135301 (2016).

[110] J. Boronat and J. Casulleras, *Monte Carlo analysis of an interatomic potential for He*, Phys. Rev. B **49**, 8920 (1994).

[111] Y. J. Hao and S. Chena, *Ground-state properties of interacting two-component Bose gases in a one-dimensional harmonic trap*, Eur. Phys. J. D **51**, 261 (2009).

[112] U. Schollwöck, *The density-matrix renormalization group*, Rev. Mod. Phys. **77**, 259 (2005).

[113] F. Verstraete and J. I. Cirac, *Matrix product states represent ground states faithfully*, Phys. Rev. B **73**, 094423 (2006).

[114] F. Verstraete and J. I. Cirac, *Continuous Matrix Product States for Quantum Fields*, Phys. Rev. Lett. **104**, 190405 (2010).

[115] M. A. Garcia-March and T. Busch, *Quantum Gas Mixturres in Different Correlation Regimes*, Phys. Rev. A **87**, 063633 (2013).

[116] E. J. Lindgren, J. Rotureau, C. Forssén, A. G. Volosniev, and N. T. Zinner, *Fermionization of two-component few-fermion systems in a one-dimensional harmonic trap*, New J. Phys. **16**, 063003 (2014).

[117] M. A. Garcia-March, B. Juliá-Díaz, G. E. Astrakharchik, T. Busch, J. Boronat, and A. Polls, *Sharp crossover from composite fermionization to phase separation in microscopic mixtures of ultracold bosons*, Phys. Rev. A **88**, 063604 (2013).

[118] M. A. Garcia-March, B. Juliá-Díaz, G. E. Astrakharchik, J. Boronat, and A. Polls, *Distinguishability, degeneracy, and correlations in three harmonically trapped bosons in one dimension*, Phys. Rev. A **90**, 063605 (2014).

[119] M. A. Garcia-March, B. Juliá-Díaz, G. E. Astrakharchik, T. Busch, J. Boronat, and A. Polls, *Quantum correlations and spatial localization in one-dimensional ultracold bosonic mixtures*, New J. Phys. **16**, 103004 (2014).

[120] S. Campbell, M. A. Garcia-March, T. Fogarty, and T. Busch, *Quenching small quantum gases: Genesis of the orthogonality catastrophe*, Phys. Rev. A **90**, 013617 (2014).

[121] M. A. Garcia-March, A. S. Dehkharghani, and N. T. Zinner, *Entanglement of an impurity in a few-body one-dimensional ideal Bose system*, J. Phys. B **49**, 075303 (2016).

[122] A. G. Volosniev, D. V. Fedorov, A. S. Jensen, M. Valiente, and N. T. Zinner, *Strongly interacting confined quantum systems in one dimension*, Nat. Commun. **5**, 5300 (2014).

[123] L. Yang, L. Guan, and H. Pu, *Strongly interacting quantum gases in one-dimensional traps*, Phys. Rev. A **91**, 043634 (2015).

[124] A. G. Volosniev, D. Petrosyan, M. Valiente, D. V. Fedorov, A. S. Jensen, and N. T. Zinner, *Engineering the dynamics of effective spin-chain models for strongly interacting atomic gases*, Phys. Rev. A **91**, 023620 (2015).

[125] L. Yang and X. Cui, *Effective spin-chain model for strongly interacting one-dimensional atomic gases with an arbitrary spin*, Phys. Rev. A **93**, 013617 (2016).

[126] R. E. Barfknecht, A. Foerster, and N. T. Zinner, *Dynamical realization of magnetic states in a strongly interacting Bose mixture*, Phys. Rev. A **95**, 023612 (2017).

[127] R. E. Barfknecht, A. Foerster, and N. T. Zinner, *Dynamics of spin and density fluctuations in strongly interacting Few-Body Syst.*, Sci. Rep. **9**, 15994 (2019).

[128] M. Płodzień, D. Wiater, A. Chrostowski, and T. Sowiński. *Numerically exact approach to few-body problems far from a perturbative regime*, (2018).

[129] H. P. Büchler, G. Blatter, and W. Zwerger, *Commensurate-Incommensurate Transition of Cold Atoms in an Optical Lattice*, Phys. Rev. Lett. **90**, 130401 (2003).

[130] A. Lazarides and M. Haque, *Strongly interacting one-dimensional bosons in optical lattices of arbitrary depth: From the Bose-Hubbard to the sine-Gordon regime and beyond*, Phys. Rev. A **85**, 063621 (2012).

[131] K. Lelas, T. Seva, H. Buljan, and J. Goold, *Pinning quantum phase transition in a Tonks-Girardeau gas: Diagnostics by ground-state fidelity and the Loschmidt echo*, Phys. Rev. A **86**, 033620 (2012).

[132] G. E. Astrakharchik, K. V. Krutitsky, M. Lewenstein, and F. Mazzanti, *One-dimensional Bose gas in optical lattices of arbitrary strength*, Phys. Rev. A **93**, 021605(R) (2016).

[133] G. E. Astrakharchik, K. V. Krutitsky, M. Lewenstein, F. Mazzanti, and J. Boronat, *Optical lattices as a tool to study defect-induced superfluidity*, Phys. Rev. A **96**, 033606 (2017).

[134] E. Haller, R. Hart, M. J. Mark, J. G. Danzl, L. Reichsöllner, M. Gustavsson, M. Dalmonte, G. Pupillo, and H.-C. Nägerl, *Pinning quantum phase transition for a Luttinger liquid of strongly interacting bosons*, Nature **466**, 597–600 (2010).

[135] G. Boéris, L. Gori, M. D. Hoogerland, A. Kumar, E. Lucioni, L. Tanzi, M. Inguscio, T. Giamarchi, C. D'Errico, G. Carleo, G. Modugno, and L. Sanchez-Palencia, *Mott transition for strongly interacting one-dimensional bosons in a shallow periodic potential*, Phys. Rev. A **93**, 011601 (2016).

[136] A. Minguzzi and D. M. Gangardt, *Exact Coherent States of a Harmonically Confined Tonks-Girardeau Gas*, Phys. Rev. Lett. **94**, 240404 (2005).

[137] A. del Campo and J. G. Muga, *Dynamics of a Tonks-Girardeau gas released from a hard-wall trap*, Europhys. Lett **74**, 8 (2006).

[138] M. Collura, S. Sotiriadis, and P. Calabrese, *Equilibration of a Tonks-Girardeau Gas Following a Trap Release*, Phys. Rev. Lett. **110**, 245301 (2013).

[139] O. M. Braun and Y. Kivshar, *The Frenkel-Kontorova model: concepts, methods, and applications*, Springer Science and Business Media (2013).

[140] T. Fogarty and T. Busch, *A many-body heat engine at criticality*, Quantum Sci. Technol. **6**, 015003 (2020).

[141] J. Settino, N. L. Gullo, F. Plastina, and A. Minguzzi. *Exact spectral function of a Tonks-Girardeau gas in a lattice*, (2020).

[142] I. Reshodko, A. Benseny, J. Romhányi, and T. Busch, *Topological states in the Kronig–Penney model with arbitrary scattering potentials*, New J. Phys. **21**, 013010 (2019).

[143] J. Maldacena, S. H. Shenkerband, and D. Stanford, *A bound on chaos*, J. High Energy Phys. **8**, 106 (2016).

[144] E. B. Rozenbaum, S. Ganeshan, and V. Galitski, *Lyapunov Exponent and Out-of-Time-Ordered Correlator's Growth Rate in a Chaotic System*, Phys. Rev. Lett. **118**, 086801 (2017).

[145] J. Chávez-Carlos, B. López-del Carpio, M. A. Bastarrachea-Magnani, P. Stránský, S. Lerma-Hernández, L. F. Santos, and J. G. Hirsch, *Quantum and Classical Lyapunov Exponents in Atom-Field Interaction Systems*, Phys. Rev. Lett. **122**, 024101 (2019).

[146] M. Heyl, F. Pollmann, and B. Dóra, *Detecting Equilibrium and Dynamical Quantum Phase Transitions in Ising Chains via Out-of-Time-Ordered Correlators*, Phys. Rev. Lett. **121**, 016801 (2018).

[147] C.-J. Lin and O. I. Motrunich, *Out-of-time-ordered correlators in a quantum Ising chain*, Phys. Rev. B **97**, 144304 (2018).

[148] C. B. Dağ, K. Sun, and L.-M. Duan, *Detection of Quantum Phases via Out-of-Time-Order Correlators*, Phys. Rev. Lett. **123**, 140602 (2019).

[149] M. Gärttner, J. G. Bohnet, A. Safavi-Naini, M. L. Wall, J. J. Bollinger, and A. M. Rey, *Measuring out-of-time-order correlations and multiple quantum spectra in a trapped-ion quantum magnet*, Nat. Phys. **13**, 781–786 (2017).

[150] M. McGinley, A. Nunnenkamp, and J. Knolle, *Slow Growth of Out-of-Time-Order Correlators and Entanglement Entropy in Integrable Disordered Systems*, Phys. Rev. Lett. **122**, 020603 (2019).

[151] M. Campisi and J. Goold, *Thermodynamics of quantum information scrambling*, Phys. Rev. E **95**, 062127 (2017).

[152] R. Lewis-Swan, A. Safavi-Naini, J. Bollinger, and A. Rey, *Unifying scrambling, thermalization and entanglement through measurement of fidelity out-of-time-order correlators in the Dicke model*, Nat. Commun. **10**, 1581 (2019).

[153] R. Hamazaki, K. Fujimoto, and M. Ueda. *Operator Noncommutativity and Irreversibility in Quantum Chaos*, (2018).

[154] A. Chenu, J. Molina-Vilaplana, and A. del Campo, *Work Statistics, Loschmidt Echo and Information Scrambling in Chaotic Quantum Systems*, Quantum **3**, 127 (2019).

[155] B. Yan, L. Cincio, and W. H. Zurek, *Information Scrambling and Loschmidt Echo*, Phys. Rev. Lett. **124**, 160603 (2020).

[156] A. D. Luca and A. Scardicchio, *Ergodicity breaking in a model showing many-body localization*, Europhys. Lett. **101**, 37003 (2013).

[157] T. Sowiński and M. Á. García-March, *One-dimensional mixtures of several ultracold atoms: a review*, Rep. Prog. Phys. **82**, 104401 (2019).

[158] K. Hashimoto, K. Murata, and R. Yoshii, *Out-of-time-order correlators in quantum mechanics*, J. High Energy Phys. **10**, 138 (2017).

[159] N. L. Harshman, *Symmetries of three harmonically trapped particles in one dimension*, Phys. Rev. A **86**, 052122 (2012).

[160] N. L. Harshman, *One-Dimensional Traps, Two-Body Interactions, Few-Body Symmetries: I. One, Two, and Three Particles*, Few-Body Syst. **57**, 11–43 (2016).

[161] N. L. Harshman, *One-Dimensional Traps, Two-Body Interactions, Few-Body Symmetries. II. N Particles*, Few-Body Syst. **57**, 45–69 (2016).

[162] D. Baye, *Lagrange-mesh method for quantum-mechanical problems*, Phys. Status Solidi B **243**, 1095–1109 (2006).

[163] S. Waldensrøm and K. R. Naqvi, *The overlap integrals of two harmonic-oscillator wavefunctions: some remarks on originals and reproductions*, Chem. Phys. Lett. **85**, 581–584 (1982).

[164] T. Grining, M. Tomza, M. Lesiuk, M. Przybytek, M. Musiał, P. Massignan, M. Lewenstein, and R. Moszynski, *Many interacting fermions in a one-dimensional harmonic trap: a quantum-chemical treatment*, New J. Phys. **17**, 115001 (2015).

[165] S. Okubo, *Diagonalization of Hamiltonian and Tamm-Dancoff Equation*, Prog. Theor. Phys. **12**, 603–622 (1954).

[166] K. Suzuki, *Construction of Hermitian Effective Interaction in Nuclei: — General Relation between Hermitian and Non-Hermitian Forms —*, Prog. Theor. Phys. **68**, 246–260 (1982).

[167] K. Suzuki and R. Okamoto, *Effective Interaction Theory and Unitary-Model-Operator Approach to Nuclear Saturation Problem*, Prog. Theor. Phys. **92**, 1045–1080 (1994).

[168] A. F. Lisetskiy, B. R. Barrett, M. K. G. Kruse, P. Navratil, I. Stetcu, and J. P. Vary, *Ab-initio shell model with a core*, Phys. Rev. C **78**, 044302 (2008).

[169] J. Rotureau, *Interaction for the trapped fermi gas from a unitary transformation of the exact two-body spectrum*, Eur. Phys. J. D **67**, 153 (2013).

[170] T. Ernst, D. W. Hallwood, J. Gulliksen, H.-D. Meyer, and J. Brand, *Simulating strongly correlated multiparticle systems in a truncated Hilbert space*, Phys. Rev. A **84**, 023623 (2011).

[171] P. Jeszenszki, H. Luo, A. Alavi, and J. Brand, *Accelerating the convergence of exact diagonalization with the transcorrelated method: Quantum gas in one dimension with contact interactions*, Phys. Rev. A **98**, 053627 (2018).

[172] P. Koscik, *Optimized configuration interaction approach for trapped multiparticle systems interacting via contact forces*, Phys. Lett. A **382**, 2561 – 2564 (2018).

[173] I. Talmi, *Nuclear spectroscopy with harmonic-oscillator wave-functions*, Helv. Phys. Acta **25** (1952).

[174] M. Moshinsky, *Transformation brackets for harmonic oscillator functions*, Nucl. Phys. **13**, 104–116 (1959).

[175] L. M. Robledo, *Separable approximation to two-body matrix elements*, Phys. Rev. C **81**, 044312 (2010).

[176] R. R. Chasman and S. Wahlborn, *Transformation scheme for harmonic-oscillator wave functions*, Nucl. Phys. A **90**, 401–406 (1967).

[177] Y. F. Smirnov, *Talmi transformation for particles with different masses (II)*, Nucl. Phys. **39**, 346–352 (1962).

[178] A. Gal, *The talmi transformation for different particles—A complete construction and new results*, Ann Phys (N Y) **49**, 341–356 (1968).

[179] T.-N. Xu, J. Li, T. Busch, X. Chen, and T. Fogarty, *Effects of coherence on quantum speed limits and shortcuts to adiabaticity in many-particle systems*, Phys. Rev. Res. **2**, 023125 (2020).

[180] J. D. Teufel, T. Donner, D. Li, J. W. Harlow, M. S. Allman, K. Cicak, A. J. Sirois, J. D. Whittaker, K. W. Lehnert, and R. W. Simmonds, *Sideband cooling of micromechanical motion to the quantum ground state*, Nature **475**, 359–363 (2011).

[181] J. Chan, T. P. M. Alegre, A. H. Safavi-Naeini, J. T. Hill, A. Krause, S. Gröblacher, M. Aspelmeyer, and O. Painter, *Laser cooling of a nanomechanical oscillator into its quantum ground state*, Nature **478**, 89–92 (2011).

[182] J. B. Khurgin, M. W. Pruessner, T. H. Stievater, and W. S. Rabinovich, *Laser-Rate-Equation Description of Optomechanical Oscillators*, Phys. Rev. Lett. **108**, 223904 (2012).

[183] S. Forstner, S. Prams, J. Knittel, E. D. van Ooijen, J. D. Swaim, G. I. Harris, A. Szorkovszky, W. P. Bowen, and H. Rubinsztein-Dunlop, *Cavity Optomechanical Magnetometer*, Phys. Rev. Lett. **108**, 120801 (2012).

[184] T. Bagci, A. Simonsen, S. Schmid, L. G. Villanueva, E. Zeuthen, J. Appel, J. M. Taylor, A. Sørensen, K. Usami, A. Schliesser, and E. S. Polzik, *Optical detection of radio waves through a nanomechanical transducer*, Nature **507**, 81–85 (2014).

[185] M. Wu, A. C. Hryciw, C. Healey, D. P. Lake, H. Jayakumar, M. R. Freeman, J. P. Davis, and P. E. Barclay, *Dissipative and Dispersive Optomechanics in a Nanocavity Torque Sensor*, Phys. Rev. X **4**, 021052 (2014).

[186] F. Armata, L. Latmiral, A. D. K. Plato, and M. S. Kim, *Quantum limits to gravity estimation with optomechanics*, Phys. Rev. A **96**, 043824 (2017).

[187] C. Biancofiore, M. Karuza, M. Galassi, R. Natali, P. Tombesi, G. Di Giuseppe, and D. Vitali, *Quantum dynamics of an optical cavity coupled to a thin semi-transparent membrane: Effect of membrane absorption*, Phys. Rev. A **84**, 033814 (2011).

[188] X. Y. Zhang, Y. H. Zhou, Y. Q. Guo, and X. X. Yi, *Photon blockade in optomechanical systems with a position-modulated Kerr-type nonlinear coupling*, J. Phys. A **51**, 095302 (2018).

[189] P. Djorwe, Y. Pennec, and B. Djafari-Rouhani, *Low-power phonon lasing through position-modulated Kerr-type nonlinearity*, Sci. Rep. **9**, 1684 (2019).

[190] X. Xiao, H. Liang, and X. Wang, *Optimal estimation of gravitation with Kerr nonlinearity in an optomechanical system*, Quantum Inf. Process. **19**, 410 (2020).

Appendix A

Appendix

In this appendix I will present some supplemental material relevant for chapter 5 in the thesis. This includes a slightly more in-depth analysis of the matrix-elements and a comparison of the position operator results with momentum operator results.

A.1 Analysis of the matrix elements K_{jk} and J_{jk}

The important coefficients that determine the behavior of the emergent matrix elements are given by Eq. (5.27). Let us first consider what happens for large m, j. To do this the behaviour of the quantities in Eq.(5.27) must first be established. The harmonic oscillator eigenfunctions evaluated at zero argument $\psi_{2n}(0)$ are given by

$$\psi_{2m}(0) = \left(\frac{-1}{2}\right)^m \left(\frac{1}{\pi}\right)^{1/4} \frac{\sqrt{2m!}}{m!}, \tag{A.1}$$

which, by utilizing Stirling's formula, can be evaluated for large m as

$$\psi_{2m}(0) \approx (-1)^m m^{-1/4} \propto m^{-1/4}. \tag{A.2}$$

The behaviour of the digamma functions for solutions of Eq. (3.18) is complicated, but numerically it is found that $\Omega^g_{2j} \propto j^{-1/4}$ for large j. The energy of the $2j$-th state can be expressed as in Eq. (3.19) in the main text. For large j, one has $\Delta_j \propto j^{-1/2}$ (see [94]).

Let us now consider the dependence of $\alpha^x_{m,j}$ on j. Using Eq. (3.19) one can rewrite the position coefficients as

$$\begin{aligned}\alpha^x_{m,j} &= a_\omega \sqrt{2m+1}\psi_{2m}(0)\Omega^g_{2j} \\ &\times \left(\frac{1}{(2m-2j+\Delta_j)} - \frac{1}{(2m+2-2j+\Delta_j)}\right).\end{aligned} \tag{A.3}$$

For $m = j$ and $m = j-1$ the fractions scale $\propto j^{1/2}$ in the limit of large j, while

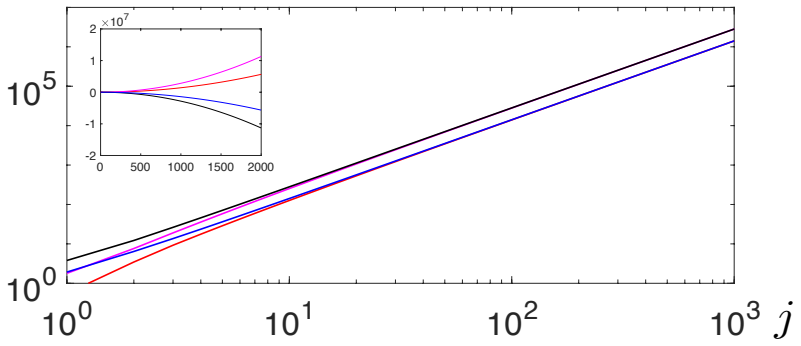

Figure A.1: The main plot shows the absolute values of $K_{j,j}$ (magenta line), $K_{j,j+1}$ (blue line), $J_{j,j}$ (red line) and $J_{j,j+1}$ (black line) as a function of j, while the insert shows the same for the true values.

the remaining terms don't scale with increasing j, which means that they become insignificant in comparison. As $m = j$ this means that the coefficients themselves scale as $\alpha^x_{j,m} \propto j^{1/2}$ in the limit of large j. From Eq. (5.24) it is clear that only terms in which $\alpha_{m,j}\alpha_{m,k}$ are large can contribute to K_{jk}. However, these are only large when $j = m, j = m+1$ and $k = m, k = m+1$ is simultaneously true which happens when $k = j, k = j-1, k = j+1$. Similarly from Eq. (5.25) only terms in which $\alpha_{n,k}\alpha_{n-1,j}$ are large contribute to J_{jk}. This is only fulfilled when $j = n-1, j = n$ and $k = n, k = m+1$ is simultaneously true, which is the case for $k = j, k = j+1, k = j+2$. So for large j these values will be dominant, as the other matrix-elements are of insignificant size in comparison. From the preceding discussion as well as the form of Eq. (5.24),(5.25) the relevant terms all scale as j^2. These observations are all confirmed by a full numerical evaluation of K_{jk}, J_{jk} with the j^2 scaling shown in Fig. A.1. Additionally, it is found that the following relation between the important matrix-elements hold $K_{j,j+1} = K_{j,j-1} = -J_{j,j} = J_{j,j+2} = -\xi_1 j^2$ and $K_{j,j} = -J_{j,j+1} = \xi_2 j^2$ even at relatively small values of j .

A.2 Correlation functions for other combinations of canonical operators

In chapter 5 the main focus was on $[\hat{x}(t), \hat{x}]^2$ as no regularisation of the delta-function is required and it contains the essential physics of the scrambling. In this section the last claim will be backed up by investigating other combinations of canonical operators. In order to do this a short-range Gaussian interaction described by $V_{\text{int}}(x) = \kappa \frac{1}{\sigma\sqrt{2\pi}} e^{-x^2/\sigma^2}$ is utilized. I consider $\kappa = 10, \sigma = 0.04$ which has an energy spectrum that corresponds well to $g = 10$ for the delta-function interaction. The time-dependent correlation functions are calculated numerically employing the Lagrange-mesh method [162] and the time-average is calculated in a time-interval $t \in [1000\pi, 2000\pi]$ which is large enough to get a representative average (see chapter 5.6.2 for a further discussion of this). In Fig. A.2(a) $\bar{I}_{AB}$ as a function of $\bar{I}_{xx}$ for a series of quenches where $\gamma \in [1, 20]$

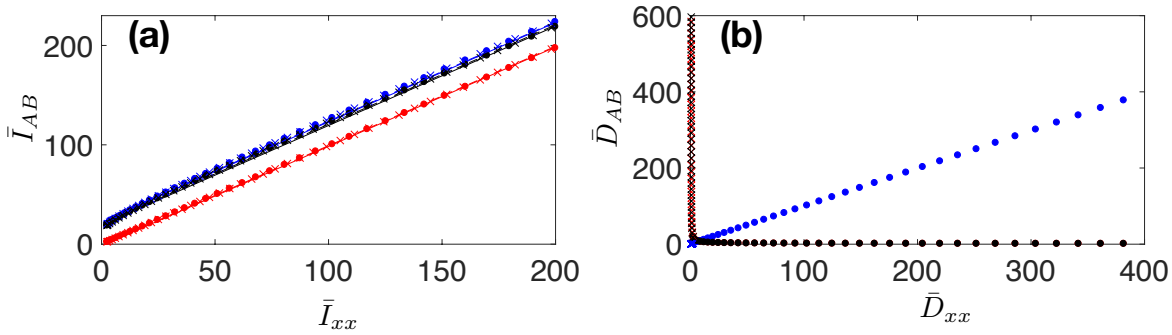

Figure A.2: (a) $\bar{I}_{xp}$ (red) $\bar{I}_{px}$ (blue) and $\bar{I}_{pp}$ (black) as a function of $\bar{I}_{xx}$ along with fits to $\bar{I}_{AB} = \bar{I}_{xx} + \text{constant}$. The crosses correspond to $\gamma > 1$, while the full circles correspond to $\gamma < 1$. (b) same as (a), but for $\bar{D}_{xp}$ (red) $\bar{D}_{px}$ (blue) and $\bar{D}_{pp}$ (black) as a function of $\bar{D}_{xx}$. Note that the black and the red are on top of each other in (b), which is why the red circles cannot be seen.

and $\gamma \in [1, 1/20]$ is shown. $\bar{I}_{AB}$ for any combination of operators only differs from $\bar{I}_{xx}$ by a constant, regardless of γ as can be seen from the graph where fits to $\bar{I}_{xx}$ plus a constant are shown. The behaviour for $\gamma > 1$ and $\gamma < 1$ is qualitatively similar, regardless of the combination of operators. In Fig. A.2(b) the same is plotted, but for $\bar{D}_{AB}$. Here the behaviour is dramatically different for different operators. $\bar{D}_{px}$ and $\bar{D}_{xx}$ (both of which probe the time-dependence of $\hat{x}(t)$) have a linear relationship. For squeezing the trap this results in linear growth of $\bar{D}_{px}$ with $\bar{D}_{xx}$ (blue full circles in the plot), while for $\gamma > 1$ they are both given by a small constant resulting in all points being on top of each other centered at (0,0) in the figure (blue crosses). $\bar{D}_{pp}$ and $\bar{D}_{xp}$ (corresponding to probing the time-dependence of $\hat{p}(t)$) also have a linear relationship, as can be seen from the plot, however, these two sets behave very differently from each other. For squeezing the trap the full black and red circles corresponding to $\bar{D}_{pp}$ and $\bar{D}_{xp}$ remain small and constant as $\bar{D}_{xx}$ grows with γ. For opening the trap on the other hand the black and red crosses grow with γ, while $\bar{D}_{xx}$ remains constant. Probing $\hat{x}(t)$ and $\hat{p}(t)$ therefore results in the opposite behaviour with respect to opening and squeezing the trap for $\bar{D}_{Ax}$ and $\bar{D}_{Ap}$ which makes the overall scrambling different. $\bar{I}_{AB}$ however, always gives a similar contribution to the scrambling, regardless of the combination of canonical operators.